THE KINETICS OF PEARLITE GROWTH IN ALUMINIUM BRONZES

Thesis presented for the Degree of
Doctor of Philosophy
of London University
by

Moodalagri Kushalrao Asundi.

Department of Metallurgy
Imperial College of Science and Technology
London SW7

August 1964

SUMMARY

The kinetics of pearlite growth in certain binary and ternary aluminium bronzes have been studied from a quantitative aspect. The investigations consisted of determinations of pearlite growth rate at several temperatures and of the corresponding interlamellar spacings. The diffusion coefficients of aluminium, zinc and tin which take part in the pearlite reaction, were determined. Some preliminary experiments on partitioning of the ternary elements were also conducted.

The growth rate - temperature curves showed a peak which was found to be associated with the ordering reaction $\beta \rightarrow \beta_1$ in these alloys. The pearlite growth rate obtained from the dissociation of $\beta_1 \rightarrow \alpha + \gamma_2$ was found to decrease with decreasing temperatures of reaction with a corresponding increase in the interlamellar spacing.

Addition of tin was found to retard the growth rate considerably through its constitutional effect by decreasing the driving potential of the reaction. The effect of zinc was similar though less pronounced and its effect on the $\beta \rightarrow \beta_1$ reaction appeared to give the impression of an enhanced growth rate.

The growth of pearlite in all the alloys is considered to be controlled by the diffusion rate of aluminium in the β phase. The diffusion coefficient of

aluminium in the β phase was found to be very much larger than in the α phase and the activation energy for diffusion almost half that in α. The diffusivities of zinc and tin in the β phase were of the same order of magnitude as that of aluminium and thus partitioning appeared to occur simultaneously during the growth of pearlite.

CONTENTS

CHAPTER I.

GENERAL INTRODUCTION.

The product of the decomposition of a single phase into two new phases, forming alternate lamellae, growing as a nodule or a cell from the parent phase is known as pearlite. Originally this term pearlite was applied to that structure observed in normalised and annealed steels, but nowadays it is also applied to the transformation product of various non-ferrous systems. A considerable amount of experimental and theoretical work has been done on the kinetics of the pearlite reaction in steels which is of great technical importance and interest. There is, however, comparatively little data on the quantitative aspects of the kinetics of eutectoid transformation in non-ferrous alloys.

The pearlite transformation has been well established as a nucleation and growth reaction and the kinetics of pearlite form an interesting aspect of the transformation. Although the determination of the growth rate is a comparatively simple matter the mechanism of growth is rather complex. In a binary eutectoidal dissociation process two new phases, of differing concentrations of constituent components, are formed. It is essential therefore that the components must diffuse to the phases in order to effect a segregation. Whether the

reaction rate is controlled by the diffusion ahead of the interface, at the interface or in one of the product phases or by any other mechanism remains to be established by experiments.

It has not been possible to derive a precise relation between growth rate and various parameters on the basis of diffusion or interface reactions. Consequently growth kinetics have been interpreted in several ways and there is a lack of general agreement. However, it is possible to determine with reasonable certainty whether volume diffusion is controlling the reaction rate or not, by analysing the various parameters essential in the establishment of a growth mechanism.

Additions of ternary elements which enhance or retard the growth rates bring in further complications in understanding the reaction kinetics and the mechanism of growth. In steels it is well known that small additions of manganese and nickel retard the growth rate of pearlite considerably while cobalt increases it. In a similar way additions of manganese, iron, cobalt and tin decrease the growth rate of pearlite in aluminium bronzes. The precise nature of the influence of the ternary elements on the growth rates is not known.

In the present investigation efforts have been directed to provide some useful data on the growth rate

of pearlite in the binary copper-aluminium system and to study the influence of small alloy additions on the growth rate of some ternary alloy systems. In order to simplify the analyses, only eutectoidal compositions have been chosen and additions of ternary elements are restricted to only a few per cent.

With this general aim in mind, the problem is to determine all the contributing factors for the growth process and to find out whether the existing theories of growth can be successfully applied. A systematic compilation of all the factors has rarely been carried out even in the case of steels where there is ample data on diffusion rates, growth rates, etc.

A venture such as this one necessarily involves, for a fuller appraisal, all the relevant data on growth rates, diffusion rates, interlamellar spacings and partitioning effects. Each of these four demand considerable time and effort. A major portion of the investigation has been devoted to the determination of the diffusion coefficients of aluminium, tin and zinc in the β phase; since no such data are available in the literature. The theoretical implications have been analysed in the same way as the ferrous pearlites, bearing in mind the special features of the copper-aluminium system.

CHAPTER II.

PREVIOUS LITERATURE.

The Pearlite Reaction in the Copper-Aluminium System:

Since the development of the isothermal techniques for the study of phase transformation phenomena in metals and alloys, the pearlite reaction in aluminium bronzes has been investigated very thoroughly. The earliest comprehensive work was by Smith and Lindlief[1] and subsequently Mack[2], Klier and Grymko[3], Haynes[4], Thomas[5], Kasberg and Mack[6], Ranzetta[7] and Ranzetta and West[8] have recorded their results of investigations of the various structures and peculiar features encountered in this system. However, there has been little quantitative work on nucleation and growth rates of the pearlite. Ranzetta and West[8] reported the growth rates of pearlite in binary and some ternary systems and Haynes[4] has made some measurements of the interlamellar spacings.

The presence of a eutectoid reaction in the copper-aluminium system at the copper-rich end can be noted from the equilibrium diagram[9] reproduced in Fig.1. The intermediate β phase dissociates eutectoidally at 565°C and at a concentration of 11.8 wt.% Al; giving phases α and γ_2. The parent phase β is an electron compound of 3/2 electron to atom ratio and has a disordered body centred cubic structure. The α phase is a face centred cubic

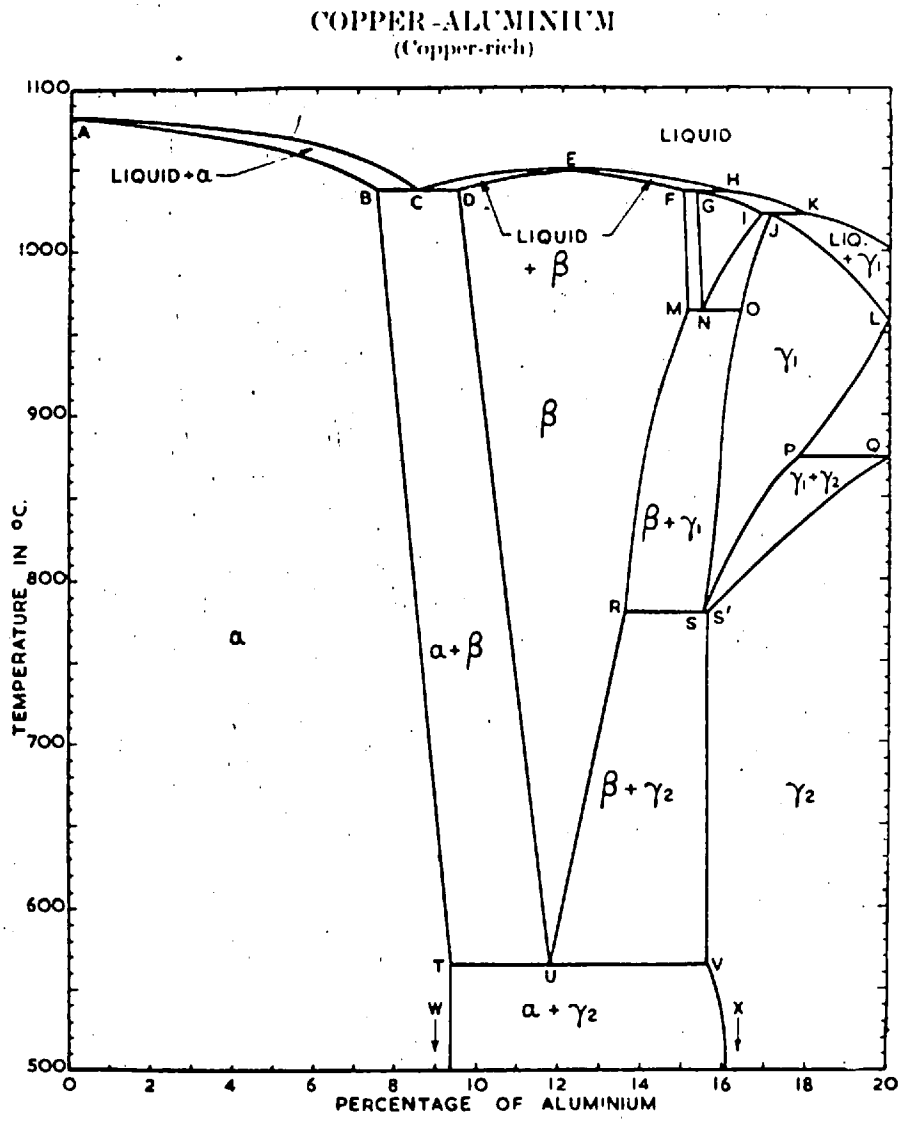

Point	A	B	C	D	E	F	G	H	I	J	K	L_A
° C.	1083	1037	1037	1037	1048	1036	1036	1036	1022	1022	1022	958
Al, %	0	7·5	8·5	9·5	12·4	14·95	15·25	16·0	16·9	17·1	18·0	20·0

Point	M	N	O	P	Q	R	S, S'	T	U	V	W	X
° C.	963	963	963	873	873	780	780	565	565	565	0	0
Al, %	15·1	15·45	16·4	17·8	20·0	13·6	(15·6)	9·4	11·8	15·6	9·4	16·2

G. V. Raynor, Institute of Metals (Annotated Equilibrium Diagram Series No. 4), 1944.

FIG. 1. The Copper Aluminium Phase Diagram.

copper-rich primary solid solution; the γ_2 phase is an intermetallic compound rich in aluminium and has a complex γ brass type cubic structure.

The stability of the β phase increases with increasing temperature and the range of composition over which it is stable widens. The phase boundaries of β rise steeply and any slight composition change from the eutectoid composition leads to the occurrence of pro-eutectoid phases during isothermal transformation below the eutectoid temperature. Thus a completely pearlitic structure can only be obtained over a very limited composition range. The products of decomposition, i.e. α and γ_2, appear to be stable between 565°C and about 400°C.

In the eutectoid alloy lamellar pearlite is formed from the β phase in the range 565°C to 527°C, and below this temperature β transforms to β_1, an ordered structure, prior to the pearlitic reaction. It has been established[10,11] that β_1 is an ordered phase and is richer in aluminium than β. For aluminium compositions of less than 12.4 wt.%, due to this reaction from $\beta \rightarrow \beta_1$, copper rich α phase is precipitated below about 510°C, the amount increasing with the lowering of the reaction temperature. Interference of the α precipitate confines the measurements of the pearlite growth rates within the temperature range 490°C to 565°C. At temperatures of 550°C and above increasing amounts of granular pearlite are formed.

The formation of β_1 from β was first observed using the optical microscope by Smith and Lindlief[1]. This reaction has interesting implications on the kinetics of pearlite growth in binary and ternary alloy aluminium bronzes. The temperature and the composition range in which both β and β_1 coexist in metastable equilibrium is shown in Fig.2. For a binary eutectoid composition alloy (11.8 wt.% Al), the highest temperature of formation of β_1 occurs at 527°C and the alloy transforms fully to β_1 below 450°C. The boundaries of the metastable phase diagram, namely the $\beta/\beta + \beta_1$ and the $\beta_1/\beta + \beta_1$ boundaries, intersect at about 545°C and at a composition given by Cu_3Al (12.4 wt.% Al).

The decomposition of β_1 to α and γ_2 in a binary alloy of composition 12.4 wt.% Al, consisting entirely of β_1, is of particular interest since a fully pearlitic structure forms over the temperature range 500°C to 400°C. The growth rates measured from this reaction would be free from the interference of α precipitate, for a much longer range of temperatures than that of $\beta \rightarrow \alpha + \gamma_2$. Details of the T-T-T diagram for a 12.4 wt.% alloy have been given by Thomas[5].

There is a general agreement about the form and position of the T-T-T diagrams of the binary eutectoid alloys. It has also been recognised that lamellar eutectoid forms in binary alloys within a composition

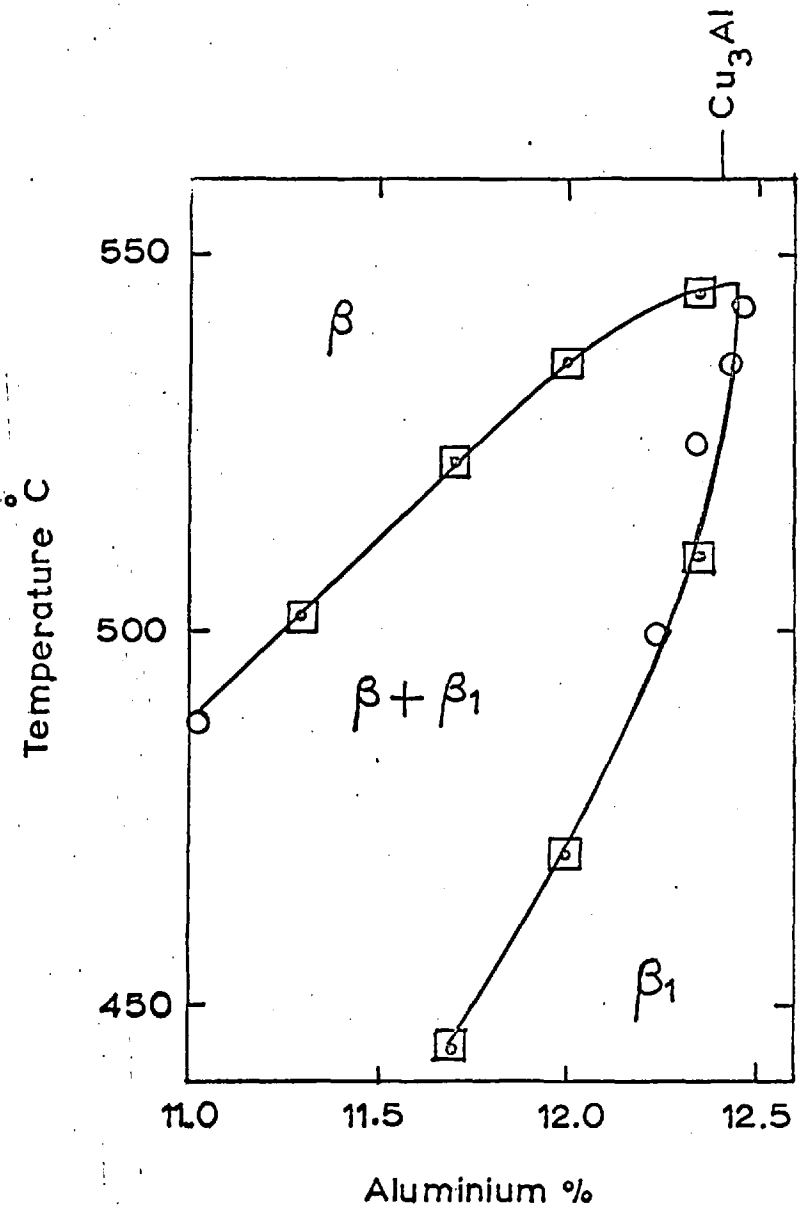

FIG. 2. Metastable Diagram For β And β_1 Phases In Binary Copper-Aluminium Alloys Containing Less Than 12.5% Al.

range between 10.5 wt.% Al and 13.5 wt.% Al.

Philip and Mack[12] studied the effects of ternary elements, silver, cadmium, indium, tin, antimony, beryllium and zinc on the eutectoid transformation in aluminium bronze. They determined the T-T-T diagrams for these alloys between 450°C and 550°C and from the results concluded that the valency of the ternary element affects the transformation kinetics. Also it was found that the eutectoid composition is shifted so as to maintain a roughly constant electron to atom ratio. In general the 'transformation start' and the 'transformation end' of the 'C' curves move away from the temperature axis, with the exception of zinc alloys. The shift in the transformation end curve may be associated with the effect of the growth rate of the pearlite. On this approximate inference they assumed that tin and beryllium decreased the growth rate more markedly than other alloy additions. Additions of any of the ternary elements investigated appeared to favour the formation of a granular pearlite.

Ranzetta and West[8] have reported the growth rates of pearlite in binary eutectoid Cu-Al and ternary Cu-Al-Mn, Cu-Al-Fe and Cu-Al-Co alloys in the range 490°C to 550°C. The variation of growth rate with temperature shows a peak between 530°C and 520°C. The additions of Mn, Fe and Co were found to retard the growth rate by up to a factor of approximately 2.

Calorimetric experiments[13] carried out show that small additions of the ternary elements mentioned above do not affect appreciably the free energy change of the eutectoid transformation, indicating that differences in kinetics cannot be explained on the basis of differences in ΔF, the free energy change.

Haynes[4] has determined the variation of inter-lamellar spacing with temperature in a binary eutectoid alloy. The results are in agreement with the observations made by Klier and Grymko[3] that the interlamellar spacing decreases initially with decrease in temperature but increases with further decrease in temperature.

Relevant Ternary Systems: Cu-Al-Sn System.

The copper-aluminium-tin system has been investigated in some detail by Leach[14] and the results on the copper-rich end of the ternary diagram have been published by Leach and Raynor[15]. The diagrams show that an addition of more than 2 wt.% Sn (1 at % Sn) results in the formation of a ternary phase (Phase T). In Fig.3 an isothermal section at 546°C is shown. It may be observed that only a small amount of tin is permissible if the product of β decomposition is to remain $\alpha + \gamma_2$. Below 540°C the $\alpha + \gamma_2$ field is not expected to show marked change.

The composition of the β phase shifts towards

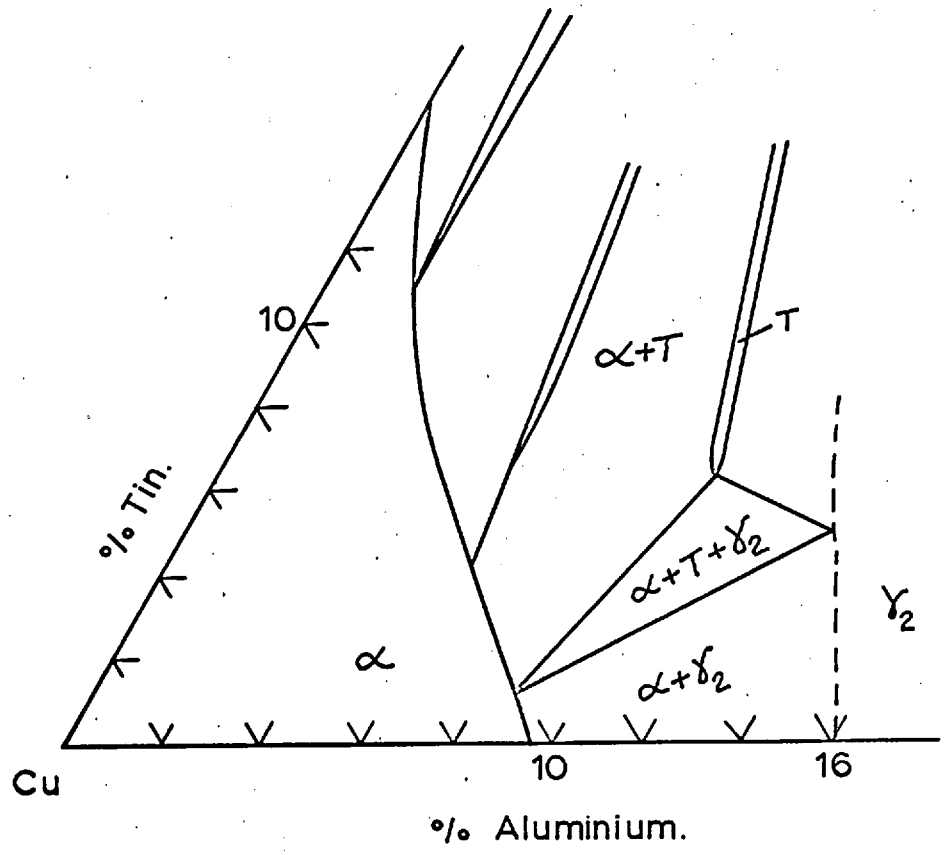

FIG. 3. The Copper-Aluminium-Tin System

546 °C Isothermal Diagram

lower aluminium contents with increasing tin contents. The eutectoid temperature is initially depressed by tin, reaching a minimum value of 548°C at about 3.5 wt.% Sn (1.75 at % Sn).

Cu-Al-Zn System

Isothermal sections of the ternary diagrams published by Bauer and Hansen[16] showed that the α, β and γ_2 phases of the binary Cu-Al and Cu-Zn systems are isomorphous and extend across the ternary diagram, in bands of constant electron - to - atom ratio, as shown in the isothermal sections reproduced in Fig.4. The β phase of the ternary system containing up to about 20 wt.% Zn can give eutectoid products. However, the β phase is stable just below the eutectoid temperature, in a three phase field which diminishes in the temperature scale as the zinc content is decreased. Recent work[17] has shown that at about 5 wt.% Zn the three phase field is sufficiently small to regard the decomposition of the ternary β as identical with that of binary β phase. The eutectoid temperature does not seem to alter noticeably at this concentration.

The Pearlite Reaction in Ferrous Systems.

In contrast to the small amount of quantitative data available on pearlite in the Cu-Al system, considerable material has been gathered in Ferrous systems.

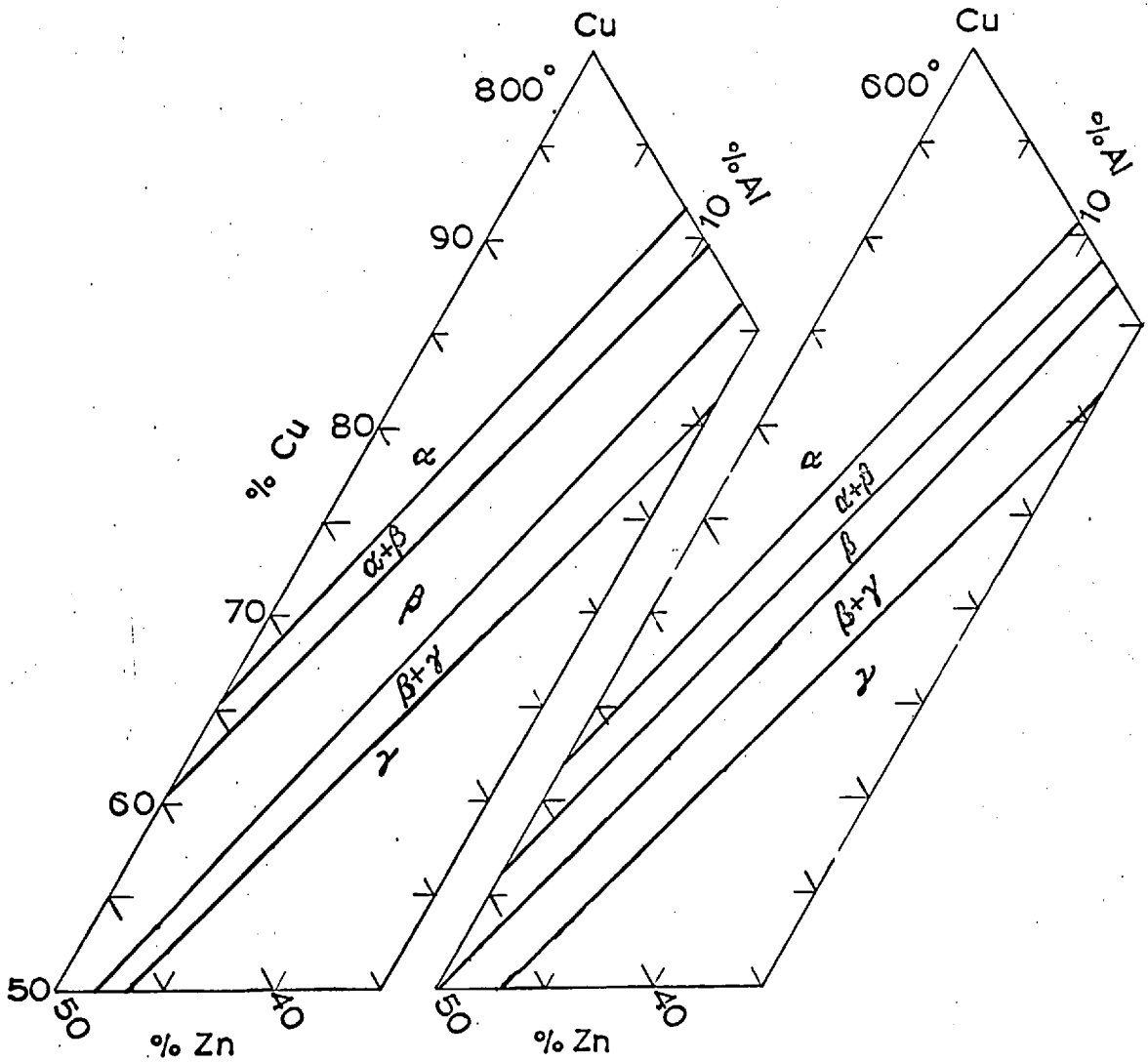

FIG. 4. The Copper-Aluminium-Zinc System;

800°C And 600°C Isothermal Diagrams.

The latter results are summarised in two excellent critical reviews[18,19]. A brief reference to the data on non-ferrous pearlite reactions has also been included in one of the two reviews[19]. Notable contributions made by several investigators and the interest stimulated in this field resulted in an organised symposium on "Decomposition of Austenite by Diffusional Processes" in 1960.

In view of the above mentioned critically assessed reviews it is proposed to give here only an outline of the important contributions to bring out the prevalent ideas of the main schools of thought on the growth mechanism of pearlite transformation.

Hull and Mehl[20] reviewed the subject of the structure of pearlite in 1942 and traced the development of the ideas on the formation of pearlite. The following is a summary of the points discussed:

a) Cementite is found to be the active nucleus in the formation of pearlite.

b) The growth of a colony of pearlite consists of sidewise nucleation and growth and edgewise growth of the ferrite and cementite plates; the edgewise growth contributing a significant proportion of the total transformation.

c) The thickness of the ferrite and cementite plates, i.e. the interlamellar spacing, is determined by the

nucleation rates of ferrite and cementite. Since these rates are increased by supersaturation of the austenite, lowering of the transformation temperature increases the supersaturation and consequently decreases the interlamellar spacing.

d) The spacing obtained by sidewise nucleation and growth is not identical to that obtained during the edgewise growth but it appears to be nearly the same.

e) Curvature in lamellae may be due to volume changes accompanying transformation and also concentration gradients around the colony may cause the lamellae to curve in order to maintain the edges of the lamellae perpendicular to the growing interface.

f) Nucleation of pearlite in steel occurs exclusively at the grain boundaries in the absence of other factors such as inclusions, undissolved carbide particles, etc.

Brandt[21] first published his theoretical analysis on the edgewise growth of pearlite by solving an appropriate diffusion equation assuming certain boundary conditions. Solutions were then compared with the data then available. The results indicated that growth rates calculated and obtained experimentally agreed within an order of magnitude. The lamellar form of pearlite, the curved interfaces between austenite-cementite and austenite-ferrite, the determining factor in pearlite spacing and the causes for increase in growth velocity with increasing

undercooling can all be deduced from purely theoretical arguments.

The solution to the diffusion equation contains terms defined by the carbon concentrations in austenite, ferrite and cementite and by the concentrations at the midpoints of the ferrite-austenite and cementite-austenite interfaces. The last two are estimated for a given reaction temperature from the extrapolated ferrite + austenite/austenite and cementite + austenite/austenite phase boundaries in the metastable region of the equilibrium diagram. The ferrite + austenite/austenite boundary can be extrapolated linearly or along a smooth curve. With the latter type of extrapolation, the terms are altered in favour of better agreement with the experimentally obtained growth rates.

The direct effect of an alloying element is to decrease the "effective" carbon content of the austenite and thus alter the values of the terms in the growth rate equations. The magnitude of the effect on other terms cannot be estimated easily.

Zener[22] reviewed the kinetics of the decomposition of austenite and was able to evolve general principles which govern the transformation, derived directly from fundamental principles.

The growth rate of a new phase into its matrix

phase is calculated on a volume diffusion model. It is assumed that the new phase has a different concentration of the solute from that of the matrix. The ratio of the concentrations on either side of the phase/matrix boundary is given by the equilibrium relations existing between the two phases, provided the interface boundary is stationary and remains plane. If the boundary moves sufficiently fast then the concentrations of the solute in both the phases remain unchanged. On the other hand, if the phase boundary movement is limited primarily by the rate of diffusion of the solute atoms away from or towards the advancing interface then an essentially equilibrium ratio of the concentrations is maintained.

The velocity of the boundary, V_B, is obtained by combining the equations of mass balance and of flux of the solute atoms. It is given by

$$V_B = \frac{\Delta C}{C_2 - C_1} \cdot \frac{D}{L} \quad \ldots\ldots\ldots (1)$$

where

ΔC- is the difference of the concentrations in the parent phase just at the advancing phase boundary and far away from it.

C_2 and C_1 are the concentrations in the matrix and the new phase respectively.

D is the diffusion coefficient of the solute in the matrix.

L is a distance related to some linear dimension of the growing phase.

The shape of the growing phase is deduced from equation (1) in the following way.

If the interface is plane, i.e. the radius of curvature is infinity, r_∞ , then the effective diffusion distance, L, becomes very large and the growth velocity diminishes. If the interface is convex towards the matrix, then L is comparable to the radius of curvature r of the interface. The smaller the radius r the greater is the velocity of growth. However, there is a critical value, r_c, to which the radius of curvature is limited; it is imposed by the change in the equilibrium relation with the change in the radius of curvature of the interface. At this value of r_c the magnitude of ΔC, which drives the diffusion, reduces to zero. The relation between ΔC and r is given by

$$\Delta C = (1 - r_c/r)\, \Delta Co \quad \ldots\ldots\ldots \quad (2)$$

where ΔCo is the equilibrium concentration difference, i.e. when $r = r_\infty$

The optimum value of the radius of curvature will be such as to make the velocity of growth a maximum. The term ΔC is proportional to $(1 - r_c/r)$ and L is proportional to r; the growth will be maximised at a maximum value of $(1 - r_c/r)/r$ which is when $r = 2r_c$.

The driving force ΔC is obviously half the maximum at $r = 2r_c$. Since ΔC is proportional to the undercooling which in turn is proportional to the change in free energy; it is deduced that only half the available free energy is utilized in the irreversible diffusion process while the remaining half is stored as interface energy.

The variation of growth rate with temperature is determined in the following way. The concentration difference, which is the driving force for diffusion, increases directly as the degree of undercooling and the effective diffusion distance is proportional to the critical radius which is inversely proportional to the undercooling. The diffusion coefficient which determines the rate of movement varies exponentially with temperature. Combining all these factors one obtains growth rate as

$$V_B \sim (\Delta T)^2 \; e^{-Q/RT} \quad \ldots\ldots\ldots \quad (3)$$

where: ΔT - degree of undercooling

Q - activation energy for diffusion

R - universal gas constant.

and T - reaction temperature in $^{\circ}K$.

Examination of equation (3) shows that V_B will go through a maximum for a certain value of ΔT.

This approach was extended by Zener to the growth of pearlite in steels. The minimum possible interlamellar spacing S' is computed by pure thermodynamic methods.

Here again, it is deduced that the maximum growth occurs when the interlamellar spacing is twice the minimum S'. By equating the available free energy, i.e. half the total free energy, to that formed as interfacial free energy a relation between the minimum possible interlamellar spacing and undercooling is derived. It is found that the spacing is inversely proportional to the degree of undercooling. From an experimentally observed spacing, which is in fact twice the minimum possible spacing, interfacial free energy is calculated. However, the value of the calculated interfacial free energy exceeds that obtained by other more direct methods by a factor of 2 to 3.

The edgewise growth rate of pearlite is represented by a similar equation such as equation (1), except that the concentration differences are now obtained by the Hultgren extrapolation below the eutectoid temperature and the concentrations C_2 and C_1 represent the concentration of carbon in cementite and ferrite respectively. The magnitude of the diffusion distance, L, is proportional to the interlamellar spacing or

$L \sim S$ i.e. $L = \alpha S$ where α is a numerical coefficient.

The temperature dependence of growth rate is given by

$$V_B \sim (Te - T)^2 . e^{-Q/RT} \quad \ldots\ldots\ldots \quad (4)$$

where Te - eutectoid temperature.

This is the same as equation (3) and shows a growth rate maximum for steels at 630°C for a known value of α. From the known values of C, C_1, C_2, S and V_B, the numerical constant α is estimated. It was expected that the effective diffusion distance would be comparable to the thickness of a cementite plate. The estimated value of α was found to be a third of the expected value.

Zener classifies the alloying elements that affect the decomposition of austenite into two main classes. There are those that retard the formation of both pearlite and bainite by about the same amount and also lower the temperature for the initiation of martensite. Manganese and nickel belong to this category. The others, of which molybdenum is a classic example, retard the formation of pearlite much more than the formation of bainite.

The explanation for the retarding effect of the elements of the second class, is the carbide forming tendency of these elements. The cementite of the pearlite contains a greater percentage of the alloying element than the ferrite and so the segregation that has to be accomplished is dependent upon the diffusion rate of the alloying elements. Since these diffusion rates are very small compared to that of carbon the pearlite formation is retarded.

Fisher[23] has modified Zener's treatment of the

growth rate of pearlite. According to Zener's equation (1) if the velocity of growth is zero then ΔC is zero and hence ΔF, the free energy change will also be zero. The system will be in equilibrium. If the phase transformation occurs at this stage then all the free energy will be retained as interfacial free energy. At the austenite pearlite interface, the interfacial tensions between the three phases must balance and this probably means equal radii of curvature for ferrite and cementite plates or in effect it amounts to equal thickness of the two plates. But the relative widths of cementite and ferrite are in the ratio 1:7 and not 1:1 (approximately) as required by the equilibrium conditions. Evidently this condition will never be achieved and therefore at zero velocity only a fraction of the free energy is transferred to the interfaces while the remainder is lost through irreversible diffusion processes.

Fisher's calculations on interfacial free energy, with the above modifications included, give one fourth the value obtained by Zener and much nearer to the values obtained by other methods.

Following the suggestion of Onsager, Fisher calculated the growth rate of pearlite by assuming the diffusion of carbon through ferrite, contrary to Zener's or Brandt's calculations. The results are somewhat better than those obtained by assuming diffusion through

austenite. Yet these calculations do not account for the growth rates encountered in high purity eutectoid steels.

Hawkes and Mehl[24] studied the effect of cobalt on the nucleation and the growth of pearlite. The rates of nucleation and growth are enhanced by the addition of cobalt in steel. Cobalt was found to decrease the interlamellar spacing through some unknown mechanism. Since growth rate and spacing are reciprocally related, as long as the growth rate increases, an increase in the growth rate is observed. They investigated the effect of cobalt on the diffusion rates of carbon in austenite. The results were inconclusive in establishing a definite increase in the diffusion coefficient of carbon due to the presence of cobalt. Even assuming an enhanced diffusion rate of carbon, they surmise that the magnitude of the effect of cobalt on the pearlite growth cannot be explained satisfactorily on this basis.

Parcel and Mehl[25] investigated the effect of molybdenum and nickel on the rate of nucleation and the rate of growth of pearlite in steels. Both molybdenum and nickel decrease the growth rate and nucleation rate. Interlamellar spacing increases with the decrease in growth rate but while the growth rate is decreased by orders of magnitude, the increase in spacing is only by a factor of two to three. Thus it is inferred that growth rate is not primarily determined by the spacing; but it

was suggested that the alloying elements might affect the diffusion of carbon and hence the growth rate.

Frye, Stansbury and McElroy[26] applied the theory of absolute reaction rate without specifying the precise mechanism by which the pearlite reaction rate is controlled. The following processes have been considered:

1. atom by atom jumps across the interface.
2. formation of groups of appropriate compositions which pass from the initial to the final state.
3. shears of a number of atoms at the interface, and
4. growth by movement of dislocations.

Each of the processes is associated with a characteristic activation energy. The net result of a transformation is the movement of an interface operated with a totalized activation energy. It is determined by substituting the known values of growth rate, free energy change and undercooling in the reaction rate equation. Interlamellar spacing and undercooling are assumed to have a reciprocal relationship to account for the decrease in interlamellar spacing with decreasing reaction temperatures.

Hagel, Pound and Mehl[27] made a calorimetric study of the austenite-pearlite transformation in order to determine the effect of ternary additions on the bulk

free energy change, as expected from Zener's approach. It is found that additions of manganese and molybdenum decrease the magnitude of the free energy change, while cobalt increases it; in terms of Zener's theory this could explain why growth rate decreases or increases.

Kramer, Pound and Mehl[28] extended the calorimetric investigation with an aim to greater calorimetric precision. They determined the free energy of formation and interfacial enthalpy in pearlite of the iron-carbon system and of the copper-aluminium system. Calculations on the interfacial free energy are made by assuming a reasonable value for entropy. From this investigation it is concluded that in the case of Fe-C pearlite only a fourth to an eighth of the total free energy change is stored as interfacial free energy, instead of half as estimated by Zener's theory. The data on the Cu-Al eutectoid alloys were inadequate to make a similar assessment for the interfacial free energy.

Hillert[29] has developed equations for the growth of pearlite from two approaches, one based on dimensional arguments of Zener and the other based on the solution of the differential diffusion equation first solved by Brandt. He finds the results of the two approaches to be identical except for a proportionality constant. The value of the constant is dependent upon the thickness of the ferrite and cementite plates of the pearlite lamellae

and hence upon the original austenite composition. In the case of ferrous pearlite with the cementite and ferrite thickness in the ratio 1:7, the value of the proportionality constant is found to be close to unity as suggested by Zener.

Hillert[29] in an effort to find out more about the critical spacing and the shapes of the pearlite-austenite interfaces, derived more sophisticated equations from the two dimensional differential equation for diffusion and from equations of growth involving thermodynamical quantities. Several interface shapes are obtained for a given growth rate with varying interlamellar spacings.

Aleksandrov and Lyubov[30] have examined the problem of the influence of alloying elements on the kinetics of pearlite transformation. The growth of pearlite is controlled by the rate of the slowest of the processes necessary for the formation of pearlite when partitioning is not taking place. These are the polymorphic change in the iron lattice and the carbon diffusion. If partitioning is occurring then the process of selective diffusion of the alloying element is also involved in the formation of pearlite.

Each of the processes was considered in developing growth rate equations and is claimed to contain no empirical constants to be determined from experimental values of the growth rate.

Results of the calculations based on the polymorphic change of the iron lattice indicate that in binary eutectoid carbon alloys the calculated growth rate values of pearlite are about 100 times higher than the experimental values for pearlite whereas for chromium steel they are much closer.

Equations derived on the basis of carbon diffusion, taking into account the stresses imposed by the transformation, give results which are closer to experimental values in the binary eutectoid but are much higher for chromium steel.

If the diffusion re-distribution of alloying element is limiting the growth of pearlite then the equation for growth can be developed from the appropriate diffusion equation and the mass balance equations. Transformation strains can also be included in such a derivation. Calculations made on chromium steel using such a relation show that the values of growth are several orders of magnitude less than the experimental values. Alloy carbide seems to have formed after the pearlite has formed. However, in molybdenum steels the growth appears to be controlled by this process. It could be that the alloy carbide is formed directly during the decomposition.

The criterion of a particular type of kinetics

predominating is determined by the difference in the activation energy of the $Fe_{\gamma} \rightarrow Fe_{\alpha}$ transformation and the activation energy for the diffusion of carbon in austenite. Change in temperature could also effect a change in the type of kinetics. For un-alloyed steels carbon diffusion seems to control the reaction rate while for chromium steels the re-ordering of the iron lattice is the controlling factor.

In the results on high purity binary alloys the disparity concerning the mechanism of transformation arises if the effect of transformation strains due to phase changes on diffusion ~~are~~ is neglected.

Entin[31] also has considered the decomposition of austenite from the aspect of the kinetics of the polymorphic change of $\gamma \rightarrow \alpha$, and ~~from~~ of the kinetics of formation of carbides. Diffusion of carbon and segregation of alloying element to the carbide control the carbide formation. It has been suggested that the effect of the alloying elements is to alter the rates of polymorphic changes $\gamma \rightarrow \alpha$ and the rates of diffusion of carbon.

The effect of manganese on the growth rate of pearlite was studied by Picklesimer et al[32]. Without proposing any particular mechanism, the investigation was aimed at developing a rate equation relating the growth rate, free energy change, an activation energy for the

growth process and a temperature term. From an assessment of such equations, it is concluded that the growth rate of pearlite is not controlled either by the diffusion of manganese or by the diffusion of carbon. The explanation for the decrease in growth rate is that there is an increase in the activation energy for the interface movement brought about by the presence of manganese.

A critical study on the theory of formation of pearlite has been reported by Hillert[33] and several interesting observations have been recorded. The active nucleus of pearlite could be either ferrite or cementite; it had generally been believed that only cementite acted as an active nucleus. The orientations of ferrite and cementite are such as to avoid forming partially coherent interfaces with the austenite matrix. Sideways growth of pearlite appear to occur not by repeated nucleation but by branching of the lamellae. Evidence for this view was obtained by examining a complete pearlite colony in three dimensions. It is noticed that such a colony is made up of two interwoven crystals, one of ferrite and the other of cementite. Only when a good co-operation between ferrite and cementite is obtained, the growth is lamellar and will be a maximum for the lowest interfacial energy between ferrite and cementite.

Darken and Fisher[34] examined the microstructural

aspects of pearlite and discussed the factors that control the growth rate. They observed by means of electron microscopy a layer of ferrite separating the pearlite and the decomposing austenite. The width of this zone was found to be about a tenth of the pearlite spacing. Substructures in pearlite colonies were attributed to polygonization and recrystallization of austenite induced by strain accompanying the transformation.

Diffusion of carbon has been assumed to be the rate-controlling factor in the growth of pearlite. The effect of alloying additions is to alter the diffusion flux though not the diffusivity of carbon. Interface mobility is considered to have no activation energy of its own. Another important aspect of this approach to the growth problem is that only a part of the total free energy change contributed to the growth, thus implying that changes in total free energy change do not necessarily dominate the growth rate.

Calculations on the growth rate in binary Fe-C alloys were made by assuming local equilibrium and utilizing ferrite diffusion data and the width of the ferrite gap. The results of the calculated values are in agreement with the experimental values. The effect of ternary elements on the growth rate is due to their influence on the activity of carbon. The data on manganese steels provide an interesting example of the

activity effect on growth rate. The calculated and experimental values agree closely.

Regarding the mechanism of pearlite formation it is considered that the deformation of austenite plays a significant part. The carbides of pearlite grow along the stacking faults in austenite. Stacking faults are created due to the shear taking place in austenite ahead of carbide. It is a consequence of the transformation of austenite to ferrite and cementite of different densities and the result of orientation relationships existing between the three phases. This could also explain the lateral growth of a colony. The spacing of pearlite varies with temperature due to the differing coefficients of thermal expansion of the three phases involved in the transformation. With decreasing temperatures the differences in lattice parameters become larger and the spacings between sheared planes become smaller, giving way to finer pearlite. In the light of such a mechanism the unusual effect of cobalt can be explained. Cobalt effectively decreases the spacing thus enhancing the reaction rate. It could be expected to lower the stacking fault energy of austenite, resulting in the ease of dissociating dislocations into partials.

Kirkaldy[35] has discussed the problems of growth of phases on the basis of volume diffusion as the rate controlling criterion with reference to the pearlite

reaction. Hillert's[29] treatment is scrutinised with the following assumptions:

1. The interface shape is very nearly plane.
2. Negligible diffusion occurs behind the interface.
3. The interface is sufficiently mobile so that the chemical reaction does not interfere in the kinetics.
4. Equilibrium segregation takes place.
5. The width of each phase is known.

The growth rate equation obtained by Hillert is substantially the same as that derived by Zener. There is a certain degree of freedom in the spacing which disallows a unique value of growth rate. Since each growth rate is associated with a particular spacing the optimising principle for a unique growth rate equation must be known. Zener argues that the system chooses the maximum rate and the spacing observed is twice that of the critical. Kirkaldy suggests that the rate of growth would be such that the transformation from austenite to pearlite attains a minimum rate of entropy production.

The effect of manganese on the growth of pearlite has been calculated by Kirkaldy[36] on a volume diffusion model. The growth of either ferrite or cementite is considered in eutectoid reactions in ternary alloys containing 1% and 2% manganese. Since the diffusion

coefficient of manganese is extremely small compared to that of carbon, the reaction product and the matrix contain the same amount of manganese. It enables one to estimate the carbon diffusion potential from the ternary diagram by specifying a tie line. Manganese is found to reduce the carbon gradient and hence the interface advance. The diffusion of carbon under a gradient of manganese is neglected. If this is also considered then a further reduction in carbon potential difference occurs, since manganese decreases the activity of carbon in γ-iron. It is therefore possible to predict, at least qualitatively, the influence of manganese on the growth of pearlite purely on constitutional and diffusion considerations.

Cahn and Hagel[19] presented a critical survey of the formation and kinetics of the pearlite reaction and reviewed the quantitative aspects of the reactions on high purity ternary alloys of iron.

Growth rate, determined by the time derivative of the largest nodule measured in isothermally transformed specimens, is some kind of a maximum growth rate. It is doubtful whether such a method is applicable if the growth rate of each nodule is not the same and/or the growth is not independent of time. There is some evidence to show that the growth of pearlite nucleated at the surface of the sample is different from that

nucleated at a grain boundary. It is difficult to explain the positive time intercept of the straight line relating time versus nodule radius. The so called 'incubation period' is larger for smaller growth rates and vice versa. It is possible that this period is related to a transient growth.

The relation between interlamellar spacing and undercooling cannot be rigorously verified since there is a considerable scatter in the experimental points and in some cases the reference temperature, from which undercooling is derived, is not known. In such a case plotting reciprocal spacing against temperature eliminates the uncertainty about the reference temperature. This relation should also be linear.

Austenite-pearlite interfaces of various shapes have been observed to exist in Fe-C-Cr alloys and a ferrite gap was noted in some instances. The gap could be due to insufficient rate of quenching.

The data available, on selective diffusion or partitioning of alloying elements into carbide or ferrite, is not complete due to the lack of important parameters such as interlamellar spacing and growth rate being reported simultaneously. This prohibits a complete understanding of this aspect of the pearlite reaction. Partitioning can occur at high temperatures but need not

occur at lower temperatures. The slow growth rate of alloy steels could be associated with the slow diffusion of alloying elements compared with that of carbon. Alloying elements seem to have little effect on carbon diffusivity. On the other hand, carbon appears to lower the activation energy for self diffusion of iron, whereas nickel, manganese and chromium may increase it. Plastic deformation (of austenite) seems to have a great effect on diffusion (of carbon) but this has not been fully investigated.

Maximum deviations from equilibrium concentrations have been worked out. If the equilibrium partitioning coefficient, defined by the ratio of the concentration of the alloying element in carbide to the concentration in ferrite at equilibrium, is less than unity then the alloying element segregates to ferrite. If it is greater than unity then the alloying element diffuses to the carbide.

Composition differences in the matrix at the interface can be estimated in binary systems by simple extrapolation of the phase boundaries provided the interface is plane; if the interface is curved then the estimation is changed. The extrapolation is not quite as simple in a ternary system and methods have been suggested to obtain approximate but meaningful data.

Cahn and Hagel[19] have evolved a different approach to the analysis of the growth problem with a knowledge of the growth rate, interlamellar spacing, diffusion coefficients and equilibrium relations.

In the solution of the diffusion equation applicable to the edgewise growth of pearlite, there are terms which indicate the thickness of enriched (or depleted) zone ahead of pearlite and also sideways fluxes that contribute to the segregation of carbon and alloying elements. The sideways fluxes are confined to a certain thickness in the austenite and are given by a parameter α_i

$$\alpha_i = \frac{GS}{2\pi D_i} \quad \ldots\ldots\ldots\ldots (5)$$

where

G - growth rate of pearlite

S - intermellar spacing

D_i - diffusion of the ith component whose enrichment or depletion is occurring

It is also related to the ratio of concentration differences as given under:

$$\alpha i = \frac{C^i_{af} - C^i_{ac}}{C^i_c - C^i_f} \quad \ldots\ldots\ldots (6)$$

where

C^i_{af} - Concentration of the ith component in austenite just ahead of centre of ferrite.

C^i_{ac} - Concentration of the ith component in austenite just ahead of centre of cementite.

C^i_c - Concentration of the ith component in cementite.

C^i_f - Concentration of the ith component in ferrite.

From these two relations, equations (5) and (6), the apparent diffusion of the species is calculated. If the apparent and experimental values of diffusion coefficients are the same then the growth is controlled by volume diffusion in the austenite. A smaller apparent diffusivity indicates that the reaction is not controlled by any diffusional process; a larger value implies that a shorter path for diffusion is operative. Application of this analysis to high purity eutectoid steels has shown that a short circuit in diffusion is most likely. It might be thought that the short circuiting may be through the ferrite since diffusion in ferrite is one hundred times faster than in austenite. However, there are other factors which rule out such a possibility.

In alloy steels, the estimation of the parameter a_i and the values of the diffusivities of the alloying elements are not accurate enough to deduce conclusively whether volume diffusion of the alloying element is the rate controlling process. There is some possibility that

a short path for diffusion, such as interface diffusion, may be controlling the growth.

At temperatures where partitioning does not occur, analysis by the above method suggests that a process other than diffusion is controlling the reaction rate. Probably the interface mobility is greatly affected and the growth is very much smaller. Since the growth is retarded, a little partitioning takes place where it need not.

This critical study on the theory of pearlite growth by Cahn and Hagel has led them to conclude that the solutions to the diffusion equations always involve a product of the growth rate and either spacing or its square. There is a need for some physical principle giving an expression relating growth rate and or spacing. The suggested extremizing principles such as 'maximising growth rate', 'minimum rate of entropy production' or the 'maximum rate of free energy decrease' have been supported only by plausible arguments rather than by any governing fundamental physical principle.

The variation of interlamellar spacing with temperature, and the effect of ternary alloying elements on the growth rates at temperatures where there is no partitioning of the alloying elements, or the effect of ternary elements on interlamellar spacing, cannot be

explained on the basis of a diffusion model alone. It is very likely that the growth is determined by a complex process involving diffusion and interface mobility.

CHAPTER III.

PREPARATION OF THE ALLOYS.

Binary eutectoid alloys demand an accurate control of the composition if pro-eutectoid constituents are to be avoided. It was noticed in initial experiments that electrolytic copper used in the preparation of the alloys tended to spurt during melting under vacuum and the losses occurring could not be controlled. It was therefore decided to melt copper first and obtain it as a consolidated ingot, prior to weighing out requisite quantities for alloy preparations. This method enabled alloys of precise compositions to be obtained without any difficulty.

All the alloys were made in an Edwards High Vacuum high frequency induction furnace. The zinc additions to prepare ternary zinc alloys were made to the appropriate binary alloys under an atmosphere of argon.

The graphite crucible used in the preparation of the alloys could hold about 2 kilograms of the alloy. Copper, obtained from melting electrolytic copper, was placed in the crucible and a weighed quantity of super-purity aluminium was placed above it in the crucible. After obtaining a vacuum of 0.5 to 0.8 microns mercury, the high frequency heating unit was switched on. Heating was done slowly until all the metal was molten and thoroughly mixed by the turbulence. Although a higher

current at this stage could hasten the mixing it was found that copper could be lost due to the high vacuum and excessive temperature.

The alloy was allowed to cool in the crucible while a refractory brick covered the top to reduce piping. Losses in making these alloys were less than 0.25% of the total metal used in preparing the alloys.

The compositions of all the alloys prepared for the investigation are indicated in Table I.

Ternary tin alloys were prepared in the same way as the binary eutectoid alloys except that the aluminium content was reduced appropriately to obtain compositions on the cutectoid line. Weighed quantity of pure tin (purity 99.95%) was placed along with copper and aluminium. The vapour pressure of tin is too small to expect any loss due to vaporization. In this ternary system a small variation in composition from the eutectoid produced a pro-eutectoid phase after isothermal treatments at 565°C. With the modified melting practice it was possible to achieve required compositions.

Ternary zinc alloys were also aimed at eutectoid compositions just as in the case of ternary tin alloys. However, zinc additions had to be made outside the vacuum furnace. First, the requisite quantities of copper-aluminium alloys were prepared in the high vacuum

Alloy	Nominal Compositions						
	Atomic Percent		Weight Percent		Chemical Analysis		
	Al		Al		Al	Cu	
Binary Eutectoid	24		11.8	-	11.90	88.14	
Binary 12.4	25		12.4	-	12.40	87.56	
	Al	Zn	Al	Zn	Al	Cu	Zn
Ternary Zinc	23.7	0.5	11.6	0.6	11.68	87.79	0.54
Alloys	23.5	1.0	11.5	1.2	11.56	87.28	1.20
	23.3	1.5	11.4	1.8	11.45	86.84	1.76
	23.1	2.0	11.3	2.4	11.33	86.45	2.25
	Al	Sn	Al	Sn	Al	Cu	Sn
Ternary Tin	24	0.1	11.7	0.2	11.81	88.07	0.094
Alloys	23.6	0.25	11.5	0.5	11.55	87.88	0.53
	23.2	0.5	11.3	1.1	11.30	87.55	1.09
	22.4	1.0	10.8	2.1		-	
	21.7	1.5	10.4	3.2	10.37	86.48	3.15
	20.8	2.0	9.8	4.2		-	

Table I

Compositions of the alloys

* In the thesis the compositions refer to the nominal compositions indicated here.

furnace. These alloys were then melted in a graphite crucible with a lid which allowed maintenance of an inert atmosphere of argon and also charging of high purity (purity 99.99%) zinc, with very little loss due to volatilization. Once the zinc dissolved in the molten alloy the stirring action of the high frequency current ensured homogeneity.

No attempt was made in any case to cast the alloy into a mould. The alloys were allowed to solidify in the crucible with a refractory brick covering the top to prevent unusually large pipe formation.

The compositions of the alloys were checked by metallographic means after giving a homogenising anneal at 900°C for 4 hours. The procedure of checking the compositions was as follows:

A small piece, cut out of the homogenised ingot, was heated to 850°C and soaked for 40 minutes and then quenched in a salt bath at 567°C for 24 hours, followed by quenching in cold water. The specimen was then sectioned and prepared for a metallographic examination in the usual way. If any pro-eutectoid α or γ_2 was found then it was estimated by a point counting method. Suitable quantities of either aluminium or copper were then added to make the alloy of requisite composition. Such a procedure was found unnecessary since the

compositions aimed at were obtained without difficulty. In the case of the 2 at % zinc alloy this showed a slight amount of γ_2 but was considered suitable for growth rate experiments without attempting to correct for the pro-eutectoid γ_2. Instead of adjusting the composition another small ingot of 2 at % zinc alloy was made by adding the appropriate amount of zinc to a vacuum melted binary copper-aluminium alloy in a gas fired furnace. There was no pre-eutectoid phase in this alloy and it was used for growth rate experiments in conjunction with the argon melted alloy.

The 12.4 wt.% aluminium alloy was prepared in the same was as the binary eutectoid by melting together requisite quantities of superpurity aluminium and consolidated electrolytic copper. The alloy ingot was homogenised as usual and a test sample, for composition check by quantitative metallography, was isothermally heat treated at 567°C for 24 hours. The quantity of pro-eutectoid γ_2 precipitated was estimated by the point count analysis and checked with the calculated values obtained from the published equilibrium diagram[9].

CHAPTER IV.

THE GROWTH RATE OF PEARLITE.

i) Introduction.

It is useful to examine the mode of growth of pearlite before attempting to describe the methods of determining the growth rate.

Lamellar pearlite consists of alternate plates of two phases, parallel or nearly parallel, in small regions known as colonies. Several colonies constitute a pearlite nodule. A single colony can grow in space by 'edgewise' and 'sidewise' growth. Whether the 'sidewise' growth occurs by repeated nucleation[18,20] or by some mechanism of branching[33] it is observed[25] that both the growth rates are very nearly the same. In practice, however, transformation takes place by the growth of the pearlite nodules and unless all the plates are normal to the interface between pearlite and the matrix, the growth of a pearlite nodule is an over all process of edgewise and sidewise growth. It has been suggested that the growth of a nodule is determined by those colonies in which the pearlite plates are normal to the interface while in others of different orientation the growth lags behind.

In the present investigation, the growth rate of the pearlite nodule is determined; that is, the rate at

which the radius of a nodule increases with time without impingement by other nodules or grain boundaries. Since the nodules are approximately hemispherical in shape, the growth rate implies the radial growth of a pearlite nodule.

There are at least three methods of measuring the growth rate of pearlite, all of them depend to some extent on the statistical methods of analysis. A brief description of each method is given below.

Method 1[37]:

Specimens are transformed for various times, t_1, t_2, t_3 ..... and a statistical distribution of various sizes, of nodules observed on a random section of the samples, is made. It is usual to count the number of nodules within a small range of diameters. The smaller the interval and the larger the number of intervals, the better is the profile of the distribution curve. From such data curves are drawn relating the number of nodules, of diameters greater than a certain value of diameter, d, to the diameter 'd'. This plot is repeated for various fixed time treatments. The incubation period is not included in the time period. A schematic graph is shown in Fig.5a. Now for any given number, the intercepts on the above sets of curves give various diameters for the corresponding times. Plotting the diameters against times gives a straight line, the

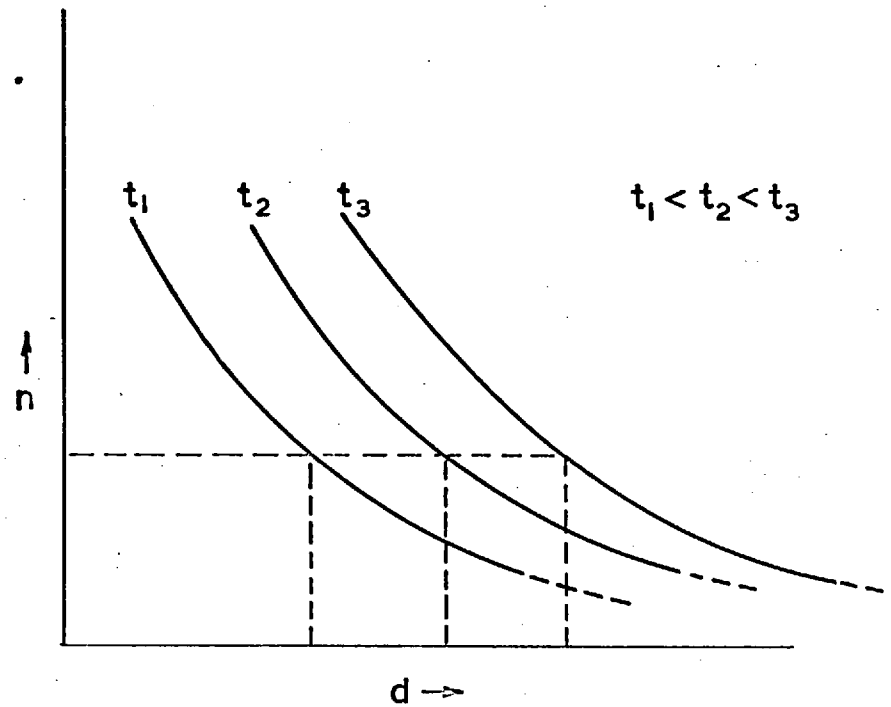

(a)

FIG 5(a) Schematic Diagram Relating The Number Of Nodules Of Diameter>d And The Diameter d.

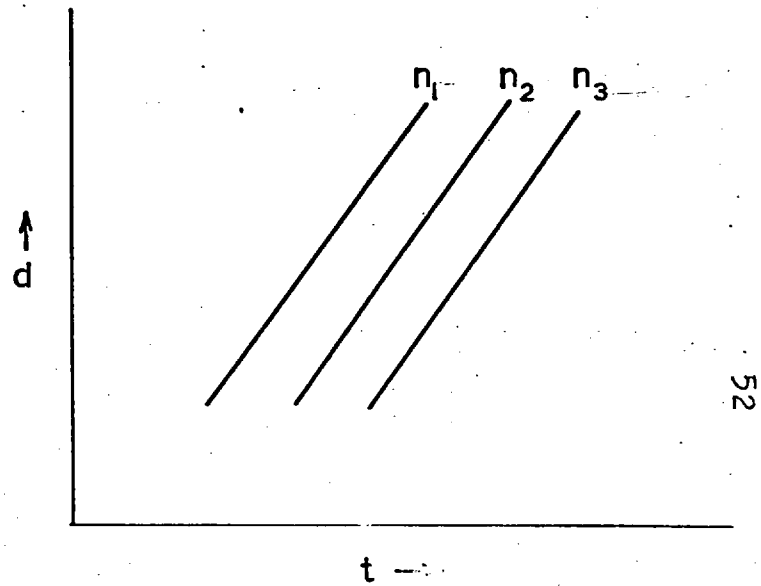

(b)

FIG 5(b) Schematic Diagram Relating The Diameter And Time.

slope of which gives twice the rate of growth. The schematic graph in Fig.5b shows the method. One can choose different numbers and obtain corresponding growth rates. If the growth rate is independent of time and the number chosen is large enough to preclude new nodules appearing then the slopes of diameter vs time linear graphs for various numbers give a constant slope. It is to be noted that the diameters mentioned refer to the spherical nodules in space and are obtained from the planar distribution data by the statistical method given by Scheil[38]. This method is obviously lengthy but it gives an average growth rate of all nodules. If there is a significant difference in the growth rates of each nodule then this method could give an indication. It has also the advantage of obtaining nucleation rates from the same data.

Method 2.

Spektor[39] has developed a method for the "determination of linear rate of transformations in solid metals", such as, for example, the rate of growth or the rate of dissolution of a phase in a matrix phase. The shape and size of the phase is immaterial; impingement and formation of aggregates do not offer any difficulty in using this method. It is assumed that all points on the interface boundary of the growing (or dissolving) phase are displaced equal distances in the direction

normal to the interface. As the method is quite general its application can be extended to the determination of the pearlite growth rate.

If the volume v of a nodule of interface area s (interface refers to pearlite/matrix and not to the interface between lamellae) increases due to the displacement, dr, of the interface then the change in volume is given, to a good approximation, by

$$dv = s\,dr \quad \ldots\ldots\ldots\ldots \quad (7)$$

The rate of change of volume is then

$$\frac{dv}{dt} = s\frac{dr}{dt} \quad \ldots\ldots\ldots\ldots \quad (8)$$

If the rate of growth $\frac{dr}{dt}$ is constant for all the nodules then the rate of change in volume of all the nodules in a unit volume of matrix will be

$$\frac{dV}{dt} = S.G \quad \ldots\ldots\ldots\ldots \quad (9)$$

where

V - volume of the nodules in a unit volume of the matrix

S - total interface boundary area in the unit volume of the matrix

G - growth rate of the nodules.

$\frac{dV}{dt}$ is the rate of change of volume transformed or the rate of change of the fraction transformed $\frac{df(t)}{dt}$.

Thus growth rate

$$G = \frac{1}{S} \cdot \frac{df(t)}{dt} \quad \ldots\ldots\ldots\ldots \quad (10)$$

The interface boundary area per unit volume, S, can be determined by the method of secants in space fully described by Saltykov[40]. It is important to note that the interface/area between two nodules of pearlite already boundary area does not include the interface impinged, but only that which divides the transforming matrix and the pearlite. The rate of change of the fraction volume transformed can be determined by the graphical differentiation of the well known kinetic curve relating the fraction transformed versus time. In the absence of such a curve it can be found by the change in volume of the pearlite over a short interval of time. The fractional volume can best be measured by the point count method.

Method 3.

This is the method that is very commonly used for the determination of the growth rate of pearlite. It is based upon the probability of finding the largest nodule in a random section in a specimen transformed isothermally for various times. It is assumed that the largest nodule is sectioned along its diameter. The nodules are assumed to be spherical (or hemispherical if nucleated along a grain boundary or specimen surface), and grow radially at a constant velocity, and the rate is time invariant. It

is necessary to allow the nodules to grow freely without impingement. The rate of change of radii of the nodules is the growth rate.

In the present investigation this last method is used and is discussed in its essential details.

ii) Experimental.

Experimental determination of the growth rate is made by observing the largest pearlite nodule in a series of samples isothermally treated for different times and obtaining the time derivative of the nodule radius. The assumption made in such a determination is that nucleation in every specimen occurred simultaneously and that the largest nodule seen is the one that nucleated first. In the aluminium bronze alloys studied in this investigation, pearlite nucleated entirely on the surfaces of the sample at higher temperatures but at lower temperatures, however, grain boundaries and minor impurities like inclusions contributed equally to the nucleation process. An earlier investigation[7] had shown that measurements on grain boundary pearlite gave rather indifferent and inconsistent results and so growth rates mentioned here refer to pearlite growth from the specimen surfaces. The advantage of surface-nucleated pearlite in growth rate determinations is that the plane of section can always be maintained normal to the plane of nucleation,

thus eliminating the doubt about the largest nodule being sectioned through its diameter.

Nucleation in these alloys was found to be sensitive to surface conditions, the rougher the surface the easier was it for nucleation to occur. In order to obtain identical conditions, on each surface all the samples were ground on a coarse 240 grit carborundum paper prior to an isothermal treatment.

The probability of finding the largest nodule in a sample varies directly as the area of the section. So a large specimen is desirable. The size suitable for experimental purposes, with some other practical considerations, was found to be approximately 3/8" cube. Usually six samples were treated simultaneously for the growth rate plot. The treatment times were chosen such as to obtain the nodules growing, as far as possible, freely without interacting with one another.

Isothermal Treatment:

Isothermal heat treatments, employed in the determination of growth rate measurements, were carried out in a salt bath consisting of equal parts of potassium nitrate and sodium nitrite mixture. The container of the salt mixtures was a stainless steel tube 4" in diameter and 12" in height. The tube was closed at one end and had a wide flange at the other. The salt level was

maintained at about 1" below the flange level. The stainless steel container slid into a vertical tubular furnace constructed from a silica tube 4½" in diameter and 12" in height. The silica tube was wound with 18 gauge nichrome wire in such a way as to obtain a maximum zone length of constant temperature. The temperature of the furnace was controlled by a Kelvin-Hughes proportional controller actuated by a chromel-alumel thermocouple placed alongside the furnace windings. Two resistors, one across the controller and another in series with the furnace, enabled the temperature to be controlled without much fluctuation. After calibrating the furnace and noting the constant zone in the stainless steel container, a steel wire gauze was placed at the centre of the constant zone. The variation of temperature across the diameter was too small to detect using a thermocouple and a portable potentiometer. The variation throughout the constant zone was less than 2°C. With this size of the salt bath the mass of six samples (at 850°C) did not alter the bath temperature to any measurable extent.

The temperature of the bath was measured by a calibrated Pt - Pt.Rh (13% Rh) couple before and soon after the heat treatment. The variation was well within ± 2°C. In certain experiments to be discussed later, the thermocouple was kept in the bath throughout the heat treatment and for these experiments the power was supplied

through a variable transformer to control the temperature to within $\pm$ ½°C.

A small tubular furnace, which could be swung away from the salt bath, was used for heating up the samples to the β phase. A soaking temperature of 850°C for 40 minutes was selected; variations of up to 50°C were found to have no observable effect on the kinetics of the reaction studied. A set of six samples tied individually to stiff nichrome wires were treated simultaneously in the soaking furnace.

The heat treated samples were quenched in cold water at predetermined intervals of time. The specimens were then sectioned by a carborundum disc in a steel jig to obtain a section normal to the surfaces which had been prepared to the same degree of roughness. The two halves of a sample were mounted in a single bakelite mount and numbered for recording purposes.

The mounted samples were prepared for metallographic examination and measurements in the conventional way. The specimens were cleaned and dried prior to electrolytic etching in a 1% chromic acid solution in water. About 6 volts was applied for 8 - 12 seconds to obtain a satisfactory etch. Pearlite was preferentially delineated leaving the untransformed matrix lightly etched. Longer time etching was effective in showing

β_1 when present in small quantities.

Nodule size was measured by a calibrated optical micrometer using a fixed magnification. The largest single nodule measured on eight sides of the sample was used in plotting nodule radius versus time graphs.

iii) Results and Discussion:

Fig.6a shows an example of a largest hemispherical nodule growing from the surface of the sample.

Fig.6b shows typical graphs of the maximum nodule radius measured against the time during which the specimens were allowed to transform at 530°C. The slopes of these straight lines give the growth rates of the pearlite nodules in the alloys mentioned on the graph. Of the 70 or so graphs of this type, almost all of them showed a good linear relationship, indicating a steady state process of growth, independent of time. It was noticed at higher temperatures of transformation that the prepared specimen surface was less favourable for nucleation and the points on the graphs showed a slight tendency to scatter. It was considered not necessary to apply any statistical method for the best fit of the points.

From the slopes of these graphs obtained at several temperatures, the growth rate versus temperature curves were obtained.

FIG.6(a) Photo - Micrograph showing an approximately hemispherical nodule of pearlite growing from the surface of the specimen. x 80

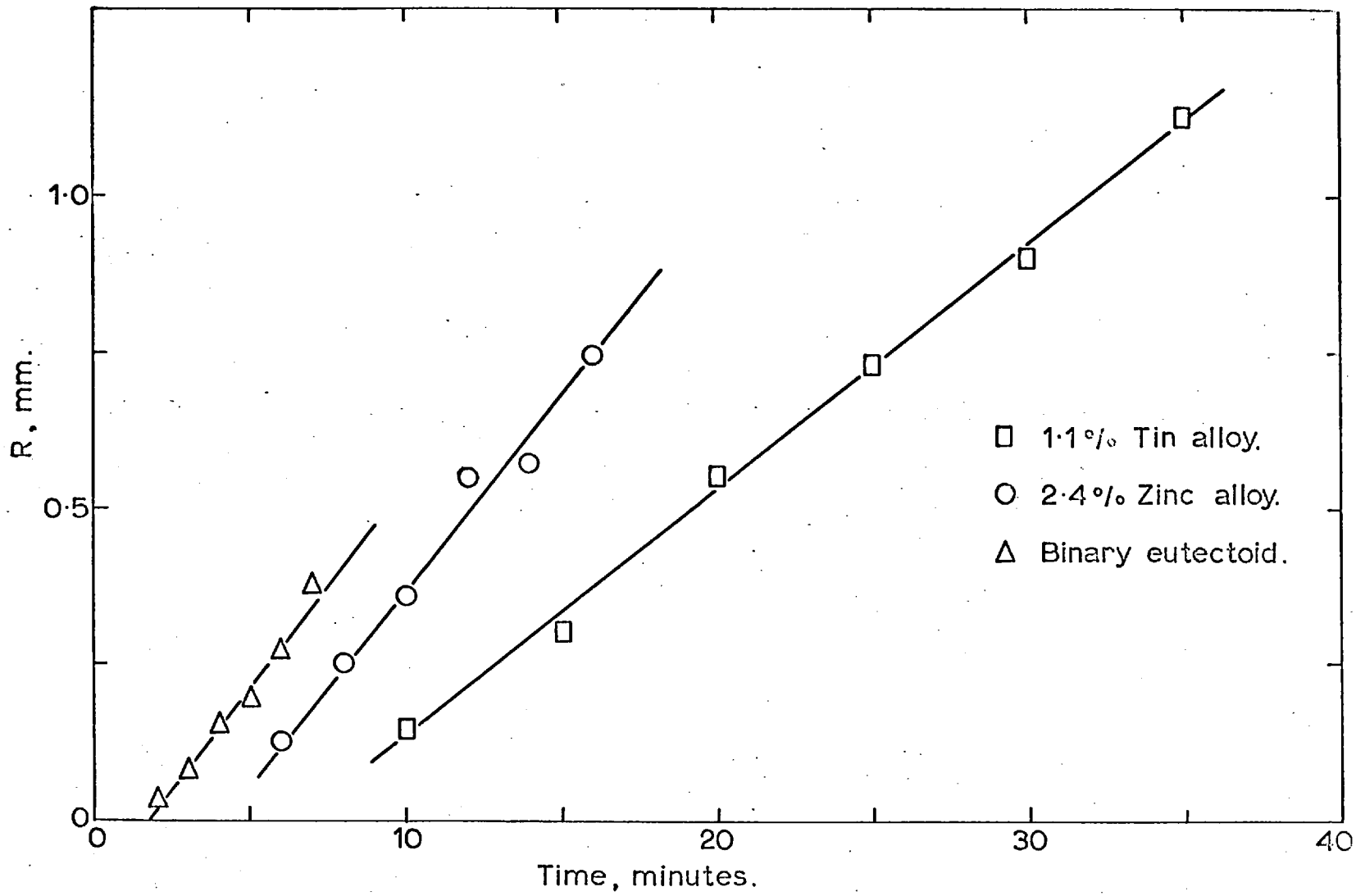

FIG 6(b) Maximum Nodule Radius(R) Vs Transformation Time At 530 °C.

The results of the two binary alloys, namely the 11.8% Al eutectoid and the 12.4% Al alloy, are shown in Figs. 7 and 8. The data on a binary eutectoid alloy obtained by Ranzetta[7,8] are also plotted in Fig.7. It may be observed that both the results are in close agreement except at temperatures below 510°C, where a slight deviation seems to occur between the two sets. This could be due to the difficulty of measurements brought about by the excessive precipitation of the α phase. It is difficult to assign an overall accuracy of growth rates as the accuracy seems to vary from temperature to temperature, but the comparison shown above gives an indication of the reproducibility of these curves.

Fig.9 is presented to show the positions of the two growth rate temperature curves obtained from the eutectoid 11.8% Al alloy and the 12.4% Al binary alloy.

The results of the three tin alloys and three zinc alloys are shown in Fig.10 and Fig.11 respectively. The data obtained from the 1.8% zinc alloy were omitted in Fig.11 for the sake of clarity. The curve for this alloy lies between the curves of the 1.2% and 2.4% zinc alloys. The 2.4% zinc alloy curve is drawn from the data of argon-melted and air-melted alloys.

In all the alloys, except the 12.4% Al alloy, the growth rate measurements were discontinued when the

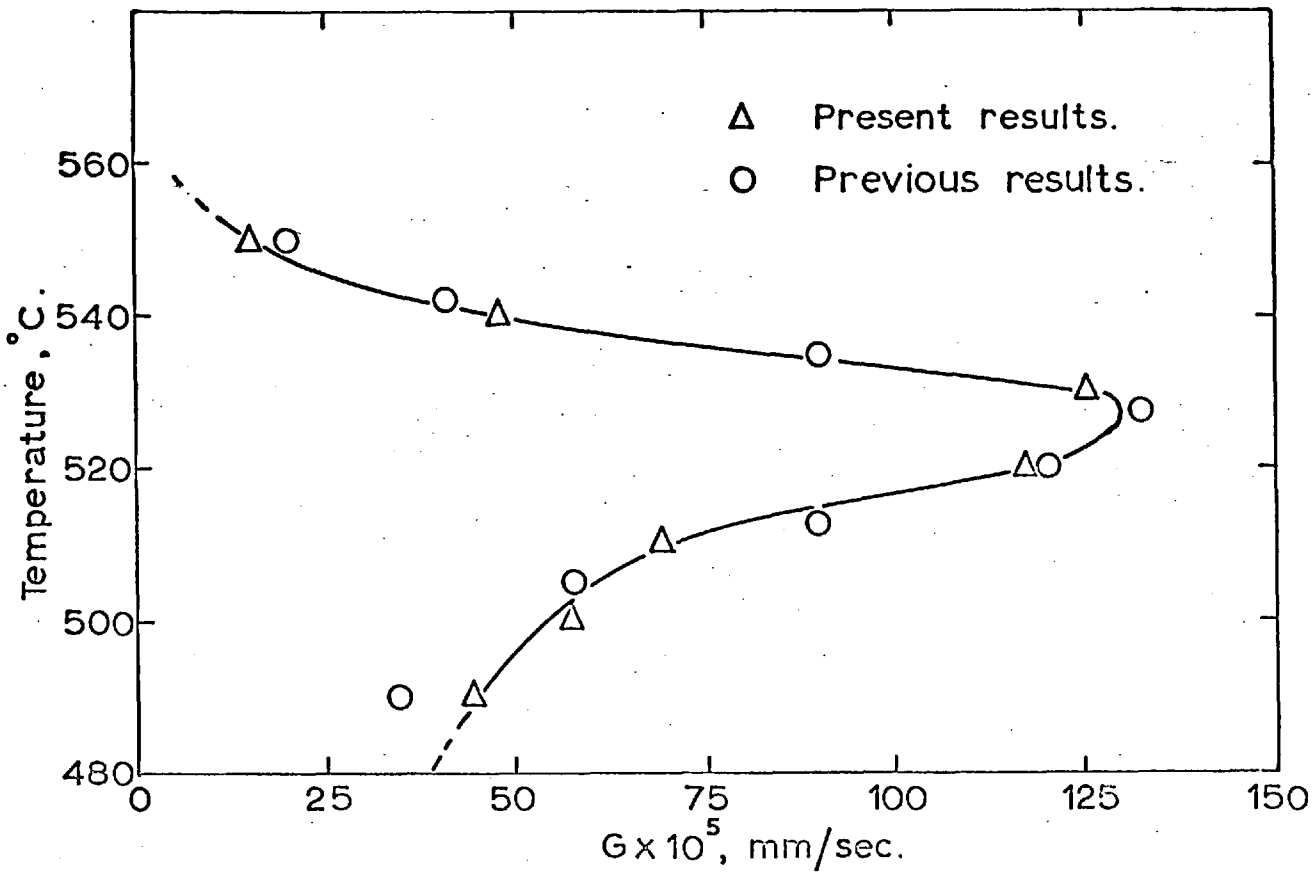

FIG. 7. Pearlite Growth Rate Vs Temperature For The Binary Eutectoid Alloy.

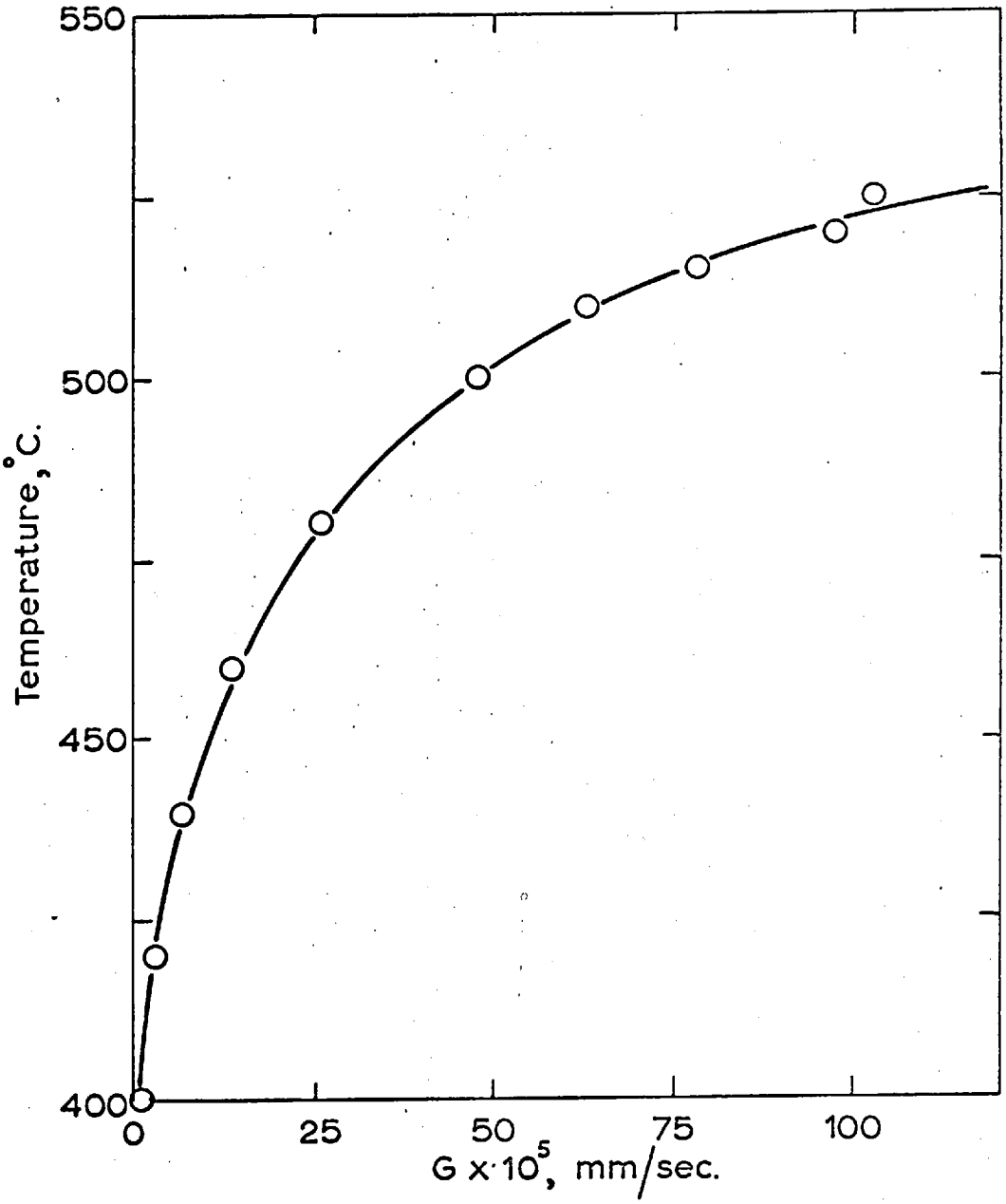

FIG. 8. Pearlite Growth Rate Vs Temperature For The Binary 12·4% Aluminium Alloy.

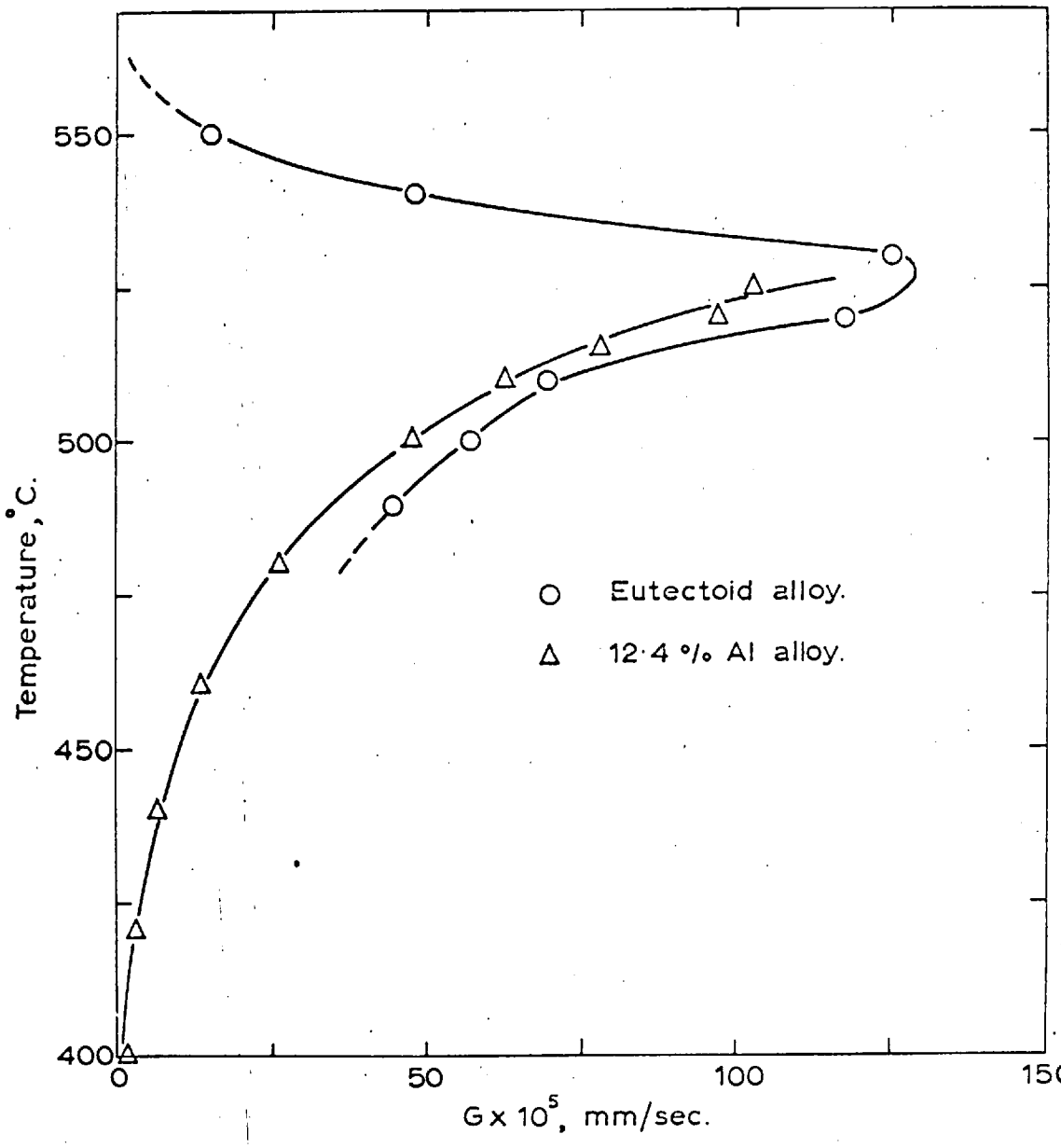

FIG. 9. Pearlite Growth Rate Vs Temperature

(Combined Figures 7 And 8)

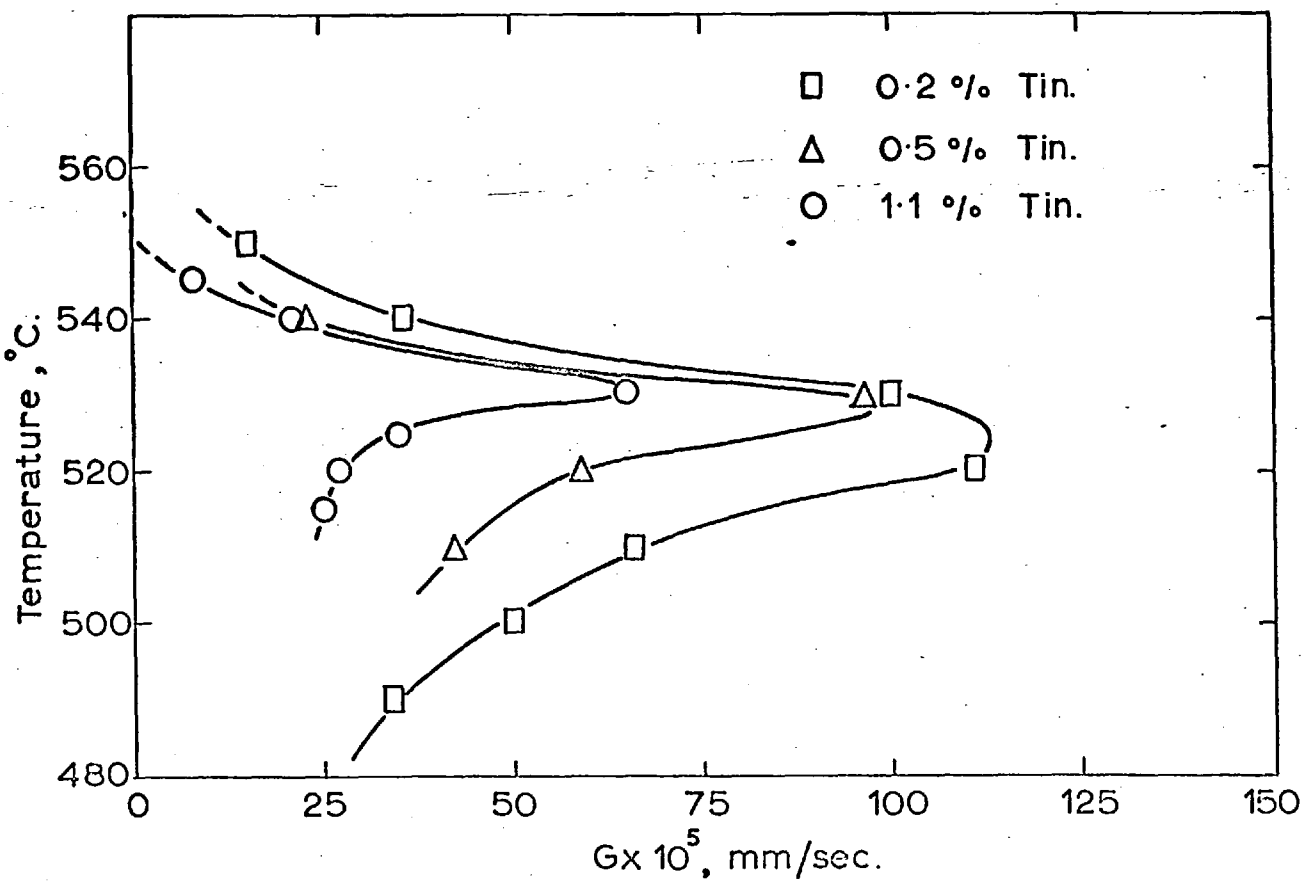

FIG. 10. Pearlite Growth Rate Vs Temperature In The Tin Alloys.

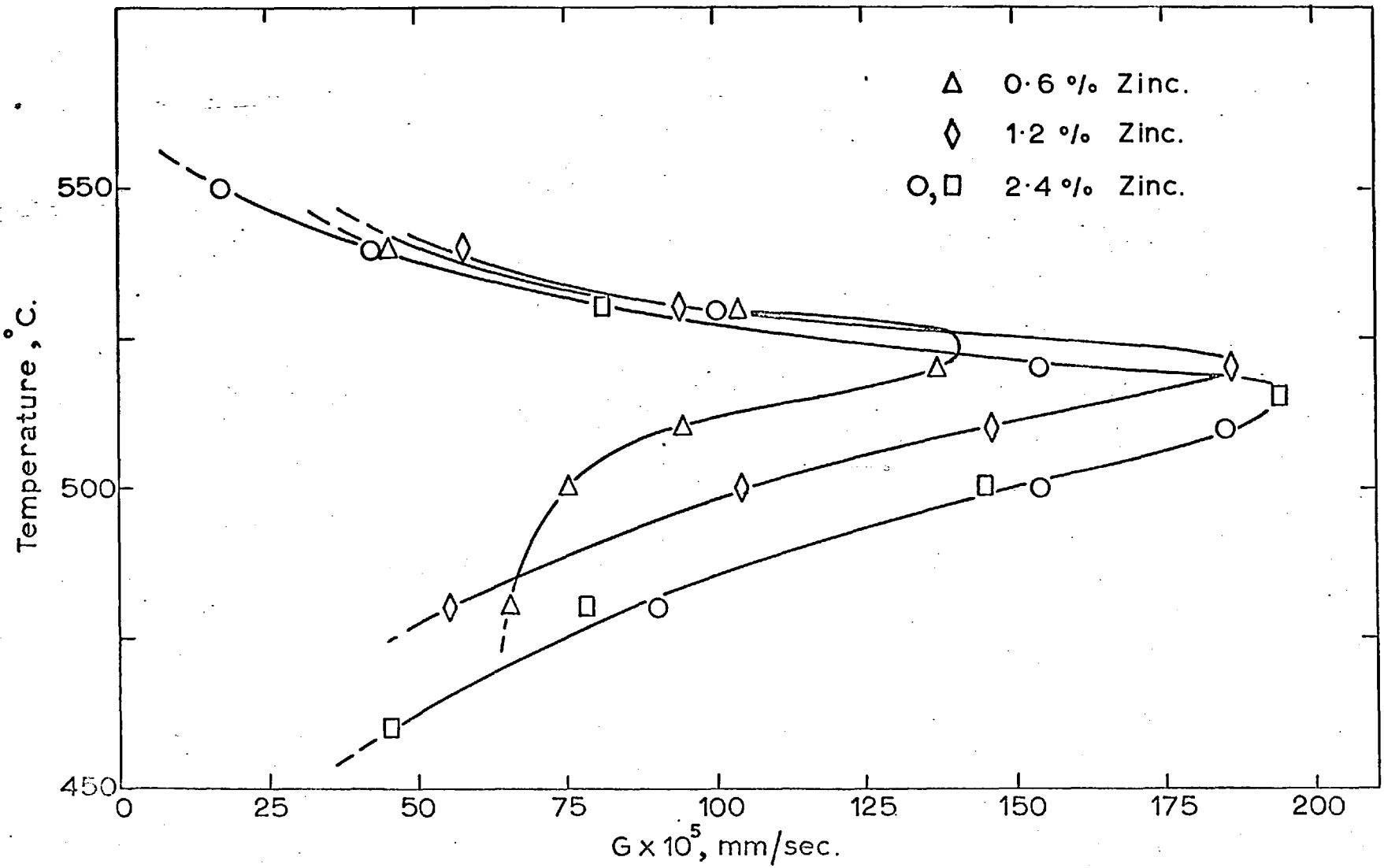

FIG. 11. Pearlite Growth Rate Vs Temperature In The Zinc Alloys.

precipitation of α, due to the formation of β_1, became excessive and the measurement of the nodule size quite difficult. In the 12.4% Al alloy above 500°C the precipitation of γ_2 increases as the temperature is raised. The γ_2 phase formation is accompanied by the formation of β around it, which in turn decomposes to give $\alpha + \gamma_2$. Measurements of the $\beta_1 \rightarrow \alpha + \gamma_2$ pearlite growth rate become prohibitive above about 525°C.

Growth rate measurements in ternary tin alloys were restricted to the 0.2, 0.5 and 1.1% Sn alloys only. In higher tin content alloys the decomposition product was rarely lamellar and did not consist entirely of $\alpha + \gamma_2$. The ternary intermediate phase T appeared and was found to be always in contact with the γ_2 phase (See Fig.12). The growth rate of the pearlite with the T phase was found to be 3.3×10^{-5} mm/sec at 540°C in an alloy containing 2.2% Sn. At higher temperatures the growth rate would be lesser still and at lower temperatures the quantity of T phase would increase. Thus it was apparent that the maximum amount of tin that can be alloyed without forming T phase is less than 2.2% Sn and therefore growth rate measurements were made only on the alloys with up to 1.1% Sn.

On the other hand, in zinc alloys no such restriction existed and it was known[17] that pearlite of $\alpha + \gamma_2$ could form in alloys containing up to about 15% zinc.

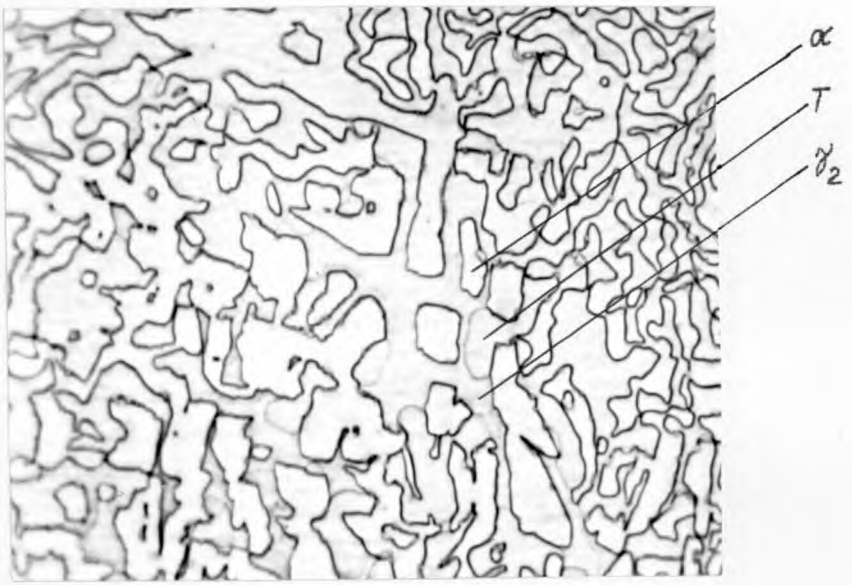

FIG.12 Structure showing the presence of T phase in the $\alpha + \gamma_2$ matrix x 1050

With more than 5% Zn the eutectoid temperature would be affected noticeably. So a maximum of 2.4% Zn was considered to be suitable for growth rate measurements and for studying the effect of zinc on the growth rate without changing the eutectoid temperature.

In binary eutectoid alloys the maximum in the growth rate occurs between 530°C and 520°C. Some attempts were made to determine the temperature of maximum growth rate by carefully controlling the temperature of the salt bath at certain fixed values and measuring the growth rates in the usual way. The maximum occurs just above 526°C, very likely at 527°C. Below 526°C and above 520°C the growth rates seem to be influenced by the rate of the reaction leading to the formation of the ordered phase β_1 from the β phase. The formation of β_1 from β is a nucleation and growth process and takes a certain amount of time for completion. The transformation time curve for such a reaction at 523°C is shown in Fig.13. It is assumed that the maximum amount of β_1 at this temperature in metastable equilibrium with β is obeying the lever rule within the metastable phase field shown in Fig.2. The rate of the reaction was found to be sensitive to the presence of inclusions, for the same degree of undercooling below the maximum at which β_1 first appears. Thus the time required could be very much shorter than shown in Fig.13. If pearlite happened to nucleate and

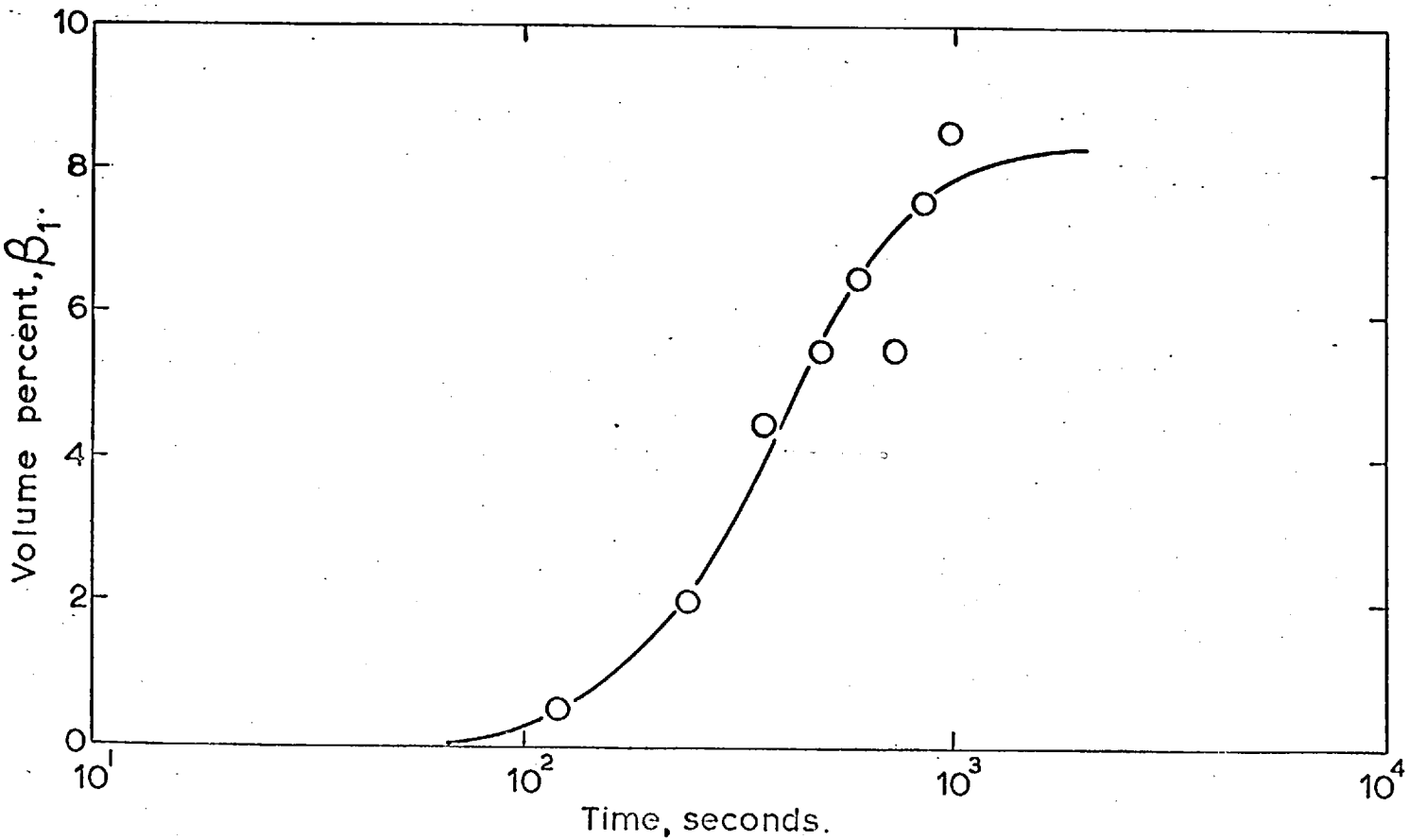

FIG. 13. Transformation-Time Curve For $\beta \rightarrow \beta_1$ At 523 °C.

grow within this time then it was observed that the growth rate of pearlite was smaller than expected. This suggested the possibility that the ordering reaction was preferred to the pearlite reaction. The growth rate of β_1 itself can be calculated by the method 2. A sample calculation made by using the reaction rate curve (Fig.13) and the quantitative measurement of the specific surface area of the β_1 particles gave a value of 6.4×10^{-5} mm/sec for the growth rate of β_1 at 10 minutes.

It is observed from Fig.10 that the addition of tin decreases the growth rate markedly. It is also noted that the temperature at which the maximum growth rate occurs increases with increasing tin content. Determinations of the highest temperature of the $\beta \rightarrow \beta_1$ transformation indicate that the peak values of growth rate correspond closely to the temperature of the beginning of the $\beta \rightarrow \beta_1$..

Results on the zinc alloys show an apparent increase in the growth rate and the peaks of maximum growth rate occur at lower and lower temperatures as the zinc content is increased. Here again the peaks correspond closely to the temperature of the beginning of the $\beta \rightarrow \beta_1$ reaction. The temperatures at which β begins to transform to β_1 in ternary and binary alloys of eutectoid compositions are given in Fig.14. The data for the binary alloys are taken from the work of Thomas[5]

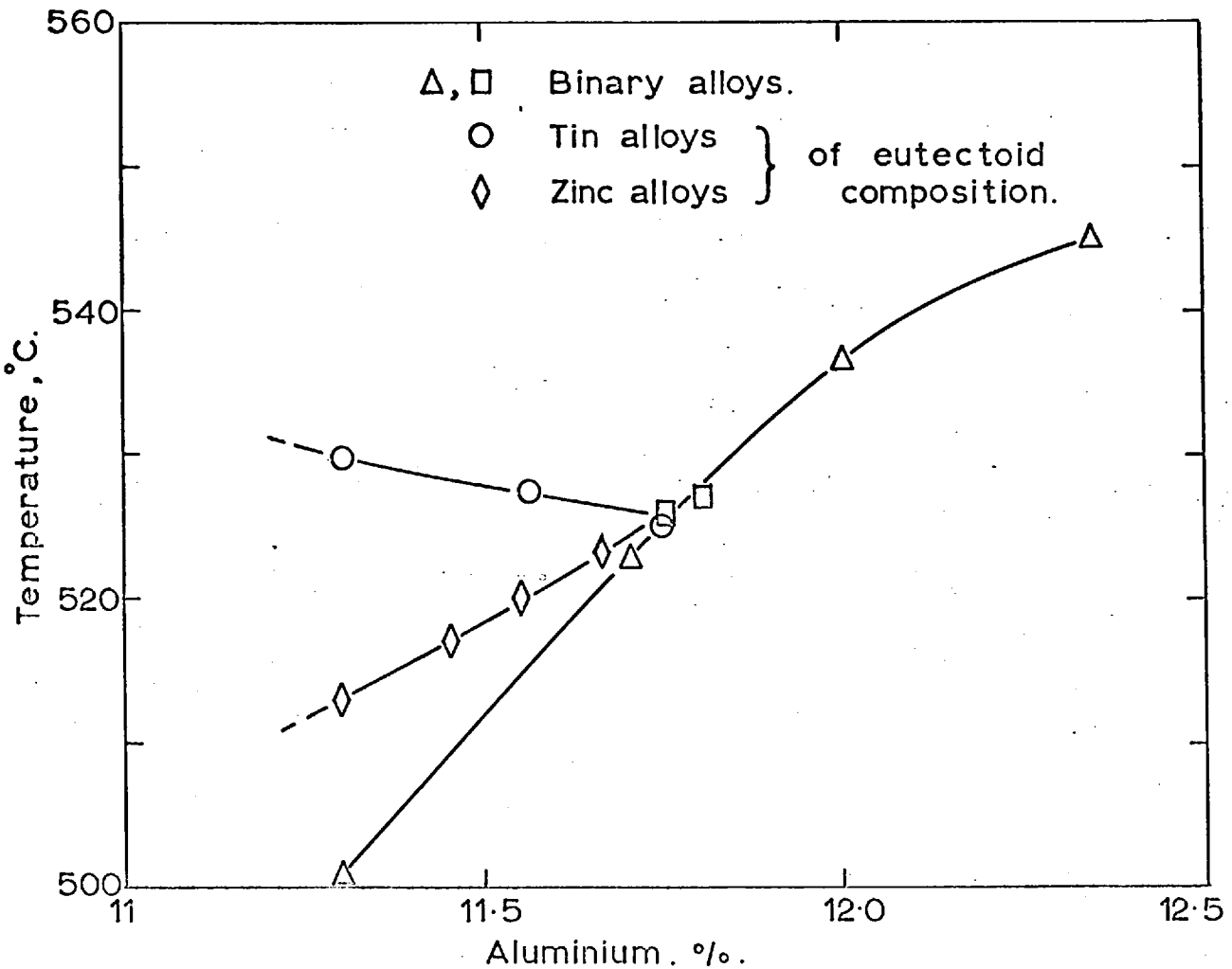

FIG. 14. The Begining Of The $\beta \rightarrow \beta_1$ Reaction In Aluminium Bronzes.

and two points from the present studies are also included. Thus it seems that the peaks in the growth rate curves of the alloys are associated with the $\beta \rightarrow \beta_1$ transformation. It is suggestive therefore to investigate the growth rate of pearlite forming from β_1 alone. The work of Thomas[5] on binary alloys and the metastable phase equilibrium relations has shown that pearlite can and does form from the decomposition of β_1 over a larger range of temperatures than the $\beta \rightarrow \alpha + \gamma_2$ pearlite. The relevant metastable phase diagram for the binary system is shown in Fig.15. The structural features of specimens treated in various regions deduced from the metastable phase relations are dealt with in detail by Thomas[5]. Here only those regions which are encountered in the study of the binary eutectoid alloy and the 12.4% Al binary alloy are discussed.

An outstanding feature of the Cu-Al system is the metastable order-disorder reaction $\beta \rightleftharpoons \beta_1$ existing below the $\beta \rightarrow \alpha + \gamma_2$ eutectoid temperature. The interactions of the $\beta/\alpha + \beta$ and $\beta/\beta + \gamma_2$ extrapolated phase boundaries are of considerable interest in the study of the structures and kinetics of the decomposition of the β phase.

Supposing a eutectoid alloy is undercooled from the β phase to just below the isothermal line passing through the point of intersection of the $\beta/\beta + \alpha$ phase boundary and the $\beta + \beta_1$ phase field (i.e. line TJK). Considering only the precipitation of α from β, the

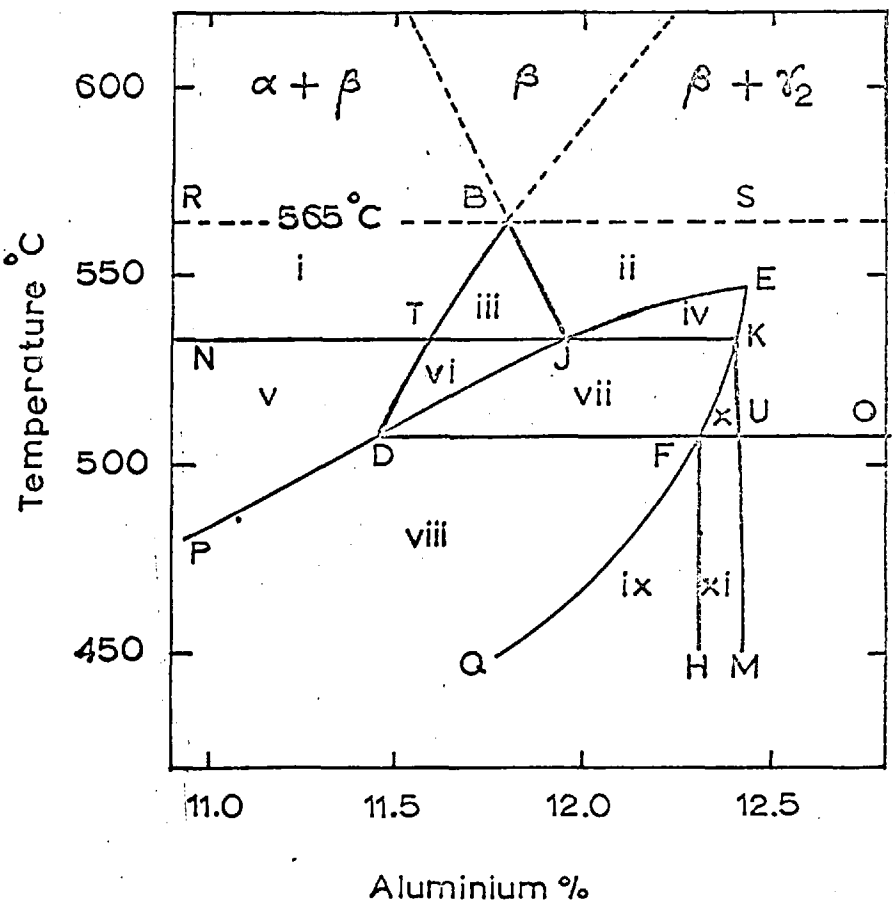

FIG.15. The $\alpha/\beta/\beta_1/\gamma_2$ Phase Diagram For Binary Copper-Aluminium Alloys Containing Less Than 12.5% Aluminium.

composition of β in contact with α gradually increases towards equilibrium. However, as soon as the concentration crosses the point J, β becomes unstable and begins to form β_1, simultaneously rejecting α. Thus a eutectoid reaction $\beta \rightarrow \alpha + \beta_1$ is evolved.

Now if the same alloy is undercooled from the β region to just above the isothermal line passing through the point of intersection of the $\beta/\beta + \gamma_2$ phase boundary and the $\beta + \beta_1$ phase field, then a rapid metastable equilibrium is established between β and β_1. Considering only the precipitation of γ_2 from β_1, the composition of β_1 in contact with γ_2 is diminished (in aluminium content) and β is formed. Thus β_1 becomes unstable with respect to $\beta + \gamma_2$. Just below this temperature β_1 precipitates γ_2 without forming β. Thus at the temperature represented by the line DFU, all the three phases are in metastable equilibrium, which suggests that a peritectoid reaction occurs, indicated by the reaction $\beta + \gamma_2 \rightleftarrows \beta_1$.

The structures observed in the regions of interest are as follows:

Region (iii): A eutectoid alloy of 11.8% Al quenched from the β phase into this region will decompose to give a eutectoid structure mostly lamellar type and a small amount of globular type nearer the eutectoid temperature. The typical structures belonging to this region are as

shown in Figs.16 (a,b,c,d,e,f).

Region (vi): Below the line TJ the alloy can dissociate to give $\alpha + \gamma_2$ as pearlite. The precipitation of α can lead to the formation of β_1 whose composition will be given by the line KF. β_1 can then precipitate α until the composition of β_1 attains line KU. β_1 can at any stage deposit γ_2 and this will result in the formation of β. The micrograph in Fig.17 shows the structure obtained just below the line TJ. The β formed due to the γ_2 precipitation from β_1 cannot be distinguished from the general background of β.

Region (vii): Metastable equilibrium will be established between β and β_1. Both β and β_1 can precipitate α and γ_2. The precipitation of α from β will convert $\beta \rightarrow \beta_1$ around α, Fig.18(a), and the precipitation of γ_2 from β_1 will convert $\beta_1 \rightarrow \beta$ around γ_2, Fig.18(b).

Region (viii): Metastable equilibrium will be rapidly established between β and β_1. α will then precipitate from either β or β_1 or from both of these phases. Precipitation of α from β will convert $\beta \rightarrow \beta_1$ (Fig.19). The composition of β_1 may attain line UM as a result of α precipitation. Only when the composition of β_1 crosses the line FH, γ_2 starts precipitating. γ_2 cannot form from β nor does its formation from β_1 give rise to β.

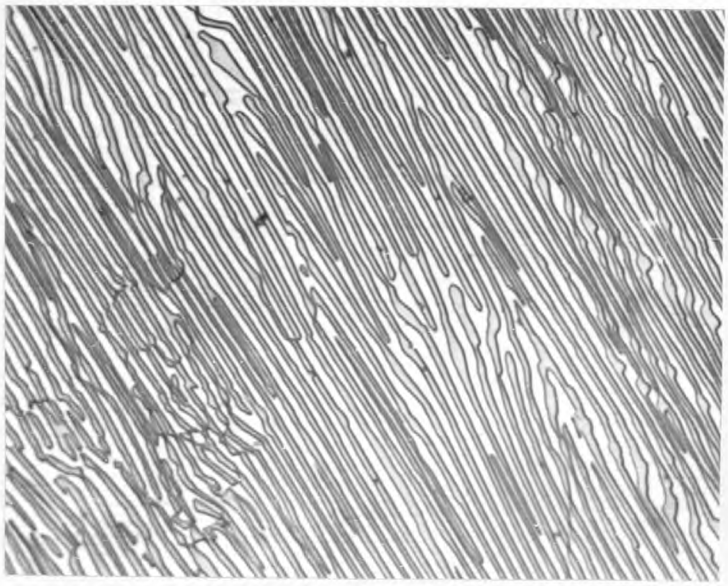

(a)

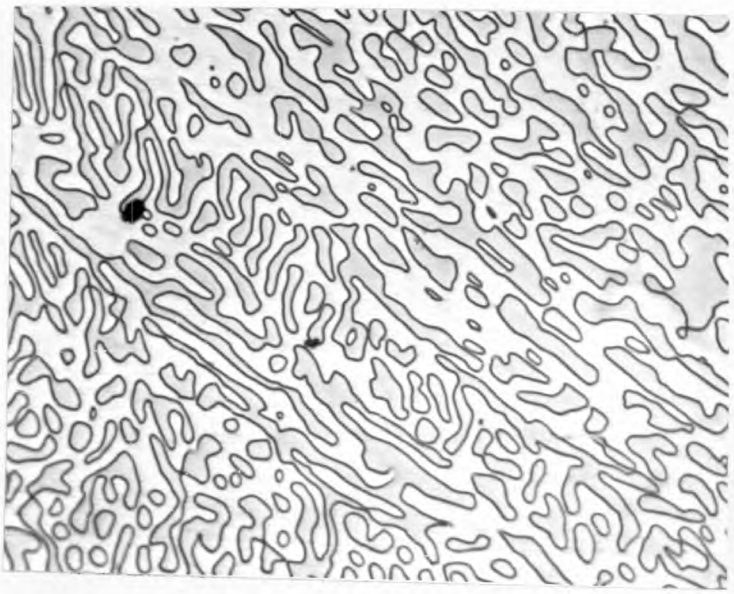

(b)

FIG.16(a,b,c,d,e,f) Typical eutectoid structures obtained in Region (iii) of Fig.15. x 250
Enlarged 4 times for reproduction.

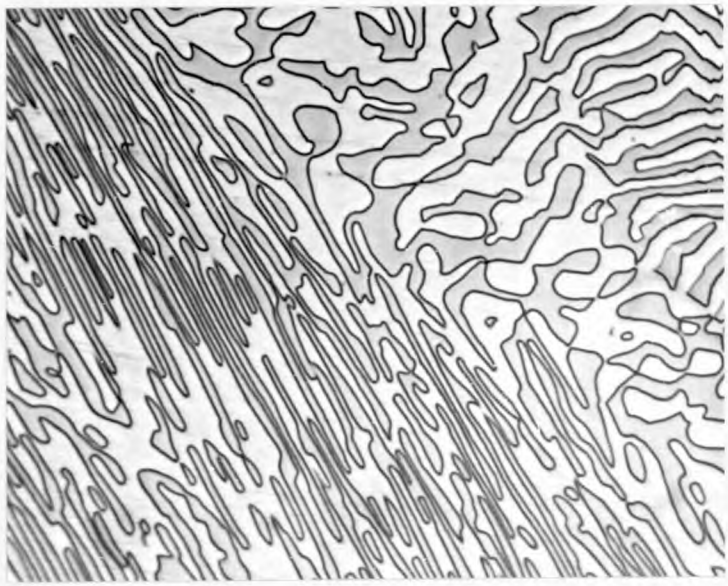

(c)

(d)

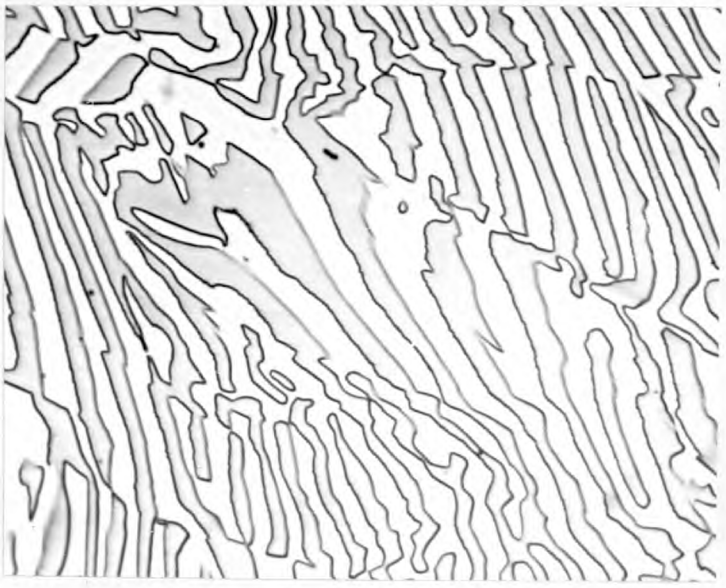

(e)

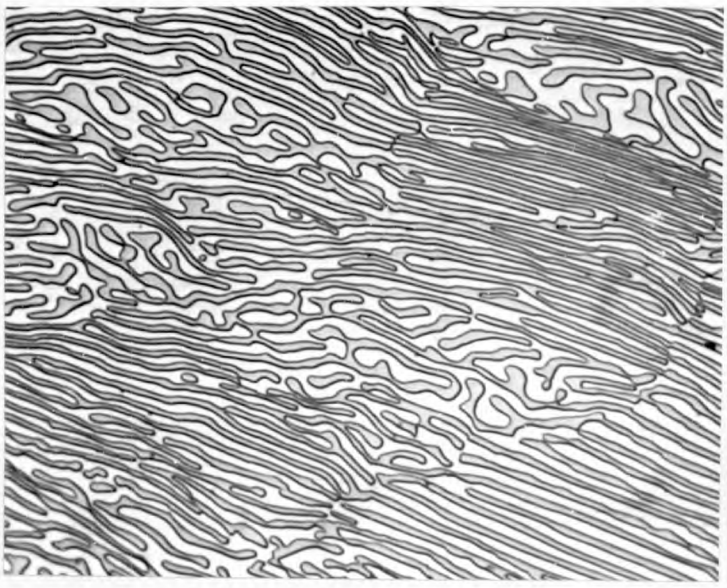

(f)

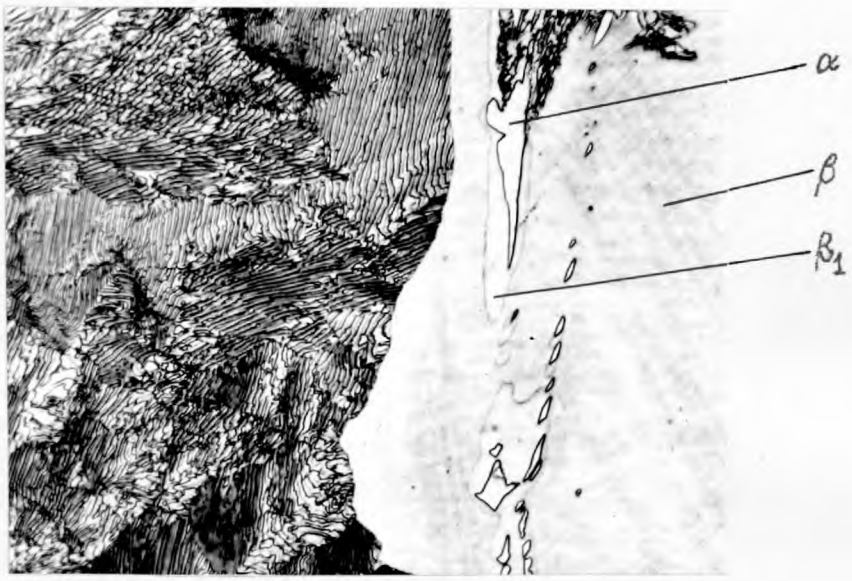

FIG.17 Precipitation of the α phase has given rise to the formation of β_1 around it. x 525

FIG.18a Precipitation of α is accompanied by the formation of β_1. x 525

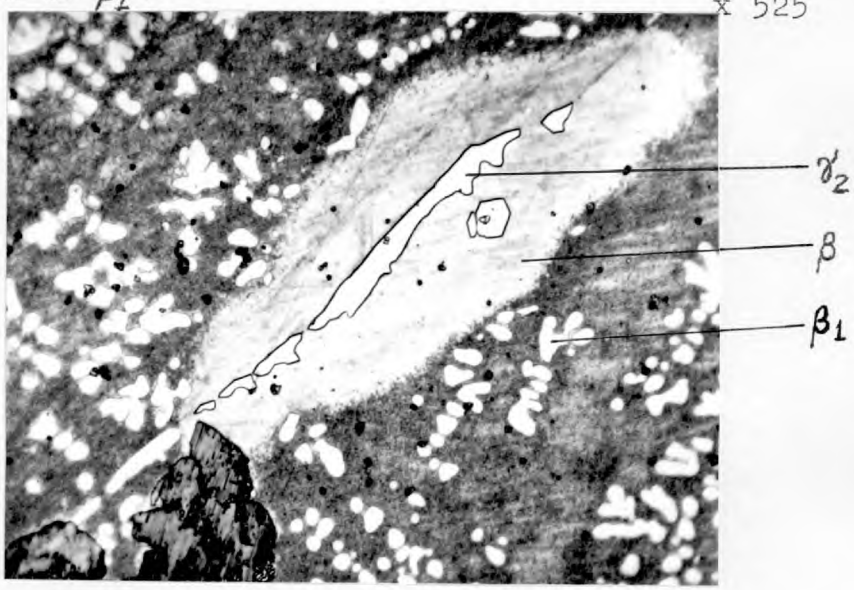

FIG.18b Same sample; precipitation of γ_2 is accompanied by the formation of β. x 525

FIG.19 Precipitation of α with the formation of β_1. The matrix is $\beta + \beta_1$ mixture. x 525

Region (x): The composition 12.4% Al lies within this range and when this alloy is quenched from the β phase in this region, β will transform rapidly and completely to β_1. Both α and γ_2 can form from β_1. The precipitation of γ_2 may convert $\beta_1 \rightarrow \beta$, Fig.20, which in turn precipitates both α and γ_2.

Region (xi): In this region β will transform rapidly and completely to β_1 and β_1 will decompose to give $\alpha + \gamma_2$; however the formation of γ_2 does not give rise to β. Fig.21.

The structural observations made in this investigation are in good agreement with those derived by Thomas[5]. The selection of the 12.4% Al alloy for the transformation of $\beta_1 \rightarrow \alpha + \gamma_2$ pearlite was based on the metastable phase diagram (Fig.15) and the range of temperature 500°C - 400°C was selected within the region (xi).

It was mentioned earlier that at temperatures near the eutectoid the transformation of $\beta \rightarrow \alpha + \gamma_2$ pearlite occurs entirely by surface nucleation and growth; an example is shown in Fig.22(a).The lamellae in this pearlite may be seen to have different angles to the interface including the parallel orientation to the growth direction Fig.22(b).

One aspect of growth rate that has so far been

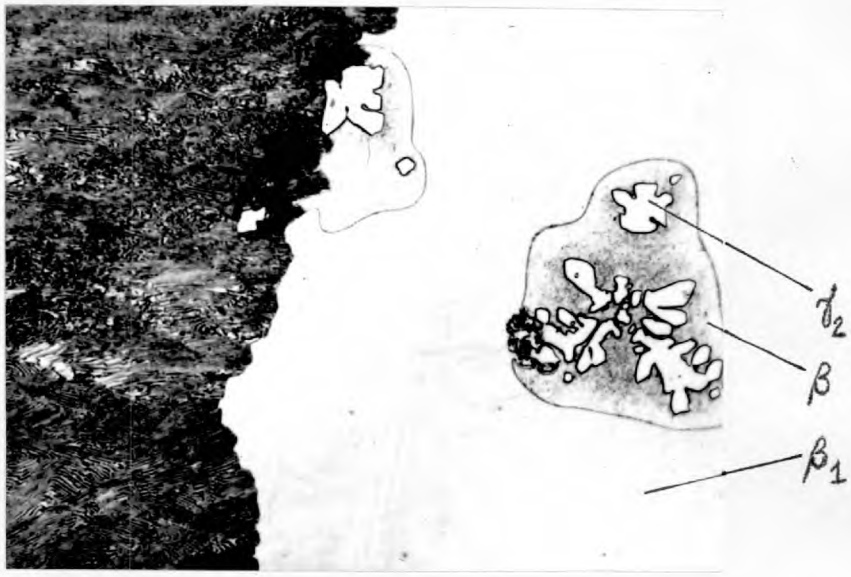

FIG.20 Precipitation of γ_2 with the formation of β. The background is β_1. Temp. 525°C. x 525

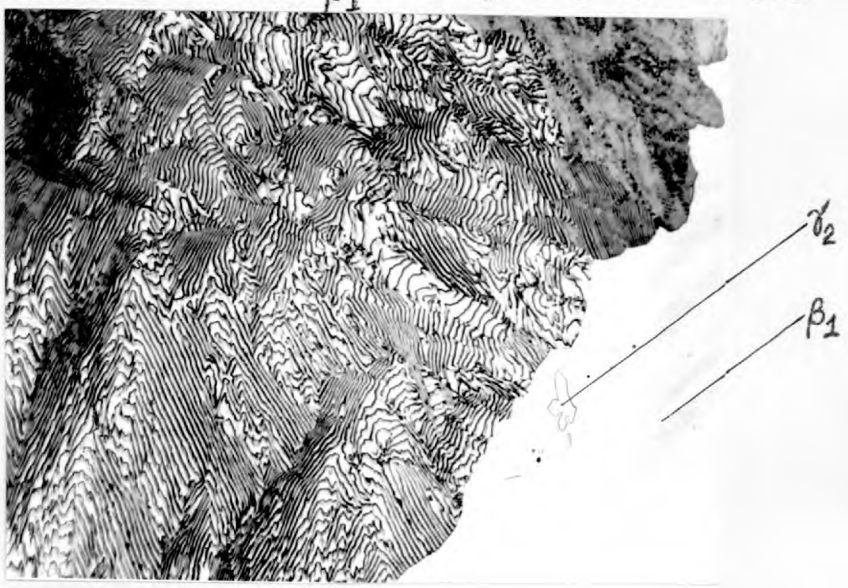

FIG.21 Precipitation of γ_2 is free from the formation of β.
Temp. 480°C. x 525

FIG. 22(a) Pearlite growing from the specimen surfaces. ~ x 7.5

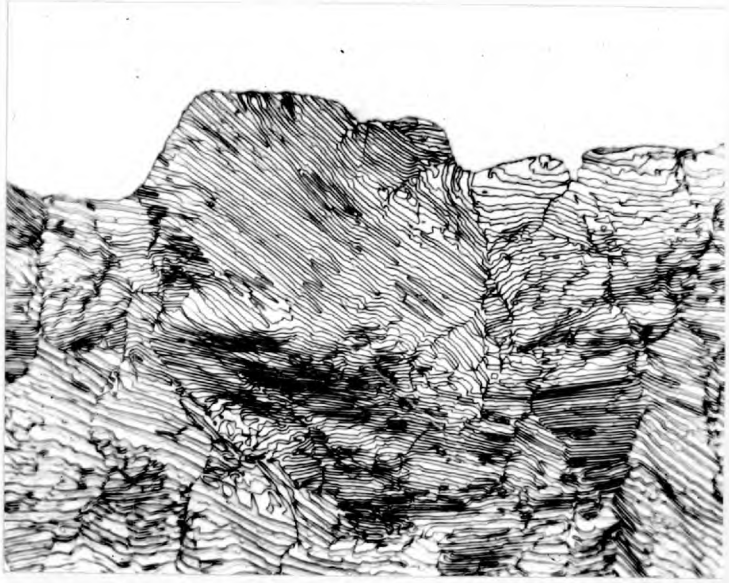

FIG. 22(b) Pearlite lamellae lying at random angles to the interface. x 525

the most difficult to interpret is the positive intercept on the time axis made by the linear nodule radius vs. time relationship for zero radius. The so called 'incubation period' may be associated with a transient growth[19]. Generally, it is observed that the incubation period is smaller for larger growth rates and larger for smaller growth rates. Fig.23 shows that this is approximately true in the case of aluminium bronzes.

The growth rate of pearlite in aluminium bronzes may be summarised as follows:

1. It is a steady state process in all the alloys studied in this investigation.

2. The effect of ternary tin and zinc additions is to change the growth rate markedly.

3. The peak in the growth rate - temperature relationship is due to the onset of the $\beta \rightarrow \beta_1$ disorder reaction.

4. The growth rate in 12.4% Al alloy decreases as the undercooling increases. ~~which is a unique feature observed in any system so far known.~~

5. The incubation period increases as the growth rate is decreased and vice versa.

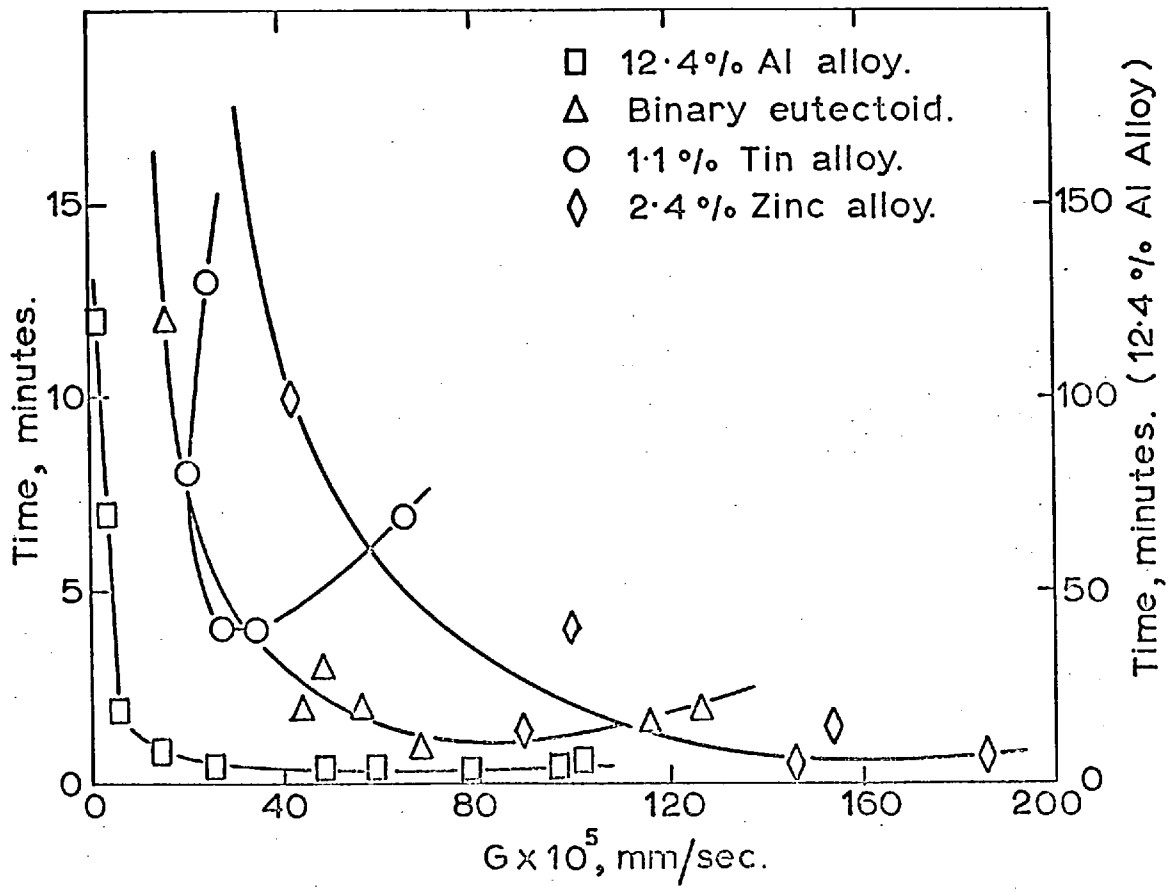

FIG. 23. Incubation Period Vs Growth Rate.

CHAPTER V.

INTERLAMELLAR SPACING.

(i) Introduction:

In a eutectoid reaction, the two phases formed by decomposition of a matrix phase quite often form lamellae, i.e. alternate plates of each of the two phases. A set of lamellae form what is known as a colony and a group of colonies constitutes a nodule. The orientation of a phase in a colony of lamellae remains constant but can vary from colony to colony.

The rate at which the nodules grow is known as the growth rate. It has been observed that the distance between the lamellae of the same phase, i.e. the interlamellar spacing, has an important bearing on the growth rate of the nodule, so that the study of the growth kinetics of pearlite would be incomplete without the knowledge of the interlamellar spacing. Since the pearlite nodules are distributed spatially, the observed interlamellar spacing (if it is assumed to be constant for all the colonies) on any random plane of section gives the apparent spacing of the lamellae. If the orientation of the lamellae can be determined then the true spacing can be calculated. Since it is difficult to determine the orientation of the lamellae, this method finds little use in determining the true

interlamellar spacing. The smallest spacing observed in a large area of pearlite nodules can be taken as the true spacing of the lamellae. It is also possible to obtain the true spacing through the measurement of apparent spacings in various colonies and applying methods of statistical mathematics. However, if there happens to be a distribution in true spacings, then the method of selecting the smallest spacing does not reveal this fact and the smallest spacing does not represent the mean true spacing. The statistical methods, on the other hand, can not only indicate the existence of a distribution in true spacing but can also give a probable distribution of the various true spacings. If the probable distribution curve shows a peak with a small standard deviation then it is appropriate to use this particular mean value of the true spacing called the mean true spacing, for analysing the growth kinetics.

(ii) Experimental Methods:

I. A comprehensive investigation on the interlamellar spacing of plain carbon and alloy steels was made by Pellisier et al[41]. Their method consisted in calculating an apparent spacing distribution by applying probability mathematics, assuming a constant spacing, So, for all colonies of pearlite which are randomly distributed in space with respect to orientation, shape and size.

Measurements made on the relative amounts of surface area, occupied by various small ranges of apparent spacings, S, were then compared with the calculated data. It was necessary that the pearlite observed was resolved completely so that apparent spacings could be measured easily. A sufficiently large area of pearlite was included to constitute a representative sample. The data were used in obtaining a cumulative percent area versus S or S/So graph. This curve was compared with the theoretical curve obtained by the formula

$$fs = \mathrm{Cos}\left(\mathrm{Sin}^{-1}\frac{So}{S}\right) = \mathrm{Cos}\left(\mathrm{Csc}^{-1}\frac{S}{So}\right) \quad \ldots\ldots (11)$$

where

fs - fraction of the area of a reference plane, such as the plane of polish, occupied by spacings up to a certain value of the apparent spacing S.

So - the true spacing.

It was found from the comparison that if the true spacing were 1.65 instead of 1, then the two curves would be close together. The matching could be improved still further if a probable distribution of the true spacing was assumed. This last step involves lengthy statistical procedures to obtain a probable distribution curve.

Hawkes and Mehl[24], Parcel and Mehl[25] and Darken

and Fisher[34] have adopted a simplified method of comparing the experimental cumulative curve with the theoretical curve and estimating the mean true spacing. Darken and Fisher[34] made the measurements on electron micrographs since the spacing was too fine to be resolved optically. Further measurements on other samples were confined to finding the minimum spacing values and correcting them to the mean true spacing by multiplying, with a factor 1.6, which gave the best match for experimental and theoretical curves.

II. There is another procedure known as the 'limit method'[42] which avoids the lengthy process of measuring areas and their apparent spacings of pearlite. It consists of using a microscope objective of known resolving power, chosen in such a way as to resolve only about 50% of the pearlite. Areal analysis of the pearlite sample is made and the mean true spacing is determined from the formula

$$So^2 = S^2 (1 - N^2) \quad \ldots\ldots\ldots \quad (12)$$

where

So - mean true spacing.

N - the fraction of the surface with an apparent spacing less than S.

S - apparent spacing measured with the knowledge of the resolving power of the objective.

This method is equivalent to fitting the experimental curve with the theoretical curve derived by Pellisier et al[41].

III. Cahn and Hagel[19] have reported that the range of true spacings, observed in a Fe - 9%Cr - 1%C alloy, is much wider than indicated by Pellisier et al[41] in plain carbon steels. Under such circumstances it is simpler to determine the smallest spacing observed which corresponds to the minimum true spacing. They suggest that an average spacing designated $\bar{S}$ may be determined on the basis of the total surface area Ac of the ferrite-carbide interfaces per unit volume. It is possible to calculate the interface surface area in a space filling volume by measurements made on a random section[43]. The relation between mean spacing and interface area is then given by

$$\bar{S} \equiv {}^{2}/_{Ac} \quad \ldots\ldots\ldots\ldots\ldots\ldots (13)$$

Experimental Procedures (Part A).

A detailed study of the spacings of the binary eutectoid alloy was undertaken to find out the distribution of apparent spacings and to compare with the theoretical curve. For this purpose a binary eutectoid specimen was transformed to completion at 555°C so that all the pearlite formed at this temperature could be resolved using an optical microscope. The experimental method employed is comparatively simpler than that of

Pellisier et al, though quite similar. Photomicrographs of the pearlite were taken on a 35 mm film at the intersections of an imaginary grid, the points of which were 0.5 mm from their nearest neighbours. Each picture covered an actual area of 0.015 sq.mm. on the specimen; 112 pictures were taken in all, corresponding to a total area of 1.68 sq.mm. The photomicrographs were taken in 3 groups of 35, 41 and 36 respectively and the distribution of spacings in each successive group was studied to determine the minimum pearlite area for a statistical representation.

The films were projected on a plane paper to a total magnification of X1000. Colonies of pearlite were marked out in pencil and the spacing determined by the linear intercept method was noted on the appropriate colony. Areas corresponding to the same spacing were cut out from the papers and collectively weighed. Thus the total area occupied by each spacing was determined. From such data a spacing versus cumulative area percent curve was plotted.

(iii) Results and Discussion (of Part A):

The experimental results of the investigation using Method I are presented in Table II and in Fig.24. The curves, relating cumulative area percent versus apparent interlamellar spacing S, show the effect of the number of micrographs analysed on the shape of curves. It may be

	Cumulative Area. Percent		
S/So So = 1μ	35 pictures	76 pictures	112 pictures
1.43	2.0	2.1	4.4
1.67	8.7	9.2	8.9
1.82	12.3	12.3	13.1
2.00	18.4	19.0	20.5
2.22	28.3	34.2	36.3
2.50	40.7	46.6	45.8
2.86	47.6	53.7	52.6
3.33	53.3	59.5	60.0
4.00	61.6	69.0	69.1
5.00	71.6	78.6	81.1
6.67	80.5	86.2	87.6
10.00	97.4	97.3	98.0

Table II

Results of the statistical analysis on the photomicrographs at S/So ratios assuming a constant interlamellar spacing if So = 1 micron

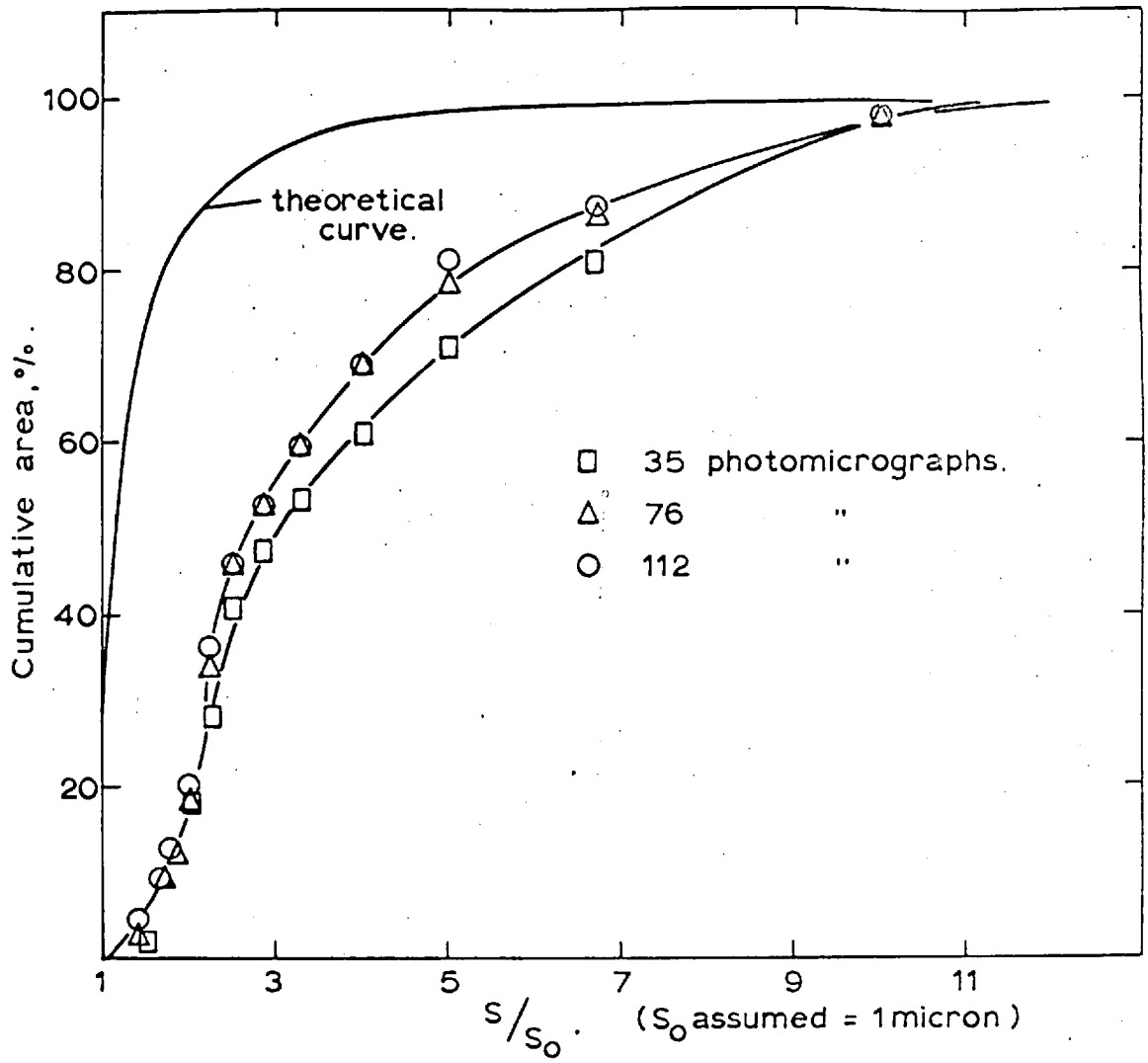

FIG. 24. Cumulative Area Percent Vs S/So In The Three Groups.

observed that the difference between 76 and 112 micrographs is quite small, indicating that about 80 micrographs would yield a representative cumulative curve. The theoretical curve, obtained from the equation (11), assuming the real spacing to be unity (or 1μ), is also shown on the same graph. It is apparent from the theoretical and experimental curves that the assumed real spacing of 1μ is not valid. To find out what value of real spacing is likely to yield a closer relation to the experimental curve, three more theoretical curves corresponding to real constant spacings of 1.5, 2.0 and 2.5μ are drawn as shown in Fig.25. In this case it seems that no particular single real spacing exists whose apparent spacing distribution would correspond to the experimental distribution. It follows that there is a distribution in real spacing. However, it is quite possible that the assumptions for obtaining the theoretical curve are not met with in the experimental one. The likely source of doubt is the assumption of randomness of the distribution of the colonies with respect to orientation, shape and size, because the entire pearlite is formed from surface nucleation at 555°C and may have preferred orientations. None the less, the true mean spacing - if it really exists in this case - is likely to be approximately 2 - 2.5 times the minimum spacing.

This detailed analysis was intended to obtain a

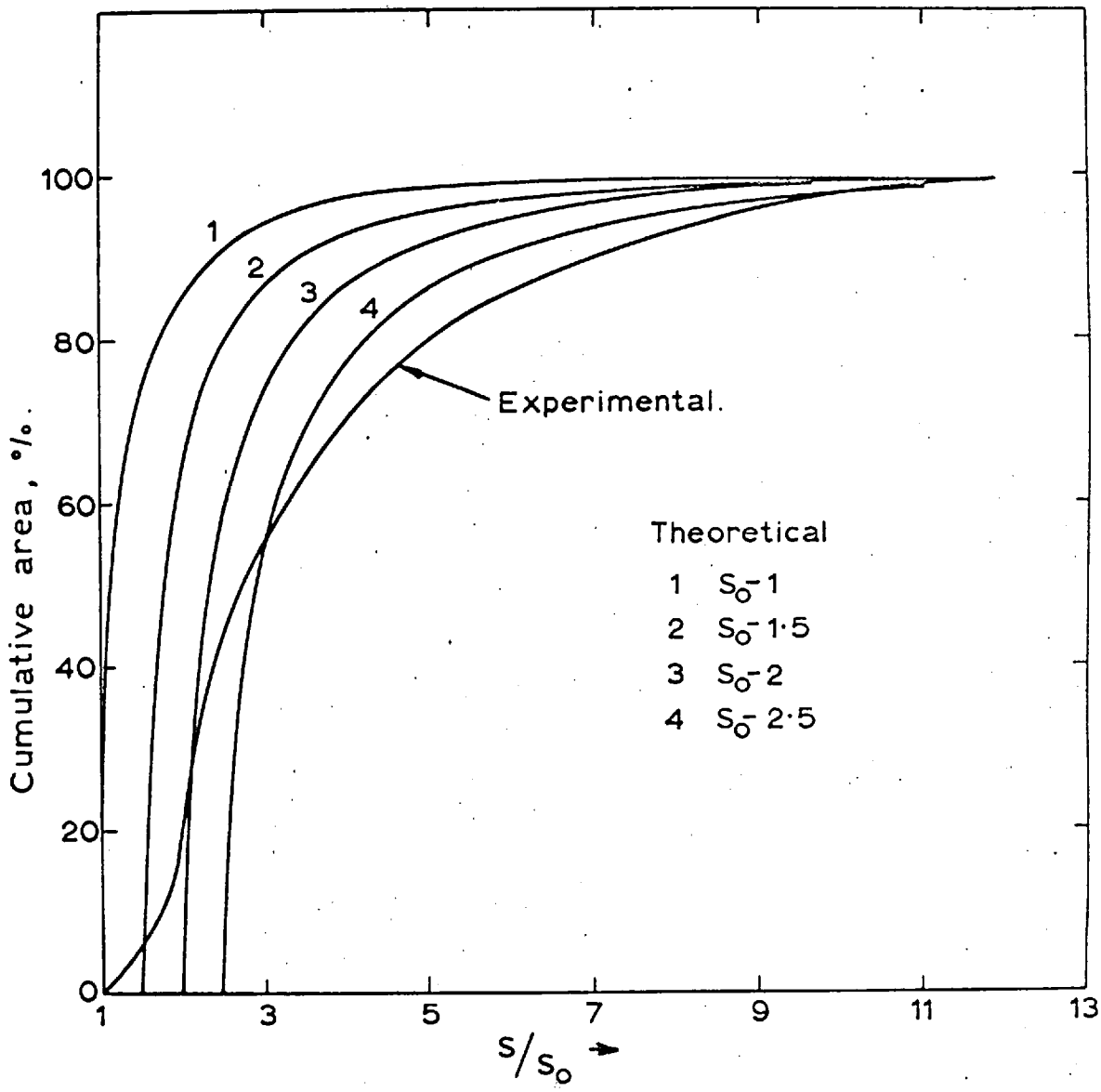

FIG. 25. Theoretical Cumulative Curves Compared With The Experimental Curve.

relation between the observed minimum spacing and the mean true spacing. It is realised that even if such a relation existed it is improbable that the same relation would be valid for pearlite formed at other temperatures or for pearlite in ternary alloys. Therefore, to obtain a mean true spacing a complete analysis on the lines investigated by Pellisier et al is necessary at all temperatures of pearlite reaction, and for all the binary and ternary alloys. Such a task would be extremely lengthy and difficult in many cases. For the purposes of analysing the kinetics of the pearlite reaction the minimum true spacing observed seems adequate and subsequent experiments were confined to searching a large area of the pearlite for the minimum spacing.

Part B:

Pearlite formed at lower temperatures in binary and ternary alloys could not be resolved in an optical microscope, hence it was necessary to use electron microscope techniques.

Preparation of Replicas:

It was possible to obtain good formvar replicas from the specimens for electron microscope studies but it was found easier to prepare carbon replicas and the electron micrographs obtained from carbon replicas were found to be better than those from formvar replicas.

The pearlite samples were ground and polished carefully to avoid scratches and were lightly etched electrolytically in an aqueous 1% chromic acid bath just as for optical microscope examination. After cleaning with alcohol and drying, the specimen surfaces were coated with spectrographic purity carbon in a vacuum chamber. The method was to place a sample at a distance of about 10 cm from a carbon arc in a vacuum glass chamber. At a pressure of less than 1μ (Hg) the carbon arc was struck with about 30 - 40 volts. A few bursts were necessary to deposit a film of carbon of sufficient thickness. The thickness of the film suitable for transmission pictures was judged from the colour of the film; when it turned light blue the deposition was discontinued and the specimen taken out. The film on the surface of the sample was scratched into small areas of 2 - 3 mm. square, approximately the size of the microscope grid. Removal of these squares of film from the sample was accomplished by electrolytic means. The same etching bath (1% chromic acid) was used. A voltage of 4 - 6 volts enabled the specimen to etch and the square pieces of the film adhering floated to the surface in about 15 - 20 minutes. These were transferred to a 50:50 nitric acid-water solution; washed for 10 minutes and transferred to a distilled water bath for 5 minutes. Finally they were carefully picked up on electron microscope copper grids

of 400 mesh size. It was found that the films had a tendency to curl up in water but this could be prevented to a large extent by adding a few drops of ethyl alcohol to the water prior to transferring on to the microscope grids. At least a dozen pieces of the film were collected from each specimen for examination.

Before examining the replicas, the electron microscopes were calibrated by using a standard replica of an optical grating, to obtain correct magnifications. The replicas from the binary eutectoid and binary 12.4% Al alloys were observed in a Hitachi electron microscope at a magnification of X5000; those from ternary tin and zinc alloys were observed in a Siemens Elmiskop I at 4400 and 7800 magnifications depending on the alloy and the temperature of transformation.

The procedure was to examine a sufficiently large number of colonies and to photograph areas judged to have the smallest spacings. The lamellar spacings on the plates were then measured using a linear intercept method and the smallest recorded was considered as the true minimum spacing for that particular temperature.

Results and Discussion (of Part B):

a) Binary Eutectoid Alloy: The results of the spacing measurements, for the various treatment temperatures, are presented in Table III. In Zener's[22] analysis of

Temp. °C	Interlamellar Spacing Å	$\frac{1}{S} \times 10^{-5}$ Å^{-1}	G x 10^5 mm/sec
490	2500	40.0	45
500	2200	45.5	57
510	2000	50.0	69
520	2200	45.5	117
530	2850	35.1	125
540	5000	20.0	48
550	10,000	10.0	15
555	14,300	7.0	8

Table III

Spacing and Growth rate

Data on the binary Eutectoid Alloy

the pearlite growth problem, the observed interlamellar spacing is expected to be twice the minimum spacing which is thermodynamically possible. Accordingly the relation between this minimum possible spacing and the degree of undercooling is given by

$$S' = \frac{2\,Te\,\sigma}{\rho Q(Te - T)} \quad \ldots\ldots\ldots\ldots\ldots\ldots \quad (14)$$

where S' - thermodynamically possible minimum spacing

Te - eutectoid temperature

T - temperature of reaction

σ - interface energy

ρ - density

Q - heat of transformation per unit mass

Thus it is deduced that the interlamellar spacing is inversely proportional to the degree of undercooling. Plotted on logarithmic paper, the spacing versus the degree of undercooling should give a linear relationship with a slope of -1. In Fig.26 such a plot from the data of table III is shown. Although the results yield a straight line the slope is -1.3. Haynes[4] has reported that the spacings in a similar alloy agree with Zener's theory in obtaining the required slope of -1. The difference between the results of the present investigation and Zener's

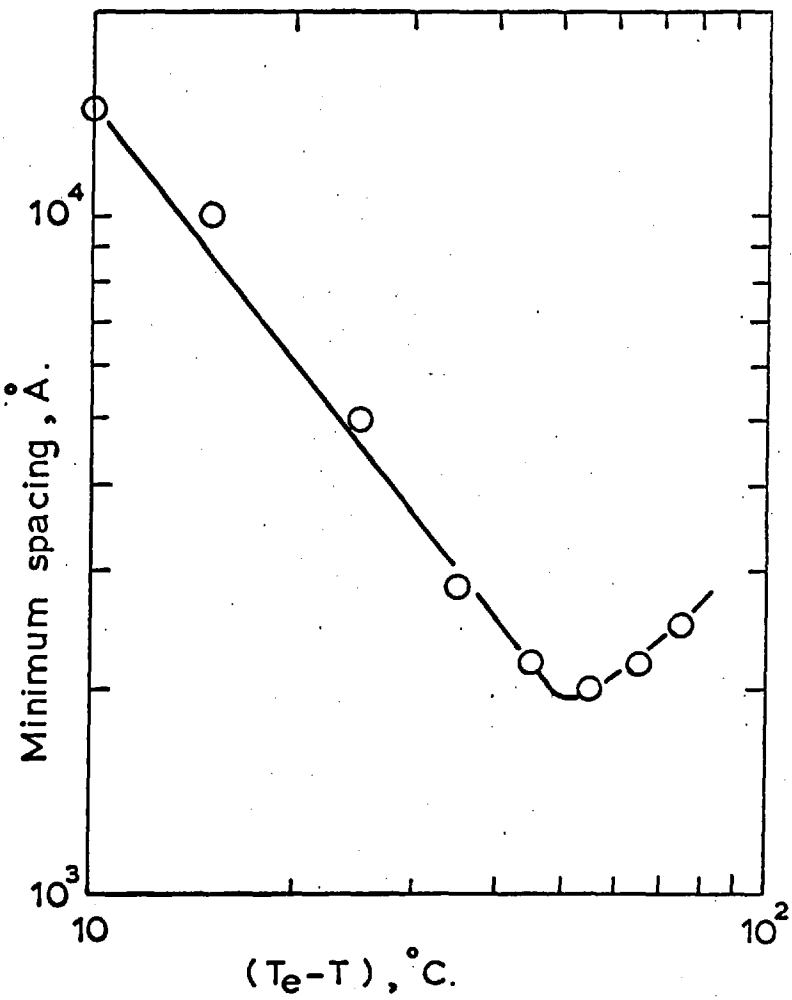

FIG. 26. Relation Between Interlamellar Spacing And Undercooling; Binary Eutectoid Alloy

derivation could be the result of an indefinite relation between true minimum spacing and the mean true spacing; the latter is the more appropriate of the values to be used in plotting the data. Accepting Zener's model, it is now possible to calculate the interfacial energy of pearlite in the Cu-Al system, from the known data of enthalpy change, density and eutectoid temperature.

An equation for the ~~straight line~~ points in Fig.26 is,

$$2S' (Te - T) = 0.0013 \text{ cm}^{\circ}\text{C}. \quad . \quad . \quad . \quad . \quad . \quad . \quad . \quad . \quad (15)$$

A value of 8.9 cals./gm. is taken for the enthalpy change from the data of Kramer et al[28]. The average density is 7 gms./c.c. and the eutectoid temperature 838°K. The value of interfacial energy calculated is 1000 ergs/cm^2. The experimental value of σ by Kramer et al is 1000 $\pm$ 600 ergs/cm^2 and was obtained from calorimetric measurements. Though the accuracy of these results is somewhat vague it does, however, strongly indicate that in the Cu-Al system Zener's analysis is reasonably valid, unlike the Fe-C system.

There is another important observation on the interlamellar spacing in Cu-Al alloys. The spacing increases after a certain minimum value has been reached, as shown in Fig.26. This is in agreement

with the earlier observations made by Klier and Grymko[3] and Haynes[4]. They considered the interference of the $\beta \rightarrow \beta_1$ reaction as the cause of this anomaly. In view of the experiments on the decomposition of $\beta_1 \rightarrow \alpha + \gamma_2$ in the present investigation, the discussion of this aspect will be taken up in the following section along with the spacing measurements of the binary 12.4% Al alloy.

(b) Binary 12.4% Al alloy:

It was mentioned in the last chapter on Growth rate that this alloy when quenched from the β phase into the temperature range 500°C - 400°C, transforms rapidly and completely to β_1 and then dissociates to $\alpha + \gamma_2$ as pearlite. The minimum interlamellar spacing was found to increase as the temperature of transformation was lowered as given in table IV. This observation is in apparent contradiction to the prediction made by equation (14), according to which spacing should continuously decrease with increasing undercooling below the eutectoid temperature. The 'eutectoid' temperature in this case refers to the temperature at which β_1 is in equilibrium with $\alpha + \gamma_2$. β_1 is a metastable phase and the metastable eutectoid temperature ($\beta_1 \rightleftharpoons \alpha + \gamma_2$) should be above the eutectoid $\beta \rightleftharpoons \alpha + \gamma_2$ temperature

Temp. °C	Interlamellar Spacing Å	Percent Area Resolved	$\frac{1}{S} \times 10^{-5}$ Å^{-1}	G x 10^5 mm/sec
400	3650	65	27.5	1
420	3350	59	30.0	3
440	2660	49	37.5	6.5
460	2660	40	37.5	13.5
480	2500	37	40.0	26
500	2150	31	46.5	47.5
510	2220	--	45.0	62.5
515	1820	--	55.0	78
520	2220	--	45.0	97
525	2630	--	38.0	102

Table IV

Interlamellar spacing, Growth rate and Percent area resolved Data on the 12.4% Al alloy

of 565°C. Thus it is not possible to obtain the same logarithmic relation between spacing and undercooling as in the binary eutectoid case since the metastable eutectoid temperature is not known. However a relation between reciprocal spacing and temperature can be obtained as indicated in Fig.27. In a normal case of decreasing interlamellar spacing with lowering of reaction temperature such a reciprocal relation can be used to find the reference temperature by extrapolation to zero $\frac{1}{S}$ value, as suggested by Cahn and Hagel[19]. This cannot be done in this particular case as the trend is in the reverse direction.

In these spacing measurements the minimum observed spacings are quoted, and it might be argued that although the minimum observed spacing may appear to be increasing the mean true spacing may in fact be decreasing. This can be tested only if the true spacing distributions for each temperature is determined. Nevertheless, in the absence of detailed analyses, a semi-quantitative check can be made. The amount of area of pearlite resolved in an optical microscope with any particular objective, is directly proportional to the true mean spacing. So if the true mean spacing also increases then an increase in

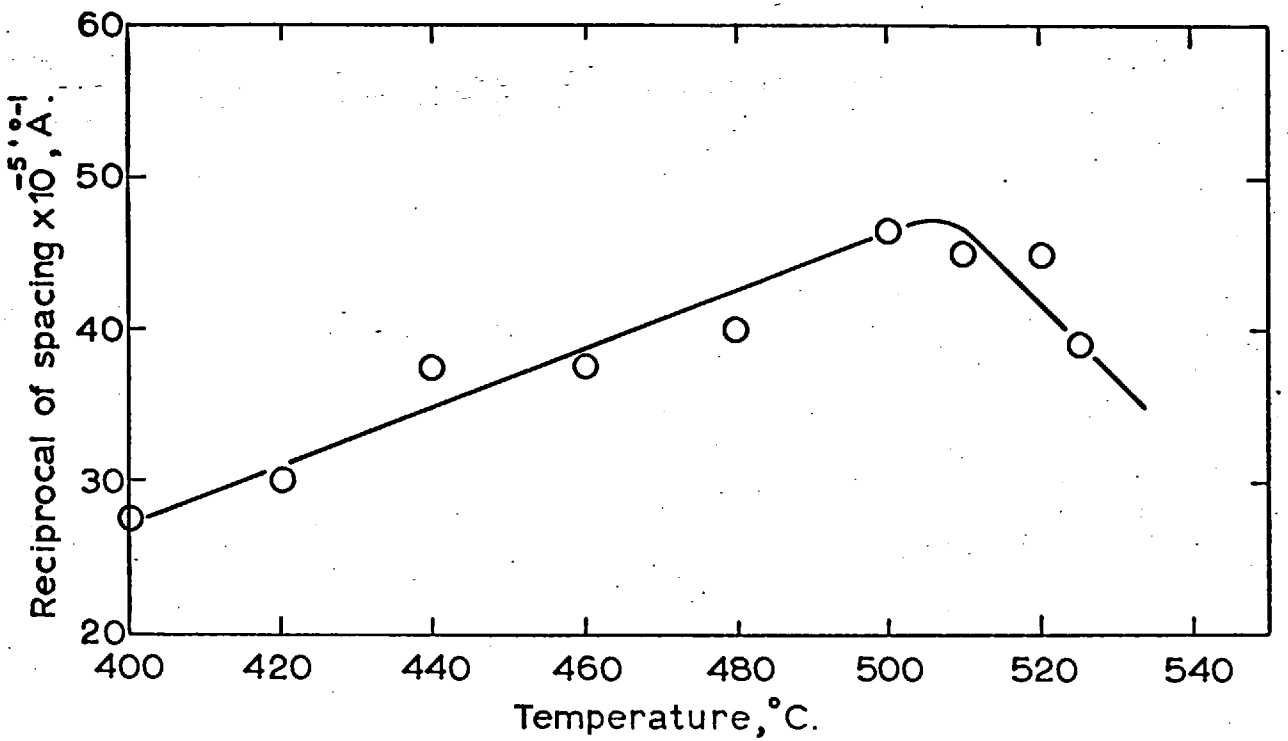

FIG. 27. Reciprocal Of Interlamellar Spacing Vs Transformation Temperature For The 12·4% Aluminium Alloy.

the fraction of area of resolved pearlite is to be expected. The results of the areal analysis of the resolved and unresolved pearlite estimated by a point count method are included in table IV Column 3. It may be observed that the spacing does increase with decrease in temperature and hence the conclusions based on minimum spacing measurements are valid.

Comparing the spacing with the growth rate in this alloy it is observed that while the spacing increases from 2200Å to 3650Å the growth rate decreases from 62 x 10^{-5} mm/sec to 1 x 10^{-5} mm/sec; so a small change in spacing appears to have a large effect on the growth rate.

Now to explain the increase in spacing reference is made to the metastable phase diagram Fig.15 and Zener's derivation of the growth rate equation (4)

$$V_B \approx (Te - T)^2 . e^{-Q/RT} \quad \ldots\ldots\ldots\ldots\ldots (4)$$

The $(Te - T)^2$ term arises from two factors, one due to the increasing gradients available for diffusion with increasing degree of undercooling, and the other due to the reciprocal relation of undercooling and interlamellar spacing. In the diagram, the boundaries KM and FH represent the compositions of β_1 in metastable equilibrium with α amd γ_2 phases

respectively. The driving potential for the diffusion process is estimated from the difference in the concentrations indicated by these lines. It is observed that the composition difference appears to be invariant with temperature and hence the gradients may be regarded as constant. Thus the growth rate equation may be represented as

$$G \sim \frac{1}{S \cdot e^{Q/RT}} \quad \ldots\ldots\ldots\ldots\ldots\ldots \quad (16)$$

$$\text{or } S \sim \frac{1}{G} \cdot \frac{1}{e^{Q/RT}} \quad \ldots\ldots\ldots\ldots\ldots\ldots \quad (17)$$

The exponential term of the diffusion increases with the decrease in reaction temperature. If the growth rate decreases faster than the increase in the exponential term, the spacing increases. In this way the apparent contradiction to Zener's analysis is explained while still retaining the reciprocity of spacing and undercooling relationship. [Para In general it seems appropriate to relate spacing with the three factors undercooling, growth rate, and the diffusion exponential term.

$$S \sim \frac{Te - T}{G \cdot e^{Q/RT}} \quad \ldots\ldots\ldots\ldots\ldots\ldots \quad (18)$$

rather than simply to the reciprocal of the undercooling. The balance between these factors determines the spacing. The most important question

that defies explanation is what determines the growth rate.

It now remains to consider the observation regarding the increase in spacing below a certain temperature and its association with the transition $\beta \rightarrow \beta_1$. The results of the binary 12.4% Al alloy and the binary eutectoid alloy are plotted in the graph, Fig.28 as $\frac{1}{S}$ vs $T^{o}C$. In the overlapping region in which both β and β_1 decompose to give $\alpha + \gamma_2$, the interlamellar spacing appears to be the same for both the alloys. With increasing amounts of β_1 in the binary eutectoid alloy the trend is towards the larger spacings of the 12.4% Al alloy. The reason is that the formation of β_1 reduces the diffusion gradient and causes the growth rate to decrease which in turn effects an increase in the lamellar spacing.

(c) Copper - Aluminium - Zinc System:

Of the four zinc alloys only the 0.6% Zn and the 2.4% Zn alloys were selected for spacing measurements. The data, presented in Table V(a) and V(b), of the minimum spacing observed at temperatures are plotted in Fig. 29 as Log S against log (Te - T). A linear relationship is observed but the slope is found to be -1.45.

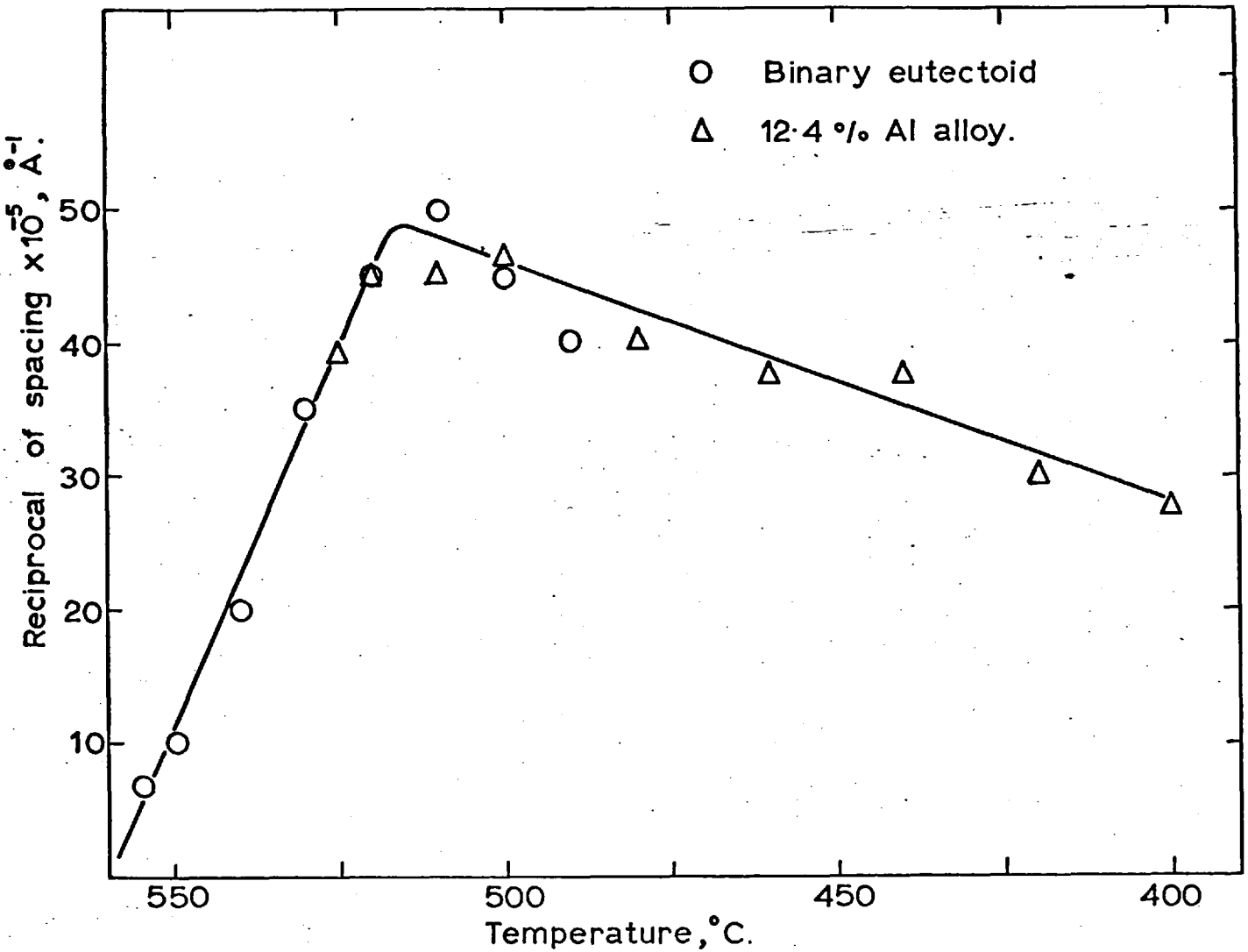

FIG. 28. Reciprocal Of Interlamellar Spacing Vs Transformation Temperature

Temp °C	Interlamellar Spacing Å	G x 10^5 mm/sec
480	2300	66
500	2100	75
510	1900	94
520	2100	137
530	3250	104
540	6500	45

Table Va

Spacing and Growth rate Data on the 0.6% Zinc Alloy

Temp. °C	Interlamellar Spacing Å	G x 10^5 mm/sec
460	2100	45
480	1600	90
500	1500	154
510	1600	185
520	1830	154
530	2210	100
540	5130	42
550	10,000	17
555	18,200	6

Table Vb

Spacing and Growth rate

Data on the 2.4% Zinc Alloy

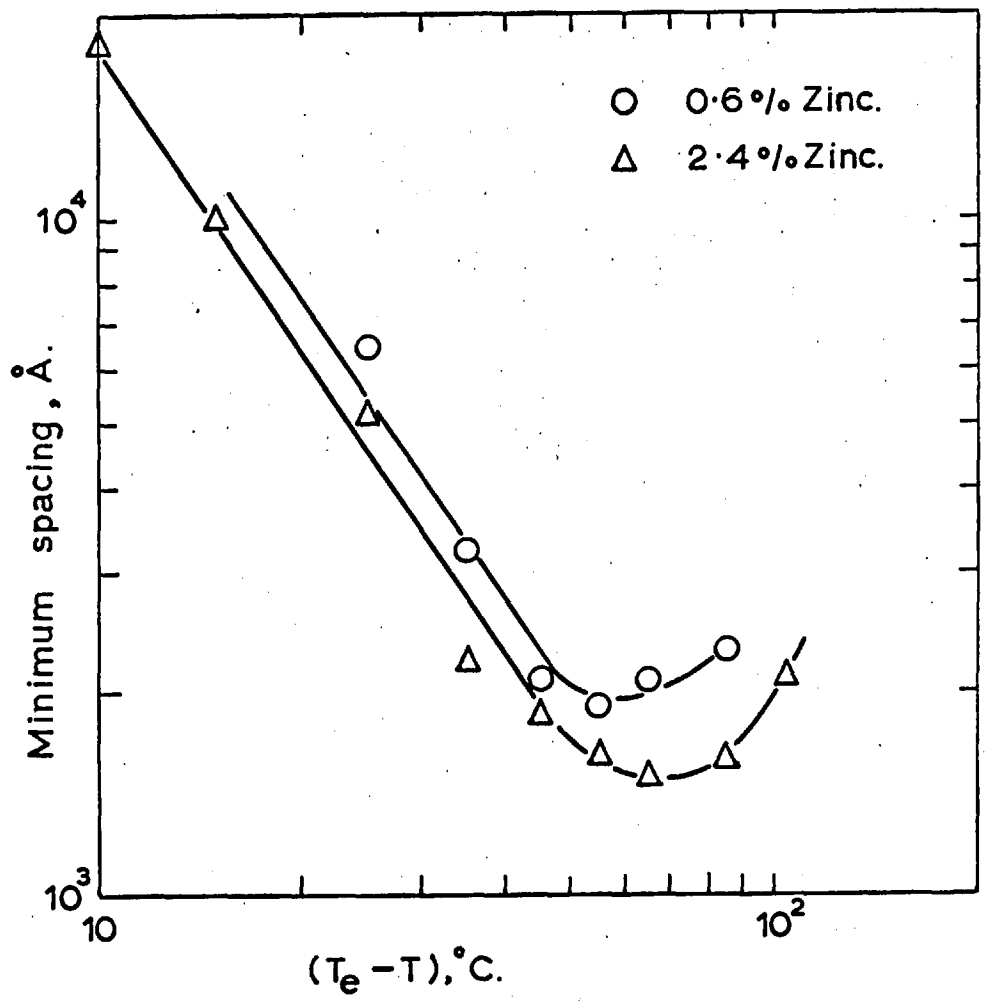

FIG. 29. Relation Between Interlamellar Spacing And Undercooling; Zinc Alloys.

It was indicated in the spacing measurements of binary alloys that the 'upturn', in the spacing vs undercooling data, is associated with the $\beta \rightarrow \beta_1$ reaction. Since in these two zinc alloys the $\beta \rightarrow \beta_1$ transformation temperatures differ by $10^{\circ}C$, it would support the view if the upturn temperatures show this difference at the the expected undercoolings. The graphs do show this effect and the difference in temperatures is $10^{\circ}C$ approximately.

(d) Copper - Aluminium - Tin System:

Interlamellar Spacing determinations were made on the 1.1% Sn alloy only. The range of temperature over which pearlite forms in this alloy is smaller than in the binary alloy or the ternary zinc alloys. A few additional samples transformed at other temperatures were also selected for spacing measurements. The results given in Table VI, are plotted in the usual way in Fig.30. The slope of the linear graph is -1.95 and the upturn in spacing coincides with the $\beta \rightarrow \beta_1$ transformation temperature.

Temp. °C	Interlamellar Spacing Å	G x 10^5 mm/sec
515	3300	25
520	3000	27
530	3300	65
535	5700	40
540	7300	21
545	8900	10

Table VI

Spacing and Growth rate

Data on the 1.1% Tin Alloy

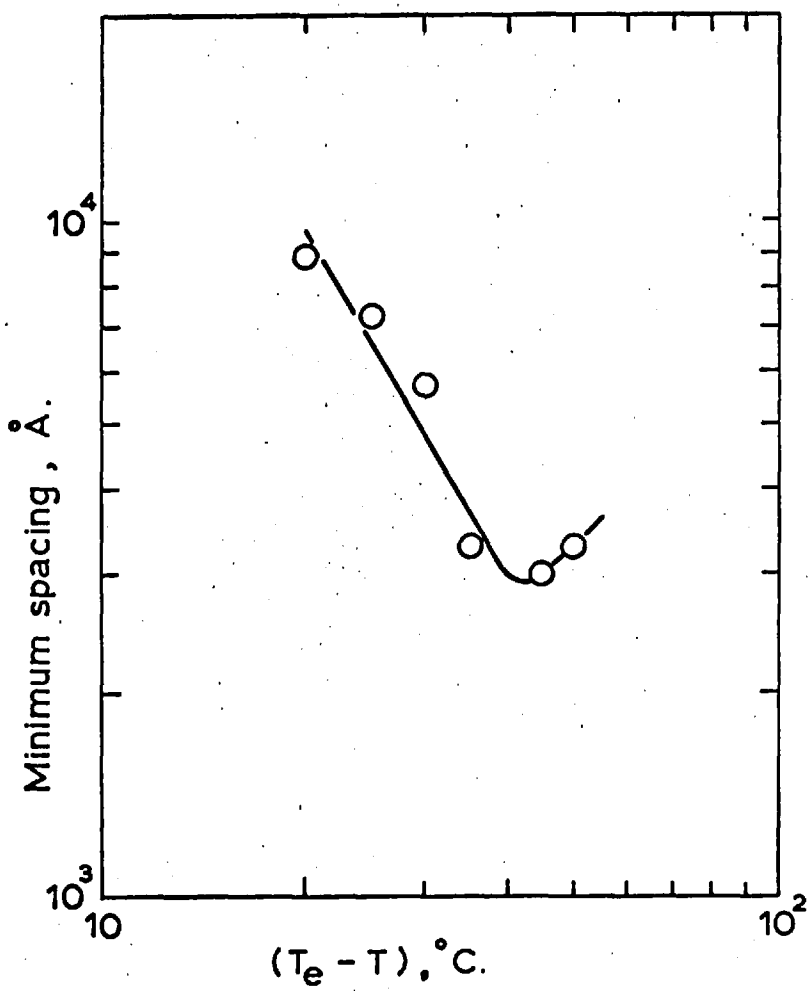

FIG. 30. Relation Between Interlamellar Spacing And Undercooling, 1.1% Tin Alloy.

CHAPTER VI.

DIFFUSION STUDIES.

A Diffusion in Binary Alloys:

(i) Introduction:

In phase transformations involving nucleation and growth processes, such as the pearlite reaction, the growth kinetics may be controlled either by interface reaction and / or by various diffusion processes. Growth kinetics would be better understood if all the diffusion rates were known. Diffusion data on carbon and other alloying elements in austenite are available. There is however no experimental information on the diffusion rates of aluminium and alloying elements in the β phase of the copper - aluminium system. In this section the results of the investigation on the diffusion coefficients of aluminium, in the β (CuAl) phase are presented.

The method adopted for the investigation employed diffusion couples in which one sample consisted of a mixture of α and β phases at the diffusion temperature selected while the other sample consisted of a $\beta_1\gamma_2$ phase mixture. With such a couple diffusion produced a region of β phase which

when quenched formed martensitic β' ; metallographic measurements of the extent of the β' region in couples reacted for different times were used to determine the rate of displacement of the β region into both the $\alpha + \beta$ and $\beta + \gamma_2$ samples.

Very recently a similar technique has been adopted by Frost and Castleman[44] on the growth kinetics of β-brass layers in saturated γ-brass vs α-brass diffusion couples. The results of their work show that interface displacements could be used for measuring diffusion coefficients and the interface equilibrium concentrations are not affected by pressure. Calculated diffusion coefficients compared within a factor of 2 with those obtained by standard methods.

The β field in the copper - aluminium system is rather narrow, and standard chemical methods would be difficult to apply in analysing concentration differences in the diffusion couple, apart from this, obtaining diffusion layers for chemical analysis is very time-consuming. However, advantage can be taken of the narrow phase field if Wagner's[45] method is adopted in determining the diffusion coefficient.

The calculation of the diffusion coefficient, using phase interface movements, was developed by

Wagner[45] and involves the assumption of a concentration independent diffusion coefficient, D_β. The interface reactions α/β and β/γ_2 are assumed to be rapid enough to be neglected. Thus the growth of the β layer is assumed to be controlled by the volume diffusion in the β. It is also assumed that the planes of discontinuity between β and $\alpha + \beta$ and β and $\beta + \gamma_2$ respectively are shifted proportionally with square root of time, i.e.

$$x_1 = k_1 2\sqrt{D_\beta t} \quad \ldots\ldots\ldots\ldots\ldots\ldots (19)$$

and $$x_2 = k_2 2\sqrt{D_\beta t} \quad \ldots\ldots\ldots\ldots\ldots\ldots (20)$$

Where x_1 and x_2 represent the distances of the planes of discontinuity from the original interface (See Fig.31(a)(b)), t is the time allowed for diffusion and k_1 and k_2 are dimensionless parameters, referring to the respective planes of discontinuity. These parameters are calculated using the compositions at the planes of discontinuity (i.e. $C_{\beta,\alpha}$ and C_{β,γ_2}) and the compositions of the samples (i.e. Co' 王 and Co'' 耳). The equations relating these quantities are given below.

$$\frac{C_{\beta\,\gamma_2} - C_{\beta,\alpha}}{C_{\beta,\alpha} - Co'} = \sqrt{\pi} \cdot k_1 \cdot \exp(k_1^2)\left[\operatorname{erf}(k_1) + \operatorname{erf}(k_2)\right] \quad \ldots\ldots (21)$$

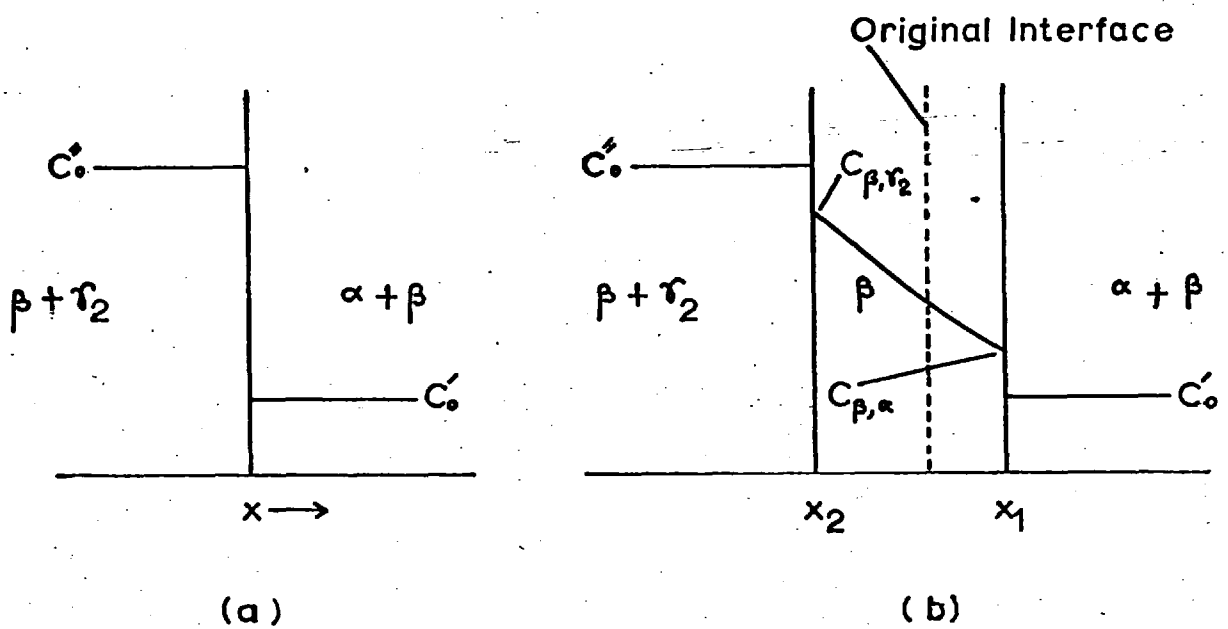

FIG. 31. Diffusion In Three Phase System

(a) At $t = 0$

(b) At $t > 0$

and

$$\frac{C_{\beta,\gamma_2} - C_{\beta,\alpha}}{C_0'' - C_{\beta,\gamma_2}} = \sqrt{\pi} \cdot k_1 \cdot \exp(k_2^2)\left[\operatorname{erf}(k_1) + \operatorname{erf}(k_2)\right] \quad \ldots \quad (22)$$

Knowing k_1 and k_2 from equations (21) and (22) and the rates of interface displacements, D_β can be calculated from equations (19) and (20). Changes in molar volume are ignored in making the calculation.

(ii) Experimental:

Two copper - aluminium alloys having compositions 13.6 and 9.1% aluminium respectively were made from electrolytic copper and superpurity aluminium. The compositions were checked by chemical analysis and by quantitative metallography. These alloys were gas melted and chill cast into 1 ¼" diameter ingots which were hot worked into 1/2" square bars and homogenised; samples 1/2 x 1/2 x 1/8" were machined to use for the diffusion couples.

A temperature range of 650°C to 750°C was selected for the diffusion experiments bearing in mind that the extent of the β field in the copper - aluminium phase diagram increases with temperature so that any errors resulting from the assumption that D_β

is concentration independent can be expected to increase with increase in temperature.

Prior to use in an experiment samples of the two alloys were heat treated to give a structure which would facilitate rapid attainment of equilibrium when the samples were eventually heated as part of a diffusion couple to a particular diffusion temperature. For the 13.6% Al alloy this initial treatment consisted of air cooling from the β range to give a relatively fine dispersion of γ_2 in β. In the case of the 9.1% Al alloy, samples were pre-annealed at the appropriate diffusion temperature followed by quenching to room temperature.

The contact surfaces for the diffusion samples were prepared to a metallographic finish, cleaned in alcohol, dried and pressed together in a steel clamp. The clamp containing the couple was placed in a stainless steel jig for insertion into a furnace, graphite powder was used to maintain a reducing atmosphere around the couple during the diffusion anneal.

The diffusion anneals were carried out in a 34" long vertical tubular furnace. The lower open end of the furnace tube was plugged with a refractory brick and the whole furnace was well insulated to

ensure against fluctuations of temperature within the furnace. Power was supplied through a variable transformer in series with a variable resistor. The temperature of the furnace was controlled by a Kelvin - Hughes proportional controller. A base metal thermocouple was used as a sensing element for the controller; the hot junction of the couple was placed near the windings of the centre portion of the furnace.

The diffusion couple was located in the furnace at the centre of a constant temperature zone 5 inches long and a noble metal thermocouple in contact with the diffusion couple served to measure the temperature. The temperatures were recorded on a Sunvic potentiometric recorder through-out the diffusion anneal. Measurements of the temperature were made with a potentiometer. The thermocouple was calibrated against the melting point of aluminium.

It took on an average 30 minutes for the diffusion couple to heat to the required temperature and then throughout the annealing period the temperature was controlled to within $\pm$ 2°C. After a suitable time the jig was removed from the furnace and water quenched. The samples were suitably sectioned and metallographically examined.

(iii) Results: and Discussion

Typical interfaces between $\beta/\alpha + \beta$ and $\beta/\beta + \gamma_2$ are shown in the photo-micrographs of Figs.32(a),(b): it is observed that the growth of β is columnar in the direction of diffusion and the effects of grain boundary diffusion can also be noticed. The $\beta/\alpha + \beta$ interface was typically parallel to the original surface of contact to within $\pm$ 1 micron. The $\beta/\beta + \gamma_2$ interface as in Fig.31(b) is less clearly defined but nevertheless could be measured to within $\pm$ 2 microns.

A typical graph showing the extent of the β region produced by diffusion at 700°C in the $\alpha + \beta$ and $\beta + \gamma_2$ samples against square root time is shown in Fig.33. The data confirm the assumption that the interface displacements are proportional to square root time, and this parabolic relationship is in agreement with the idea that the growth of the β region is controlled by volume diffusion. This latter point is especially important in view of the fact that the samples of the couples did not weld together but separated after removal from the clamp, presumably due to a **very thin** oxide film.

The calculated values of D_β for the various temperatures used are shown in Table VII, together

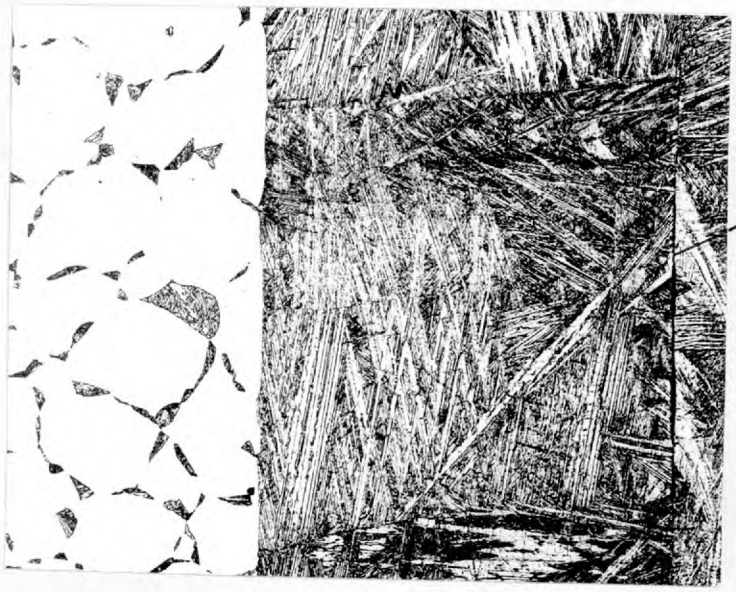

FIG.32(a) Microstructure of the β / $\alpha+\beta$ interface after 4 hours at 700°C. x 150

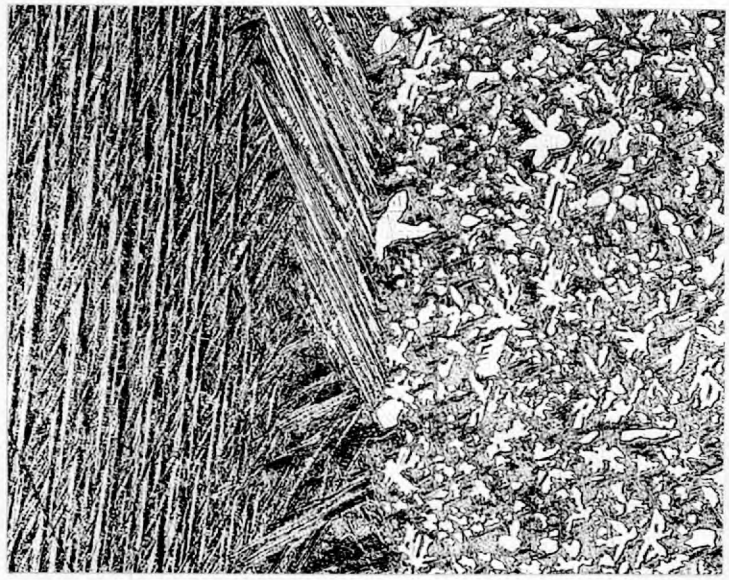

(b) Microstructure of the β / $\beta + \gamma_2$ interface in the same diffusion couple. x 150

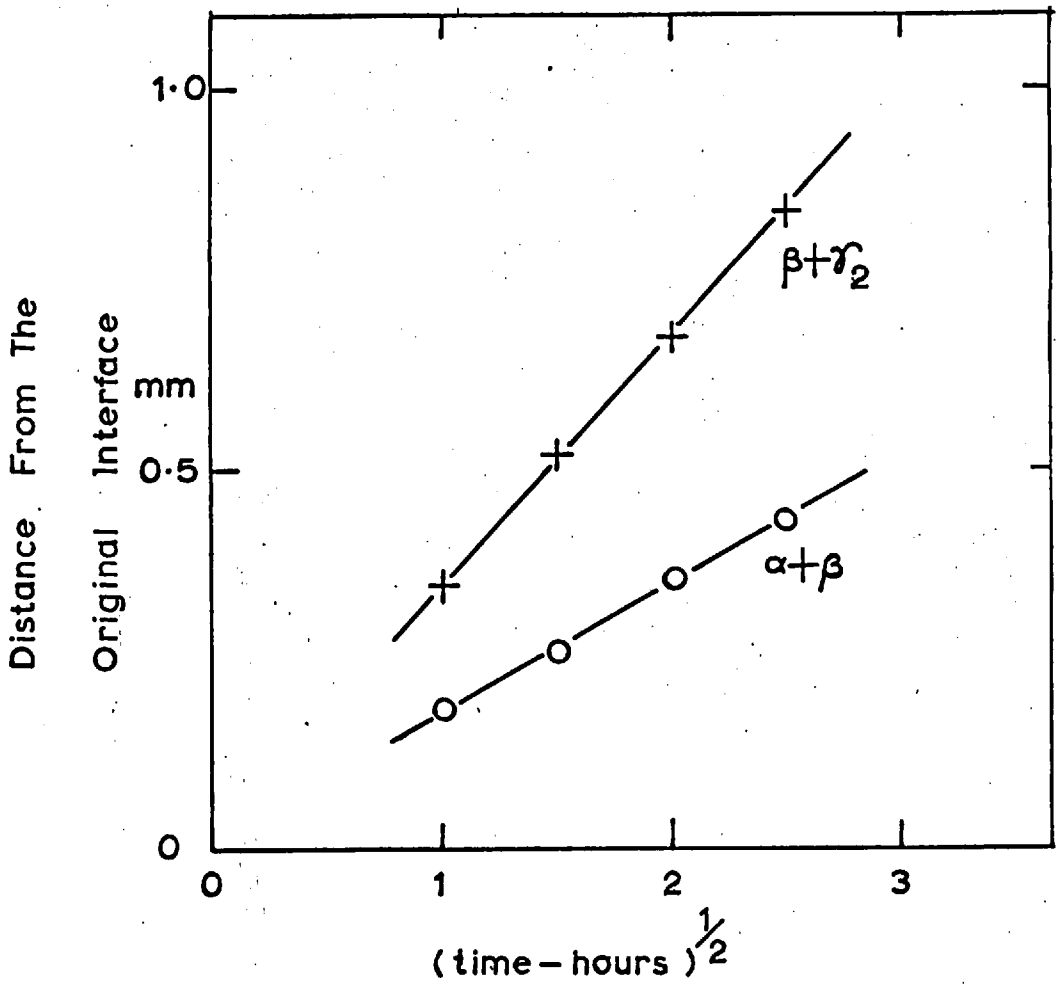

FIG. 33. Growth Of β In α+β And β+γ2 Fields At 700 °C

	Temp °C	$x_1/\sqrt{t}$ mm/h$^{1/2}$	k_1	$D^\beta k_1$ cm^2/sec	$x_2/\sqrt{t}$ mm/h$^{1/2}$	k_2	$D^\beta k_2$ cm^2/sec
1	646	0.082	0.290	5.6×10^{-8}	0.142	0.507	5.5×10^{-8}
2	672	0.116	0.338	8.2×10^{-8}	0.211	0.633	7.8×10^{-8}
3	700	0.166	0.382	1.3×10^{-7}	0.327	0.762	1.3×10^{-7}
4	725	0.230	0.420	2.1×10^{-7}	0.458	0.960	1.6×10^{-7}
5	750	0.272	0.455	2.5×10^{-7}	0.631	1.20	1.9×10^{-7}

Table VII

Diffusion coefficient of aluminium in the β phase using k_1 and k_2 parameters

with the rates of displacements of the interfaces ($x_1/\sqrt{t}$ and $x_2/\sqrt{t}$) derived from data such as are illustrated in Fig.33, and values of k_1 and k_2. These last mentioned were obtained by using a graphical method for solution of the equations (21) and (22) and taking values of C_{β,γ_2} and $C_{\beta,\alpha}$ from the copper - aluminium phase diagram[9].

It was found that for the temperatures 646°, 672° and 700°C the values of D_β obtained from the two different parameters k_1 and k_2 agree very closely, whereas for 725° and 750° somewhat differing values were obtained. This is thought to be probably due to the wider compositional range of the β field at these higher temperatures and hence the composition dependence of D_β becoming more significant. The heating-up time of the couple assembly to the annealing temperature was not considered; the use of rates of displacements in the calculation eliminates the errors introduced.

In Fig.34 the data are shown as an Arrhenius plot which gives a value of 27.5 K.Cals/mol. for the activation energy of diffusion. The straight line is drawn based mainly on the lower temperature points assuming the composition dependence of D_β is less significant at these temperatures.

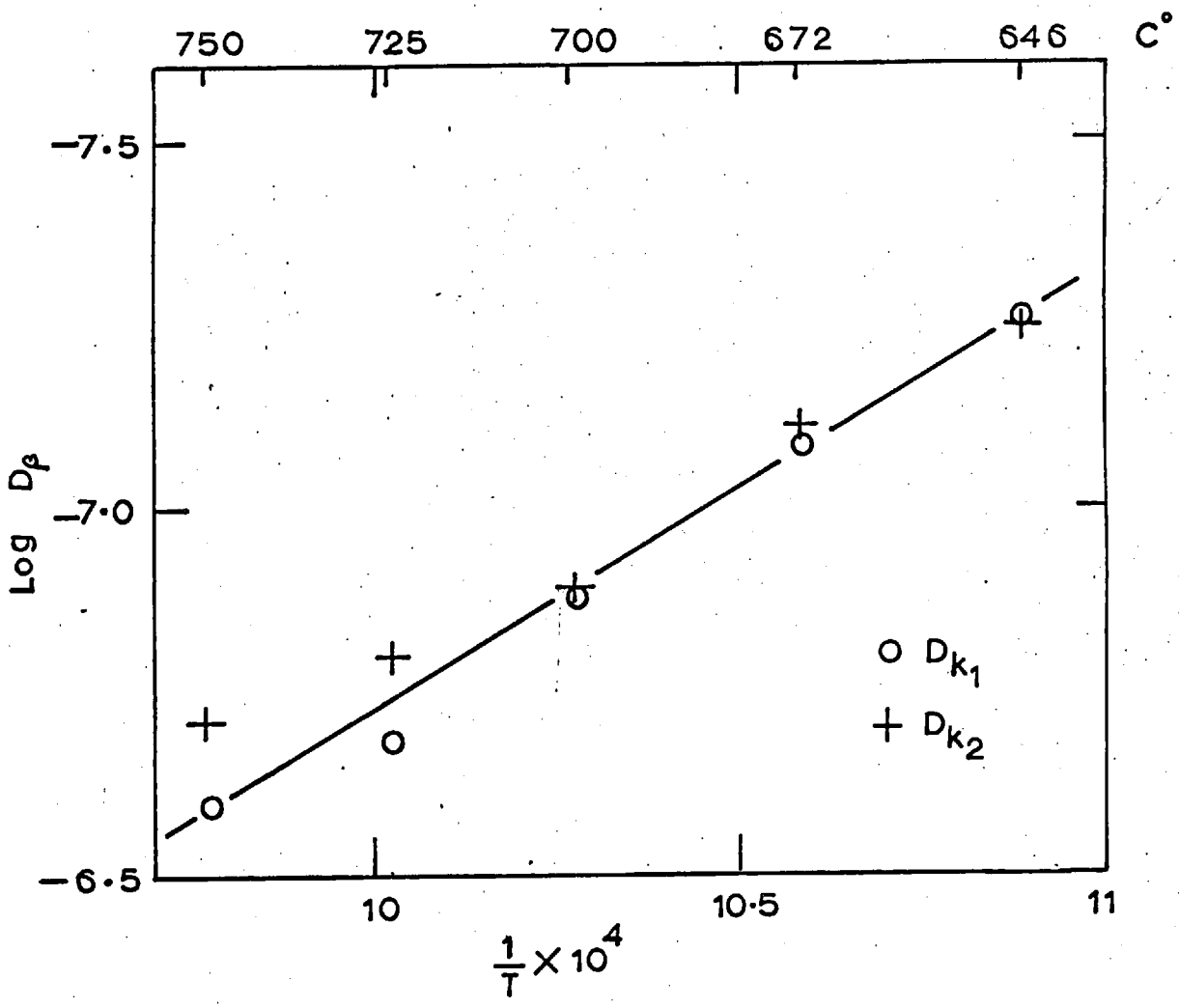

FIG. 34 Temperature Dependence Of Diffusion Coefficient

Comparison of the present data with those of Rhines and Mehl[46] for the diffusion in α - CuAl alloys shows that the diffusion coefficient is greater in the β phase and the activation energy is almost half that in α. This is consistent with results obtained on other systems in which both α and β phases have been studied, e.g. Cu-Zn[47,48].

A check was made on the present results by another series of controlled diffusion experiments but with different couple conditions. The appropriate equations developed for the purpose and the results obtained thereby are given in the Appendix. The results of these experiments substantiate the values obtained in the main investigation.

B Diffusion Studies in the Ternary Alloys:

(i) Introduction:

There has been comparatively little work done on diffusion in multicomponent systems because of the complicated nature of the diffusion process and the experimental difficulties in determining the various interacting coefficients. A well known example of ternary diffusion is due to Darken[49]. In the Fe - C - Si system it was observed that carbon diffused from a uniform composition in the

Fe - C / Fe - C - Si couple such as to segregate to the Fe - C part of the couple because of the activity gradient introduced by the silicon. Similar experiments have been made with other alloying elements in ferrous systems, but ternary diffusion involving carbon is different from the cases involving substitutional elements with respect to the rates encountered. The diffusivity of carbon is extremely high compared to most of the alloying elements so that some simplification of the solutions to the diffusion equation is possible as pointed out by Kirkaldy[50]. Diffusion in substitutional multicomponent systems has been examined and the results obtained in the Cu - Zn - Al system have been discussed by Kirkaldy et al[51]. The present investigation uses this analysis.

The generalized flux equation for linear diffusion is given by

$$J_i = - \sum_{k=1}^{n-1} D_{ik} \cdot \frac{\partial C_k}{\partial x} \quad \ldots\ldots\ldots\ldots \quad (23)$$

where n - the number of components.

In a three component system there are two independent concentrations whose flux equations would be

$$J_1 = - D_{11} \frac{\partial c_1}{\partial x} - D_{12} \frac{\partial c_2}{\partial x} \quad \ldots\ldots\ldots\ldots \quad (24)$$

$$J_2 = - D_{21} \frac{\partial c_1}{\partial x} - D_{22} \frac{\partial c_2}{\partial x} \quad \ldots\ldots\ldots\ldots \quad (25)$$

If the concentration differences are small the Dik terms may be regarded as independent of concentrations. The flux equations combined with mass balance equations give the diffusion equations

$$\frac{\partial c_1}{\partial t} = D_{11} \frac{\partial^2 c_1}{\partial x^2} + D_{12} \frac{\partial^2 c_2}{\partial x^2} \quad \ldots\ldots\ldots\ldots \quad (26)$$

$$\frac{\partial c_2}{\partial t} = D_{21} \frac{\partial^2 c_1}{\partial x^2} + D_{22} \frac{\partial^2 c_2}{\partial x^2} \quad \ldots\ldots\ldots\ldots \quad (27)$$

where D_{11} - diffusion of component 1, (say Al), under its own gradient.

D_{12} - diffusion of component 1 under a gradient of component 2, (say the ternary element Zn or Sn).

D_{22} - diffusion of component 2 under its own gradient.

D_{21} - diffusion of component 2 under a gradient of component 1.

The above equations (26) and (27) have been solved in terms of error functions with certain boundary conditions. If suitable experiments are designed then the 'off diagonal', D_{12} and D_{21}, diffusion coefficients can be determined. For this it is necessary that at least one of the independent concentrations has a large gradient in order to obtain substantial cross effects. In the ternary alloys of Cu - Al - Zn (or Sn) the concentration of either aluminium or ternary element can only be varied within a limited range if the composition is to remain in the single phase β region. The only approach, in the diffusion work in the present case, is then to vary the concentration of the ternary alloying element, within a very narrow range.

The components of the diffusion couple with these conditions would be a binary eutectoid alloy and a dilute ternary alloy of eutectoid composition. Since in such a couple the concentration difference of aluminium is small it is expected that the off diagonal coefficient D_{21} will be very small and may be assumed to be zero. Redistribution of aluminium from a nearly equal concentration state due to the concentration difference of the ternary alloying element is effected primarily by the coefficient D_{12}.

It was not possible to determine the distribution of aluminium with the electron - probe - micro - analysis which was employed for the determination of alloy concentrations.

Ternary Cu - Al - Zn alloys

(ii)a Experimental:

Diffusion couples were prepared from a binary eutectoid and a ternary alloy whose aluminium content was so adjusted as to be in the eutectoid valley. This ternary alloy contained 11.5% Al and 2.4% Zn and was the one that was used in the growth rate experiments. The couple alloys were in the fully homogenised and quenched condition showing the β' martensitic structure. Square sections of 1/2 x 1/2 x 1/8 in. were machined from the binary eutectoid alloy while rectangular sections of 1/2 x 3/8 x 1/8 in. were machined from the zinc containing alloy. The size difference enabled the alloys to be readily distinguished from one another. The surfaces of contact were prepared to a metallographic finish, washed in alcohol and dried before clamping the polished surfaces together in a steel clamp. The diffusion anneal experiments were carried out exactly as described previously in the case of the binary alloys. The temperatures

selected were 750, 725, 700, 675 and 650°C. The couples were quenched after a suitable time, sectioned and suitably mounted in bakelite. After polishing the sectioned surface, graduation marks were scribed parallel to the original interface on either side of it at intervals of 127 microns. Concentration penetration curves for zinc were obtained by analysing concentrations of zinc at the intervals marked on the specimen. The analysis for zinc was done in a Cambridge Scanning Electron probe X-ray micro-analyser. It consists of using a focused electron beam to excite X-rays from a region in the surface of the specimen, and then subjecting the X-rays to a spectral analysis to obtain the chemical composition of the region. The concentrations reported are accurate to $\pm$ 0.05 wt% Zn.

(iii) Results:

A typical concentration distance curve is shown in Fig.35, for the distribution of zinc. Concentrations are plotted in atomic percent so that the Matano method can be applied for the determination of diffusion coefficients.

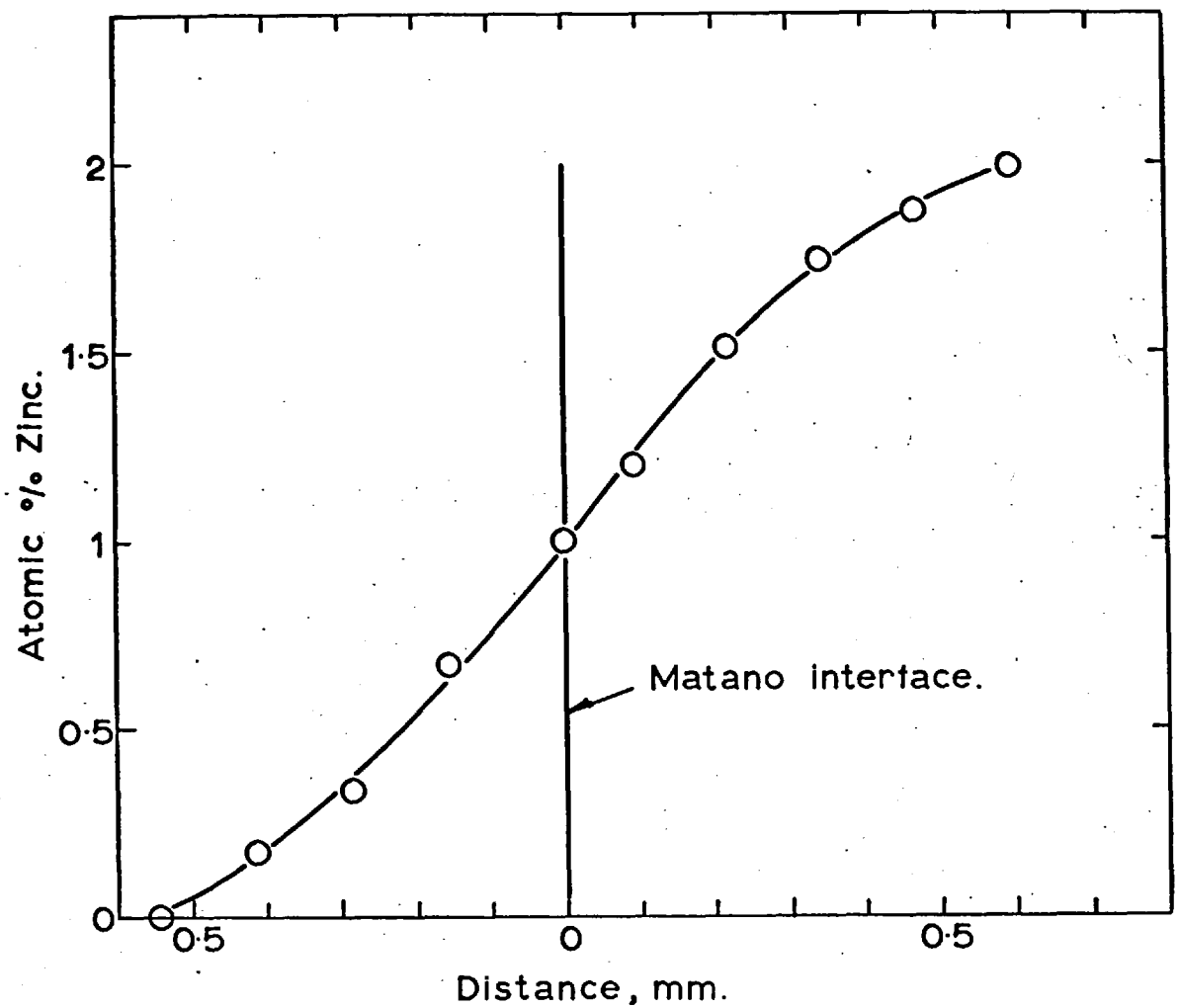

FIG. 35. Concentration Distance Curve For Zinc,

750 °C – 2 Hours.

The relevant diffusion equation in this case is

$$\frac{\partial C_2}{\partial t} = \frac{\partial}{\partial x}\left(D_{21}\frac{\partial C_1}{\partial x}\right) + \frac{\partial}{\partial x}\left(D_{22}\frac{\partial C_2}{\partial x}\right) \quad \ldots\ldots \quad (28)$$

Since D_{21} is assumed to be zero, it becomes

$$\frac{\partial C_2}{\partial t} = \frac{\partial}{\partial x}\left(D_{22}\frac{\partial C_2}{\partial x}\right) \quad \ldots\ldots\ldots\ldots\ldots\ldots \quad (29)$$

The solution to this equation can be obtained with appropriate boundary conditions and the assumption of a parametric form combining the time space variation of concentration

i.e. $C = C(\lambda)$ where $\lambda = x/\sqrt{t}$

The solution is

$$D_{22} = \frac{1}{2t} \cdot \frac{dx}{dC_2} \cdot \int_0^{C_2} x \, dC_2 \quad \ldots\ldots\ldots \quad (30)$$

The integration was carried out graphically between the limits $C_2 = 0$ to $C_2 = 0.5\%$. The reciprocal of the concentration gradient at this composition was determined from the slope of the concentration distance curve. Knowing the time of the diffusion anneal D_{22} was calculated.

As the concentration difference is small it may be possible to apply the Grube method. To explore this possibility, the ratio of the

concentration at any particular distance to the maximum concentration is plotted against the distance on probability paper. One such plot is given in Fig.36 which shows a linear relationship indicating the independence of diffusion coefficient on concentration within this concentration range. The diffusion equation in such a case is

$$\frac{\partial C_2}{\partial t} = D_{22}\frac{\partial^2 C_2}{\partial x^2} \quad \ldots\ldots\ldots\ldots\ldots\ldots\ldots\ldots (31)$$

The solution suitable for the Grube method is

$$C_2 = \frac{C_o}{2}\left[1 - \operatorname{erf}\left(\frac{x}{2\sqrt{D_{22}t}}\right)\right] \quad \ldots\ldots\ldots\ldots (32)$$

where C_2 - concentration of zinc at a distance x after a time t

C_o - maximum concentration of zinc

All terms except D_{22} are known experimentally and using tables of probability integrals the diffusion coefficient D_{22} can be evaluated.

Diffusion coefficients calculated by both the methods are presented in table VIII and in the Arrhenius plot in Fig.37. The slope of the best fit straight line gives an activation energy of diffusion of 30.2 K.Cals/mol. It may be seen that both the

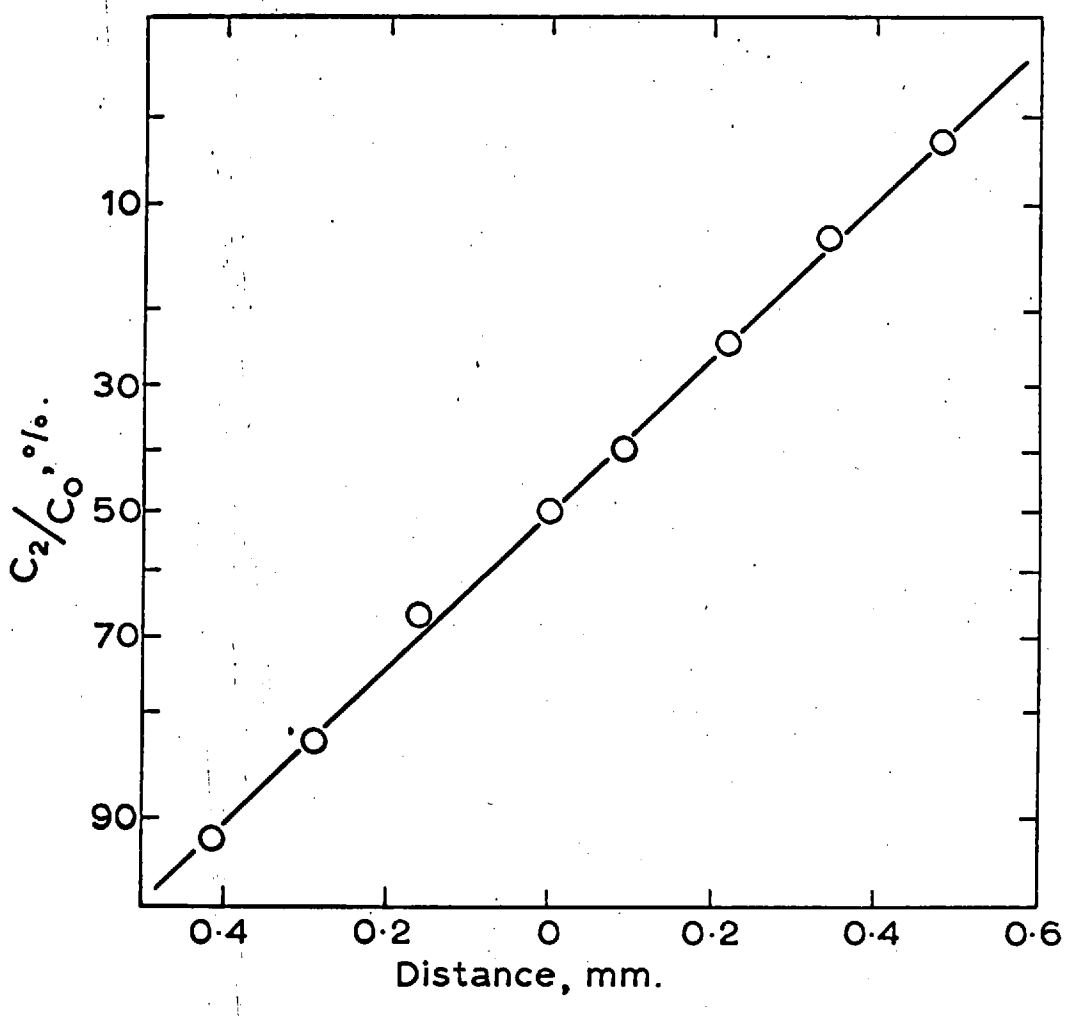

FIG. 36. Probability Plot For The Zinc Alloy, 750°C - 2 Hours

Temp °C	D_{β}^{Zn} cm^2/sec 0.5% Zn Matano	$D_{at.\beta}^{Zn}$ cm^2/sec 0.03 cm Grube
650	1.0×10^{-8}	1.3×10^{-8}
675	1.7×10^{-8}	1.7×10^{-8}
700	1.8×10^{-8}	2.2×10^{-8}
725	4.5×10^{-8}	4.8×10^{-8}
750	5.0×10^{-8}	6.2×10^{-8}

Table VIII

Diffusion coefficient of zinc in the β - Cu - Al phase obtained by the Matano and the Grube Methods

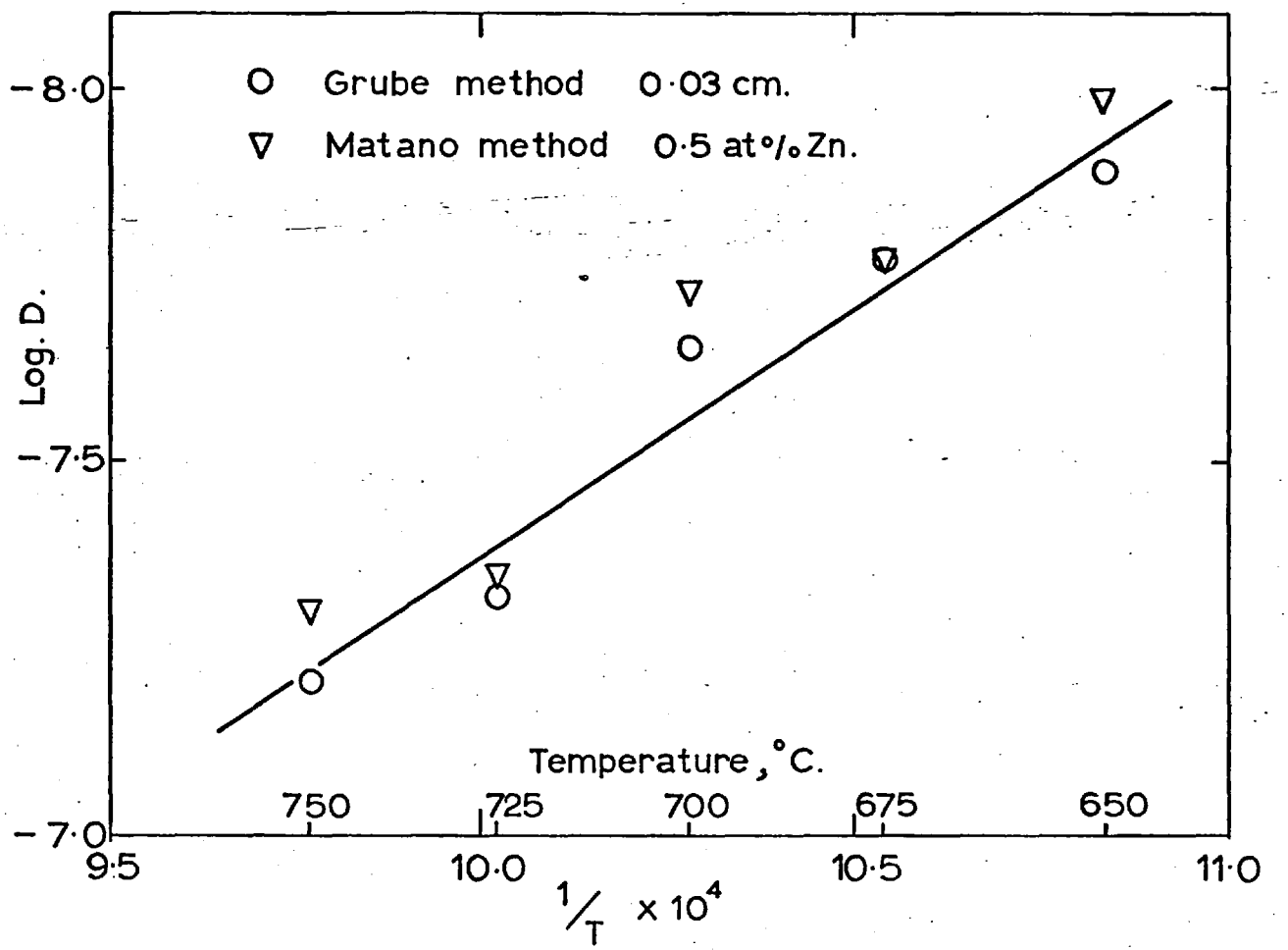

FIG. 37. Temperature Dependence Of Diffusion Coefficient Of Zinc In The β (CuAl) Phase.

methods give very nearly the same values for diffusion coefficients, implying that the diffusion coefficient of zinc is insensitive to concentrations in the range 0 to 2.4%.

Diffusion in Ternary Cu - Al - Sn alloys

(ii)b Experimental:

The experimental methods were similar to those described in the Cu - Al - Zn section. The ternary alloy contained 3.2% Sn (1.5 at %) and 10.4% Al. Three couples were annealed at 725, 700 and 675°C. In addition to couples made as described for the Cu - Al - Zn, several couples of binary eutectoid and ternary tin alloys were prepared by spot welding 3/8 x 3/8 x 3/16 in. pieces of the two alloys. The welding occurred over a small region approximately 3/16 in. diameter. It was found that the weld interface was deformed due to the temperature and pressure at the time of welding. This resulted in a non-planar interface in several cases. Only three couples had reasonably flat interfaces and were subsequently analysed for diffusion work. One of these couples was made up of 4.2% Sn (2.0 at % Sn) and 9.8% Al, and a binary eutectoid alloy. The welded couples were annealed at 603°C and 760°C for suitable periods and quenched.

Specimens for the micro - analyser were prepared as before and the concentrations of tin determined at regular intervals. A typical concentration - distance curve for the tin alloy is shown in Fig.38.

Diffusion coefficients were calculated by the Grube method. The probability plot, Fig.39, indicated that the Grube method could be applied without serious error.

(iii)b Results:

The diffusion coefficients calculated for the various temperatures are given in table IX. The activation energy for diffusion, calculated from the slope of the Arrhenius plot Fig.40, was 28.6 K.Cals/mol.

It may be observed from the results of welded and clamped couples that there is no noticeable effect due to welding. This is not surprising since in binary alloys non - welding of the couples did not inhibit diffusion and the results showed consistent parabolic growth of the β phase. It is very likely that an extremely fine film of oxide, which allows atoms to diffuse through, prevents the welding of the couples during annealing.

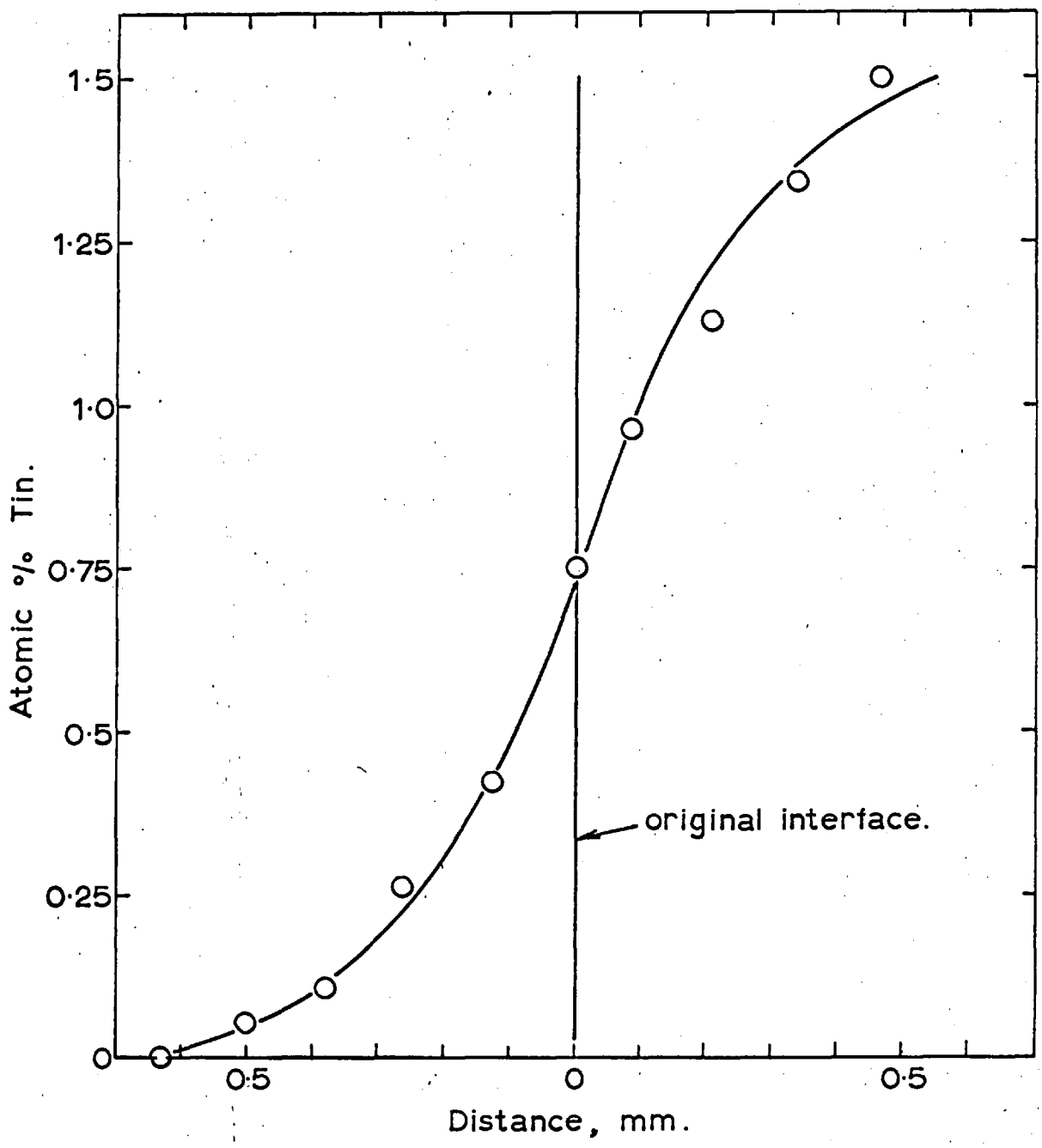

FIG. 38. Concentration Distance Curve For Tin, 725 °C – 4 Hours.

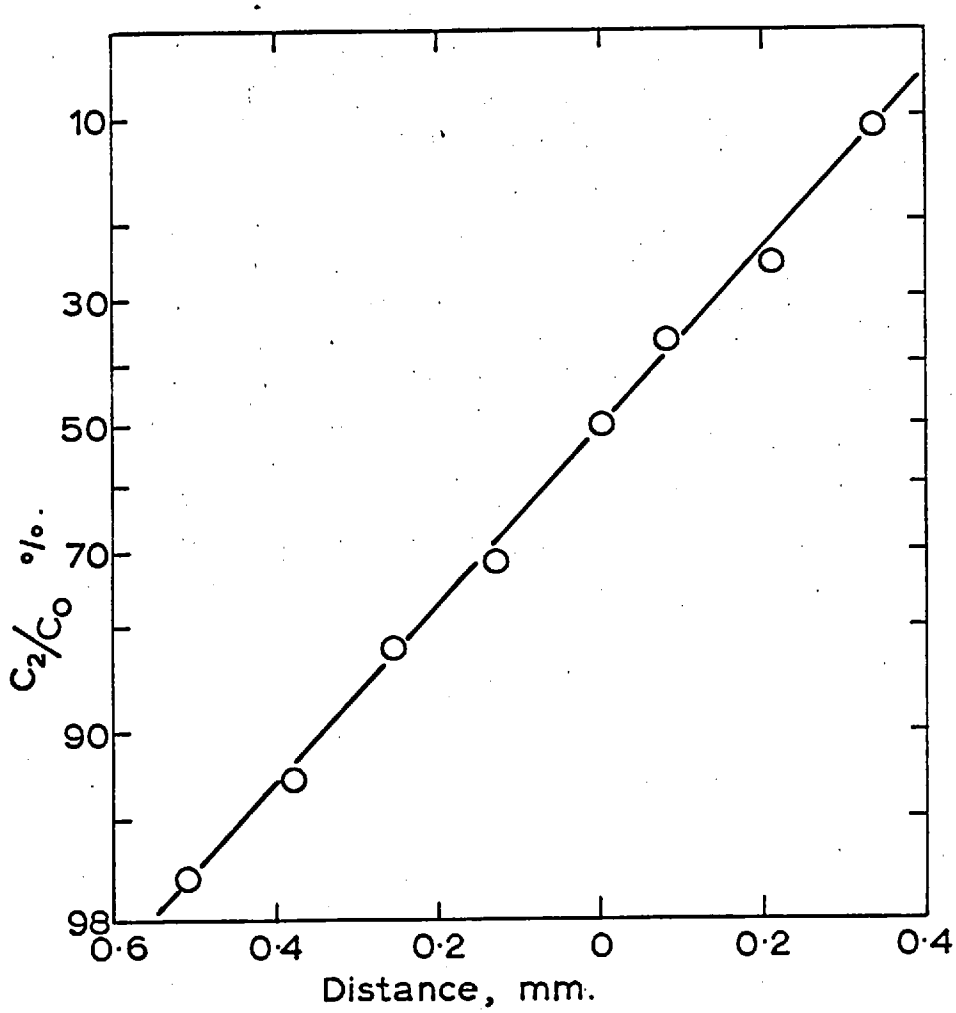

FIG. 39. Probability Plot For The Tin Alloy, 725 °C – 4 Hours

Temperature °C	D_{β}^{Sn} cm^2/sec
603 - Weld Couple	5.2×10^{-9}
675 - Clamped Couple	1.5×10^{-8}
700 - " "	2.3×10^{-8}
725 - " "	2.8×10^{-8}
760 - Weld Couple with 3% Tin	7.1×10^{-8}
760 - Weld Couple with 4% Tin	5.1×10^{-8}

Table IX

Diffusion coefficient of tin in the β - Cu - Al

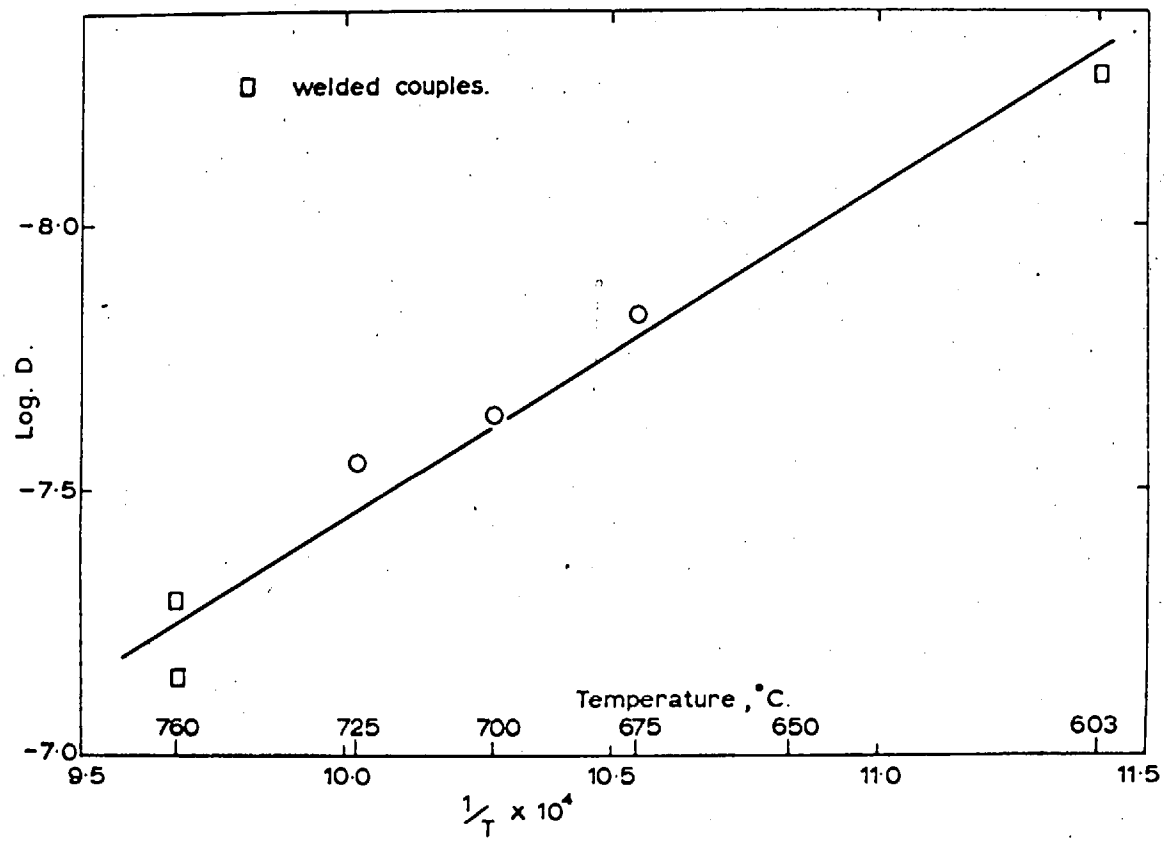

FIG. 40. Temperature Dependence Of Diffusion Coefficient Of Tin In The β (Cu Al) Phase.

(iv) Discussion

The results of these experiments have indicated that the diffusion rates of zinc and tin are very similar to one another in β - CuAl and have approximately equal activation energies for diffusion. Small concentration differences seem to have no significant effect on the diffusion coefficients. Comparison between the diffusion coefficients of aluminium in β - CuAl with those of zinc or tin shows that aluminium diffuses somewhat faster than either zinc or tin by a factor of about 5.

Now for the pearlite growth problem it is important to know, not only the diffusion rates of aluminium, zinc or tin but also the interacting off - diagonal coefficient D_{12}. However the determination of the coefficient D_{12} is through its effect upon the distribution of aluminium in a diffusion couple of initial uniform composition of aluminium[51]. The maximum difference ΔC_1 in the concentration of aluminium is given by[51]

$$\Delta C_1 = \frac{D_{12}}{D_{11}} \cdot \frac{C_{20} - C_{21}}{2} \cdot \frac{1}{1 - \phi} \left[\operatorname{erf} \frac{\lambda_m}{2\sqrt{D_{11}}} - \operatorname{erf} \frac{\lambda_m}{2\sqrt{\phi D_{11}}} \right] \quad \ldots \quad (33)$$

where

C_{20} - concentration of ternary element in binary eutectoid at $x > o$ and $t = o$; $C_{20} = 0$ in the present case

C_{21} - concentration of the ternary element in the ternary couple at $x < o$ and $t = o$ i.e. C_{21} = concentration of the ternary alloy

$$\phi = \frac{D_{22}}{D_{11}}$$

and λ_m = maximum value of $\lambda = \frac{x}{\sqrt{t}}$

Equation (33) is obtained from the error function solution to the diffusion equation (26) with certain boundary conditions.

In the present case it was not possible to determine experimentally the distribution of aluminium in such a couple. Kirkaldy et al[51] have indicated that when the coefficients D_{11} and D_{22} are of the same magnitude the off - diagonals tend to become moderated. It is therefore assumed that the coefficient D_{12} is quite small.

CHAPTER VII.

PARTITIONING.

(i) Introduction

During the growth of pearlite in ternary alloys, the ternary alloying element can segregate to either of the two phases of pearlite depending upon the temperature of transformation, the growth rate of pearlite, the interlamellar spacing and the diffusivity of the element in the matrix or in one of the product phases or along the interface. This selective segregation has been termed partitioning. At some relatively low temperatures partitioning may not occur during the growth and therefore the two phases may show the same concentration of the ternary element in the two phases of pearlite as in the matrix. Thus it may be argued that the ternary element does not influence the growth rate at these temperatures where partitioning is not taking place.

In alloy steels it is known[32,52,55] that elements like chromium, vanadium, tungsten, molybdenum and manganese partition to the carbide and elements like nickel, cobalt and silicon partition to the ferrite. Investigations on the partitioning of molybdenum in Fe - C - Mo steels have been reported

by Bowman[52,53,54] and the partitioning of silicon and nickel to ferrite by Kuo and Hultgren[55]. Recently Pickelsimer[32] and others have studied the partitioning behaviour of manganese in steels. However, only in the case of manganese, have the data been complete regarding the temperature effect of partitioning.

The results have indicated that partitioning to selected phases occurs at high subcritical temperatures where the diffusion rates of the ternary elements are comparatively higher and there are longer times available for the formation of carbide and ferrite because of the slow growth rates of pearlite. At lower temperatures partitioning may not take place, and hence there is no diffusion of the ternary element to either of the phases. The growth rate may then be regarded as independent of the diffusion of the ternary element. Under these circumstances the explanation for the effect of the ternary element on the growth rate has to be modified. Kirkaldy[36] has explained that the addition of manganese changes the constitutional diagram so as to reduce the carbon potential and thus reduce the growth rate. It was suggested[19] that since non - partitioned pearlite is not an equilibrium product, the free energychange from austenite to

pearlite is less than it would be with the equilibrium product, and hence the growth rate would be smaller.

(ii) Experimental Method

In ferrous systems the partitioning experiments consisted in transforming austenite to pearlite and then extracting the carbides electrolytically. The separated carbides were analysed chemically as well as by X - ray techniques. This method was not applied to the Cu - Al - Zn and Cu - Al - Sn systems as preliminary experiments indicated that the separation of γ_2 (or α) phase was difficult.

If a powder sample of the alloy were to be transformed to pearlite then the lattice parameter of either α or γ_2 obtained by transforming the alloy at different reaction temperatures would indicate the change if there is a partitioning occurring.

Experimental Procedure

Filed powders of 300 mesh were obtained from homogenised samples of binary eutectoid, 2.4% zinc and 1.1% tin alloys, and were sealed in small silica tubes under vacuum. After soaking in the β region the samples were transformed to pearlite in salt baths at 550, 540 and 520°C and then quenched in water. X - ray Debye - Scherrer pictures of the

transformed powders were taken with a 11.483 cm. camera, using Cu - Kα radiation. A set of samples were kept in a salt bath at 550°C for 10 days to determine the equilibrium lattice parameter of α. Well defined F.C.C. lines (belonging to the α phase) were measured with the aid of a travelling microscope.

(iii) Results and Discussion

The results of the lattice parameter measurements are presented in table X. The partition experiments were intended for determining the temperature at which the ternary element ceased to segregate to a particular phase. As is observed from the table X, there is no change in the lattice spacings of the α phase. The results of the equilibrium samples are the same as those of shorter times and lower temperatures. The binary alloy was intended for comparison purposes.

The results show that equilibrium concentrations of the ternary alloying element in α phase are achieved during the formation of the pearlite. Zinc or tin are able to diffuse to the α phase rapidly enough so that the pearlite reaction is not limited by the rate of diffusion of these

Alloy	Lattice Parameter A		
	520°C - 8 mts	540°C - 10 mts	550°C - 10 days
Binary Eutectoid	3.666	3.666	3.666
Cu - Al - Zn	3.667	3.667	3.667
2.0 at % Zn			
Cu - Al - Sn	3.668	3.668	3.668
0.5 at % Sn			

Table X

Lattice parameter of the

α - phase in Pearlite at temperatures

elements. This is not surprising since the diffusion experiments, described in the last section, showed that the rates of diffusion of zinc or tin in the β (Cu - Al) phase are of the same order of magnitude as that of Al in the β phase. On the other hand in ferrous pearlites, the rate of diffusion of carbon is several orders of magnitude larger than any substitutional alloying element and the formation of pearlite is possible without the appropriate partitioning of the ternary element.

CHAPTER VIII.

DISCUSSION ON THE GROWTH KINETICS OF PEARLITE.

(i) Introduction

The theoretical developments of the kinetics of pearlite growth have so far been specifically referred to the pearlite in ferrous systems. In the present investigation an attempt is made to apply the basic ideas to the pearlite growth problem in binary Cu - Al and ternary Cu - Al - Zn (or Sn) alloys. Hence it is felt necessary to develop the essential details of the ferrous pearlite problem prior to their adaptation. A critical assessment of the applicability is also given.

A mechanism of growth of pearlite from austenite was first discussed by Mehl[56]. It was by then recognised that such a process consisted in the formation of ferrite and cementite from a homogeneous austenite phase. The reaction was expected at the interface without involving the matrix lying at a small distance away from the interface. Since the growth rate was found to be constant with time it was

deduced that a steady state process was achieved. The bulk of the pearlite reaction was assumed to be due to the growth of the lamellae in the edgewise direction. Mehl proposed that the growth rate was dependent upon the active concentration gradient set up in the austenite just ahead of the interface, the interlamellar spacing and the diffusivity of carbon in austenite. Hultgren[57] suggested a method of obtaining the carbon concentrations ahead of the centres of the ferrite and cementite lamellae by extrapolating the equilibrium Austenite + Ferrite / Austenite and the Austenite + Cementite / Austenite phase boundaries into metastable regions as shown in Fig.41. This would enable the concentration gradients to be calculated. With the foregoing considerations Mehl[56,18] obtained the growth rate equation

$$G = \frac{K D^{\gamma}_{c}}{S_o} \quad \ldots\ldots\ldots\ldots\ldots\ldots\ldots\ldots\ldots\ldots (34)$$

where

G - growth rate in units of mass / unit area - sec

S_o - interlamellar spacing

D^{γ}_{c} - diffusivity of carbon in austenite

K - a proportionality constant inclusive of concentration difference

(ii) Diffusion Equations

The growth rate equation (34) is valid regarding its general applicability but the limitations of each of the terms have been recognised after a detailed analysis. Since the growth process was considered a steady state phenomenon, independent of time, it implied that the concentration gradients set up in front of the pearlite - austenite interface remained fixed, assuming there was no displacement of the pearlite relative to the austenite due to volume changes. Hull and Mehl[20], therefore suggested that a differential equation in two dimensions should be solved to obtain the areal distribution of carbon concentrations within the small distance in austenite. It was necessary to assume that the pearlite lamellae were normal to the moving interface and maintained a constant spacing. A schematic three dimensional model was depicted (See Fig.42) to show the distribution of the concentration contours.

Brandt[21] obtained a solution to the diffusion equation to evaluate K in equation (34) assuming a

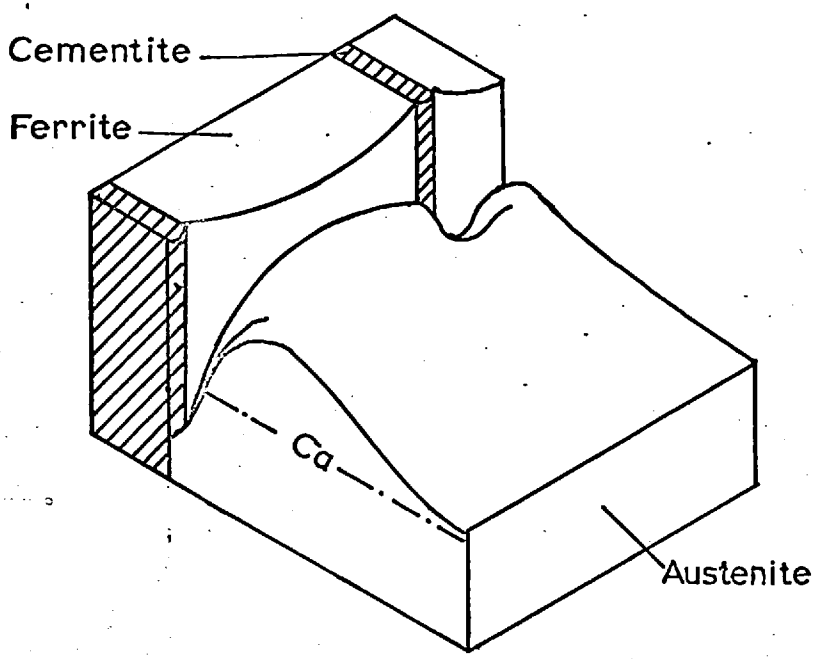

FIG. 42. Three Dimensional Model Showing Schematic Concentration Contours

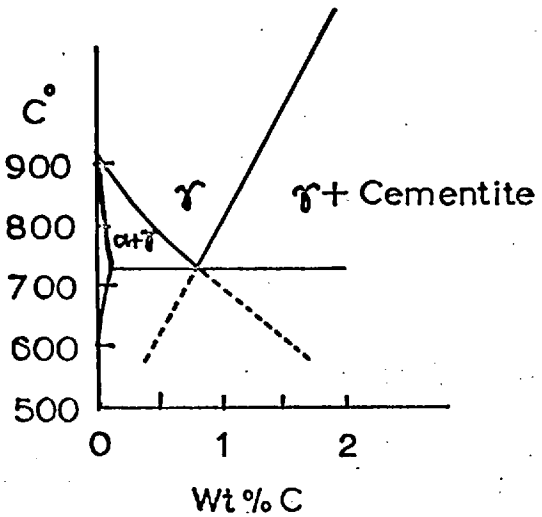

FIG. 41. The Hultgren Extrapolation Of The Phase Boundaries

concentration independent diffusion coefficient. Since the interface was moving with a constant velocity G, a set of rectangular co - ordinates was chosen such that the x and y axes were normal and parallel to the direction of growth respectively and moved with the same velocity G. The diffusion equation in two dimensions

$$\frac{\delta C}{\delta t} = D\left\{\frac{\delta^2 C}{\delta x^2} + \frac{\delta^2 C}{\delta y^2}\right\} \quad \ldots\ldots\ldots\ldots\ldots\ldots (35)$$

then transformed to

$$\frac{\delta^2 C}{\delta x^2} + \frac{\delta^2 C}{\delta y^2} + \frac{G}{D} \cdot \frac{\delta C}{\delta x} = 0 \quad \ldots\ldots\ldots\ldots (36)$$

The general solution to this equation for a system, periodic in the y direction and moving with a constant velocity G in the x direction is given by

$$C - C_o = \sum_{n=-\infty}^{n=+\infty} K_n e^{-a_n x} \cos b_n y \quad \ldots\ldots\ldots (37)$$

where

$$b_n = \frac{2\pi n}{S_o} \quad \ldots\ldots\ldots\ldots\ldots\ldots\ldots\ldots (38)$$

$$a_n = \frac{G}{2D}\left[1 - \sqrt{1 + \left(\frac{4\pi nD}{GS_o}\right)^2}\right] \quad \text{for } n < o. \quad \ldots (39)$$

$$a_n = \frac{G}{2D}\left[1 + \sqrt{1 + \left(\frac{4\pi nD}{GS_o}\right)^2}\right] \quad \text{for } n \geqslant o. \quad \ldots (40)$$

and C_o } constants determined by the
K_n } boundary conditions

Equation (37) is applicable to each phase and the constants C_o and K_n s are to be determined by the appropriate boundary conditions. In the case of austenite one of the conditions is that the carbon concentration sufficiently far away from the interface is the same as the original carbon concentration, Ca, in austenite. This condition will be satisfied only if $K_n = 0$ when $n < o$ and $C_o = Ca$. It still remains to determine an infinite number of constants, K_n s ($n \geqslant o$) with the knowledge of other boundary conditions, but that being impracticable only a few terms in equation (37) are used. i.e.

$$C - Ca = K_o e^{-a_o x} + K_1 e^{-a_1 x} \cos b_1 y. \quad \ldots (41)$$

Defining

Caf - as the carbon concentration in austenite ahead of centre of ferrite lamellae

Cac - as the carbon concentration in austenite ahead of centre of cementite lamellae

Cf - as the carbon concentration in ferrite

Cc - as the carbon concentration in cementite

and applying the conditions that there is no carbon concentration discontinuity in austenite along the interface and that the growth velocity is controlled by the diffusion of carbon in austenite, Brandt obtained an expression eliminating the unknowns in solution (41) as given below.

$$P = 1 + N\frac{L^2/1 + P_+ L}{M + L^2/1 + P)} \quad \ldots\ldots\ldots\ldots\ldots (42)$$

$$\text{where } P = \left[1 + \left(\frac{4\pi D}{GS_o}\right)^2\right]^{1/2} \quad \ldots\ldots\ldots\ldots\ldots (43)$$

$$\left.\begin{aligned} N &= 2\frac{Cc - Ca}{Ca - Cac} \\ M &= \frac{Caf - Ca}{Ca - Cac} \\ L &= \frac{Ca - Cf}{Cc - Ca} \end{aligned}\right\} \quad \ldots\ldots\ldots\ldots\ldots (44)$$

Knowing all the five concentrations P can be evaluated. The value of K in equation (34) may then be obtained from equation (43) as

$$K = 4\pi(P^2 - 1)^{-\frac{1}{2}} \quad \ldots\ldots\ldots\ldots\ldots\ldots (45)$$

Growth rates, calculated from the known values of concentrations, diffusion coefficient in austenite and interlamellar spacing, agree with those obtained from experimental values, within an order of magnitude. It appears that such calculations cannot be made any more precise[18] because of the nature of the variations in each term and the approximations assumed in the derivations of the equations.

The value of K depends upon the actual concentrations at the midpoints of the ferrite and cemintite lamellae and have been obtained by assuming metastable equilibrium conditions which may not be truly valid.

The diffusion coefficient is assumed to be independent of carbon concentration which is only an approximation. In fact both the activation energy for diffusion and the diffusion coefficient change with the carbon concentration and therefore the diffusion rates are expected to vary considerably from the region ahead of cementite to the region ahead of ferrite. It has been assumed in Brandt's

analysis that the austenite - pearlite interface is not providing a diffusion path, however this might be a possibility. There is also a probability of a diffusion path through the ferrite, since the diffusion coefficient of carbon in ferrite is very much larger than in austenite. It is clear that to represent the diffusion of carbon with a single value is an over - simplification of the complicated mechanism of diffusivity.

The interlamellar spacing value is the mean true spacing value. It is not definitely established whether a mean true spacing really exists in all systems. The distribution in true spacings may not indicate a definite mean value and in such a case the spacing cannot be represented by a single value.

Considering all these possible uncertainties the calculated growth rates invariably differ from the experimental values. It may be pointed out that the experimental values too are probably an average of several growth rates of individual pearlite nodules.

Instead of comparing the experimental and calculated growth rates, a different approach is given by Cahn and Hagel[19] which analyses the results

with a view to establishing the most likely mechanism operating in the system. For austenite, the limits in the summation series of equation (37) are from $n = o$ to $n = +\infty$. It is deduced that the $n = o$ term expresses the band of austenite ahead of pearlite, to which the diffusion processes are confined. The thickness of this band for any component i is given by D_i/G. The terms $n = 1$ onwards contribute towards side - ways fluxes resulting in carbon and alloy segregation. The extent of side - ways diffusion in austenite is given by $\frac{1}{a_1}$. From equation (40) it is possible to examine this thickness as a function of a parameter α_i defined by

$$\alpha_i = \frac{GS_o}{2\pi D_i} \quad \ldots\ldots\ldots\ldots\ldots\ldots\ldots\ldots (46)$$

If the diffusivity of an ith component is very high then the value of α_i will be very much less than 1 and

$$\frac{1}{a_1} \simeq \frac{S}{2\pi} \ll \frac{D_i}{G} = \frac{1}{a_o} \quad \ldots\ldots\ldots\ldots\ldots\ldots\ldots\ldots (47)$$

Thus side - ways thickness will be less than the diffusion zone. On the other hand if the diffusivity is very small then $\alpha_i \gg 1$, which gives

$$\frac{1}{a_i} \simeq \frac{1}{a_o} = \frac{D_i}{G} \ll S/2\pi. \quad \ldots\ldots\ldots\ldots\ldots\ldots (48)$$

The side - ways thickness is confined to a thickness of D_i/G which is smaller than $S/2\pi$.

Now the parameter α_i can be related to the concentrations just as in the case of the proportionally constant K. If α_i is assumed to be small compared to unity then equation (43) can be approximated as $P = \frac{2}{\alpha_i}$, and equation (42) may be written as

$$\frac{2}{\alpha_i} = 1 + N \frac{1 + L}{1 + M} \quad \ldots\ldots\ldots\ldots\ldots\ldots (49)$$

Substituting the values of N, L, and M it becomes

$$\alpha_i = \frac{C^i_{af} - C^i_{ac}}{C^i_{c} - C^i_{f}} \quad \ldots\ldots\ldots\ldots\ldots\ldots (50)$$

where the terms now refer to the actual concentrations of the ith component at points indicated previously. In a binary Fe - C system there is an upper limit to α_i to which the ratio of the concentration differences can reach. This limit is designated as α_o and is obtained by the Hultgren extrapolation technique. The value of α_i can also be determined through

equation (46) by the values of G, S_o and D_i. If both these quantities α_o and α_i are equal then it is deduced that the rate of carbon diffusion in austenite is controlling the pearlite growth rate. If α_i is greater than α_o then a faster diffusion path is operative. If α_i is less than α_o, then a process other than diffusion in austenite is controlling the growth rate. In the theories of Zener[22] and Brandt[21] the values of α_o and α_i are taken as equal.

It is convenient to compare α_o and α_i by an equivalent method of comparing the apparent diffusivity, Dapp, given by

$$Dapp = \frac{GS_o}{2\pi\alpha_o} \quad \ldots\ldots\ldots\ldots\ldots\ldots\ldots (51)$$

with experimentally determined diffusivity values (Dexp). The results may then be summarised as follows

$\alpha_o = \alpha_i$;	Dapp = Dexp	Diffusion in austenite is rate controlling
$\alpha_o < \alpha_i$;	Dapp > Dexp	Shorter diffusion path in austenite is operative
$\alpha_o > \alpha_i$;	Dapp < Dexp	A process other than diffusion is rate controlling

According to this analysis Cahn and Hagel[19] found that in the case of high purity Fe - C alloys the apparent diffusivity values exceeded those of experimental ones by about two orders of magnitude and hence concluded that a shorter diffusion path was in evidence. Diffusion through ferrite was ruled out on morphological grounds. It appears that the discrepancy could be due to neglecting the effect of strains, introduced in austenite during the volume changes in pearlite, on the diffusivity of carbon[30]. If the deformation of austenite ahead of pearlite due to the volume change is considered this may account for the enhanced diffusion rate and for the lamellar structure of pearlite[34]. Minor impurities in commercial purity steels may affect the deformation characteristics and thus show a decreased growth rate of pearlite compared to high purity Fe - C alloys[58].

(iii) Pearlite Growth Mechanism in the Binary Copper - Aluminium System

The Cu - Al system resembles the Fe - C system so far as the pearlite reaction is concerned. Now the concentrations refer to aluminium contents in the phases as indicated below.

Caf $\equiv C_{\beta\alpha}$ - concentration of Al in β ahead of centre of α

$Cac \equiv C_{\beta\gamma_2}$ - concentration of Al in β ahead of centre of γ_2

$Cf \equiv C_{\alpha}$ - concentration of Al in α

$Cc \equiv C_{\gamma_2}$ - concentration of Al in γ_2

$Ca \equiv C_{\beta}$ - concentration of Al in β

$C_{\beta\alpha}$ and $C_{\beta\gamma_2}$ can be determined from the extrapolated $\beta + \alpha$ / β and $\beta + \gamma_2$ / β equilibrium phase boundaries below the eutectoid temperature. C_{α} and C_{γ_2} are obtained from the equilibrium diagram (fig.1). The phase diagram has been well established and the extrapolation is straight forward. The main difficulty arises when the metastable $(\beta + \beta_1)$ loop intersects with the extrapolated boundaries. It prevents an accurate determination of the quantity $(C_{\beta\alpha} - C_{\beta\gamma_2})$, since α and γ_2 phases are precipitated not only from β but also from β_1. Values of $(C_{\beta\alpha} - C_{\beta\gamma_2})$ below 527°C are therefore arbitrary and are at best reasonable estimates. However, despite this major interference the results show a definite controlling mechanism.

The calculated apparent diffusivities and the experimental values are presented in Table XI and are shown in Fig.43. It is observed that the agreement between the two sets is quite close indicating that the diffusion of aluminium in the β phase is the

Temp °C	Dexp cm^2/sec	Dapp cm^2/sec Binary Eutectoid	Dapp cm^2/sec 12.4% Al alloy
555	9.0×10^{-8}	9.3×10^{-9}	
550	9.4×10^{-9}	7.5×10^{-9}	
540	7.6×10^{-9}	7.3×10^{-9}	
530	6.2×10^{-9}	8.0×10^{-9}	
520	5.0×10^{-9}	4.5×10^{-9}	
510	4.0×10^{-9}	2.9×10^{-9}	1.4×10^{-8}
500	3.2×10^{-9}	2.6×10^{-9}	1.0×10^{-8}
490	2.5×10^{-9}	2.4×10^{-9}	
480	1.9×10^{-9}		6.5×10^{-9}
460	1.2×10^{-9}		3.8×10^{-9}
440	6.9×10^{-10}		1.8×10^{-9}
420	3.9×10^{-10}		1.0×10^{-9}
400	2.2×10^{-10}		3.8×10^{-10}

Table XI

Apparent and experimental diffusivities of aluminium in the β - phase

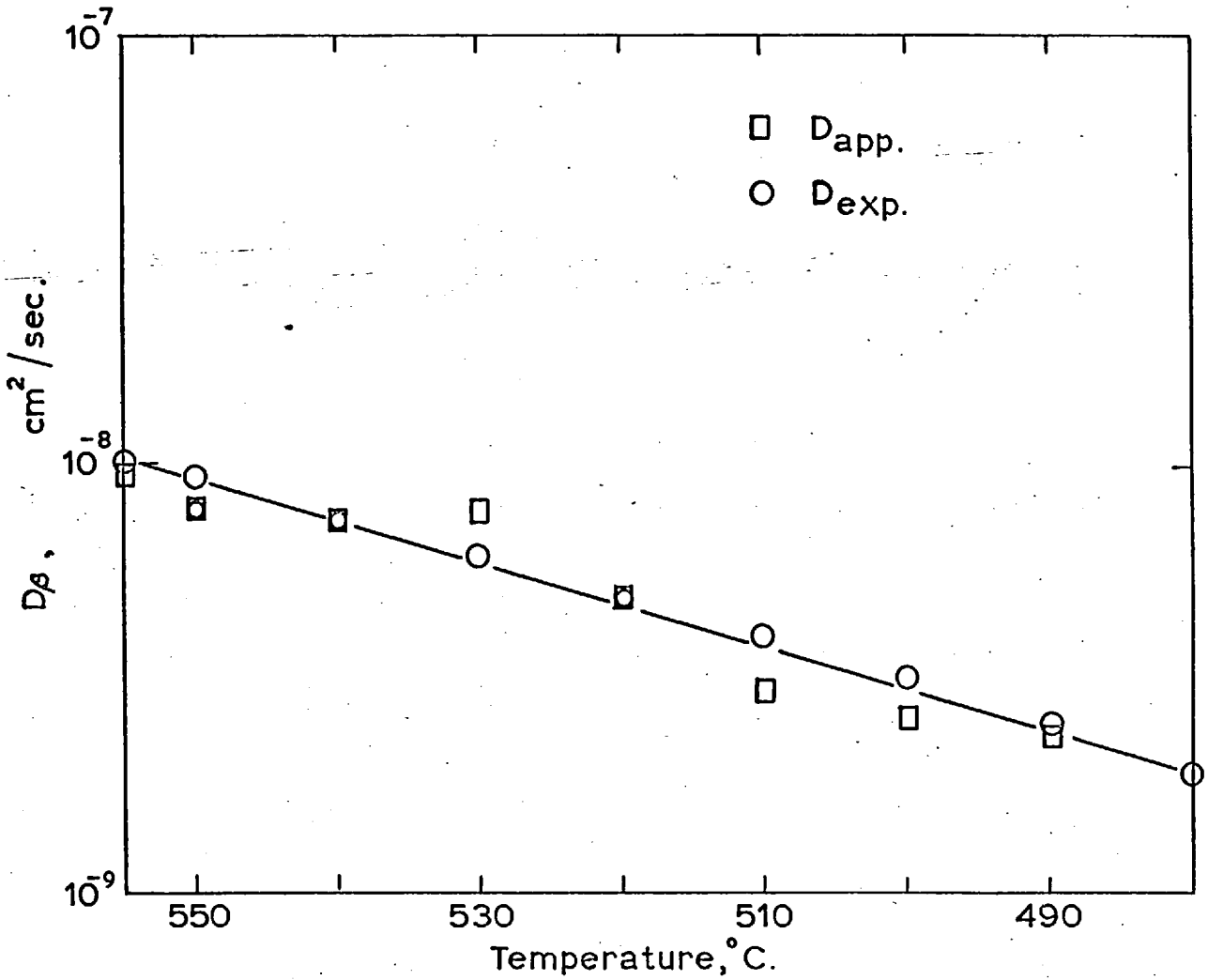

FIG. 43. Apparent And Experimental Diffusivity Values At Transformation Temperatures, Binary Eutectoid Alloy.

rate - controlling process in the growth of pearlite. Spacing data used in the calculations are the minimum observed and might be considered inappropriate; however it is indicated (in Section V on spacing) that the mean true spacing cannot possibly be more than about twice the minimum, so it would make a difference by a factor of two only. The diffusion values and the growth rate data are the average values. Taking into consideration all such variations the values of Dapp and Dexp are within sufficiently close limits to regard them as practically identical. Cahn and Hagel[19] have given a single instance in Cu - Al pearlite in which the values of Dapp and Dexp differ by orders of magnitude. However, accurate diffusion and growth rate data were not available and the calculations seem very approximate.

The growths of pearlite in the Fe - C and the Cu - Al systems may now be compared to observe the essential differences between the two systems.

The diffusion rate of aluminium in the β phase is several orders of magnitude larger than in the α phase whereas carbon diffuses faster in ferrite than in austenite. Because of the large difference in diffusivities between α and β phases, the contribution from diffusion along the pearlite - β interface may

be expected to be small compared with the contribution from the volume diffusion in the β; while in the pearlite - austenite case it could be the other way. Analysis on interface diffusion mechanism by Cahn and Hagel[19] shows inconclusive results. It has been suggested that in the austenite - pearlite reaction carbon may segregate to the carbide through ferrite for reasons of higher diffusivity in the ferrite phase; such a possibility in the β - pearlite case is remote. The volume change associated with the β pearlite transformation is expected to be small since the average density of pearlite is nearly the same as that of β; on the other hand the dissociation of austenite to pearlite is accompanied by sufficient volume change to cause deformation of austenite ahead of the pearlite interface.

The ratio of the thickness of α : γ_2 is approximately 1 : 1 (Fig.44) whereas for ferrite : carbide the proportion is 7 : 1. This may account for the interfacial free energy values showing good agreement for Cu - Al pearlite but not for Fe - C pearlite. For the same reasons (of equal thickness) equilibrium concentrations of aluminium are more likely to be attained in Cu - Al pearlite at the interfaces of α and γ_2 than in austenite at the

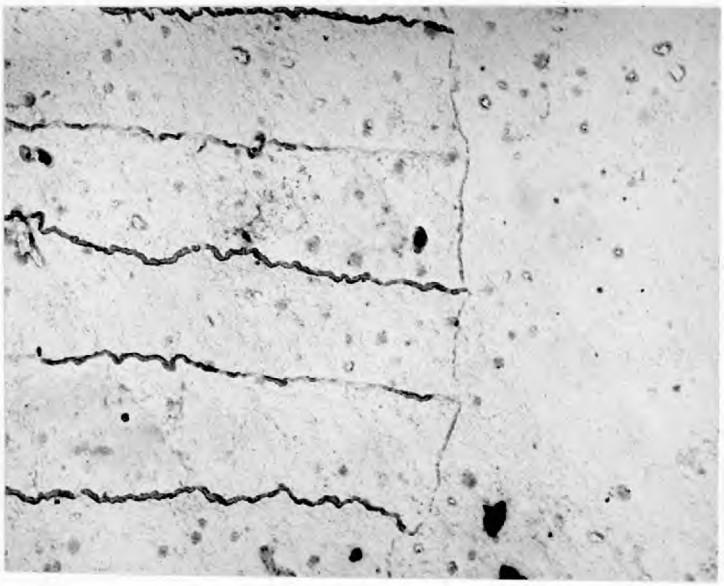

FIG.44 Thickness of the α and γ_2' phases in pearlite. x 10,000

Enlarged to 1.25 times for reproduction.

ferrite and cementite interfaces[23]. The planar interfaces (Fig.44) observed may obviate the use of Thomson's relation.

It appears from the above considerations that Cu - Al pearlite conforms to the theory much more closely than does the Fe - C pearlite for which the theory was developed.

Binary 12.4% Al alloy:

It has been already indicated that a 12.4% Al alloy when quenched from the β phase to a temperature below 500°C transforms rapidly to β_1 which gives the reaction $\beta_1 \rightarrow \alpha + \gamma_2$. The phase boundaries of this metastable phase are shown in Fig.15 as determined by metallographic observations[5]. A noteworthy feature of this system is that the $\beta_1 + \alpha$ / β_1 and the $\beta_1 + \gamma_2$ / β_1 boundaries are nearly parallel to the temperature axis. It suggests that the quantity $(C_{\beta_1\alpha} - C_{\beta_1\gamma_2})$ is approximately constant below 500°C. Assuming C_α and C_{γ_2} to have the same values as for the $\beta \rightarrow \alpha + \gamma_2$ transformation, apparent diffusivity values have been calculated with the aid of data on G and S_o for this alloy. The results are given in table XI and in Fig.45. The experimental data of diffusion coefficients are the same as in the previous case.

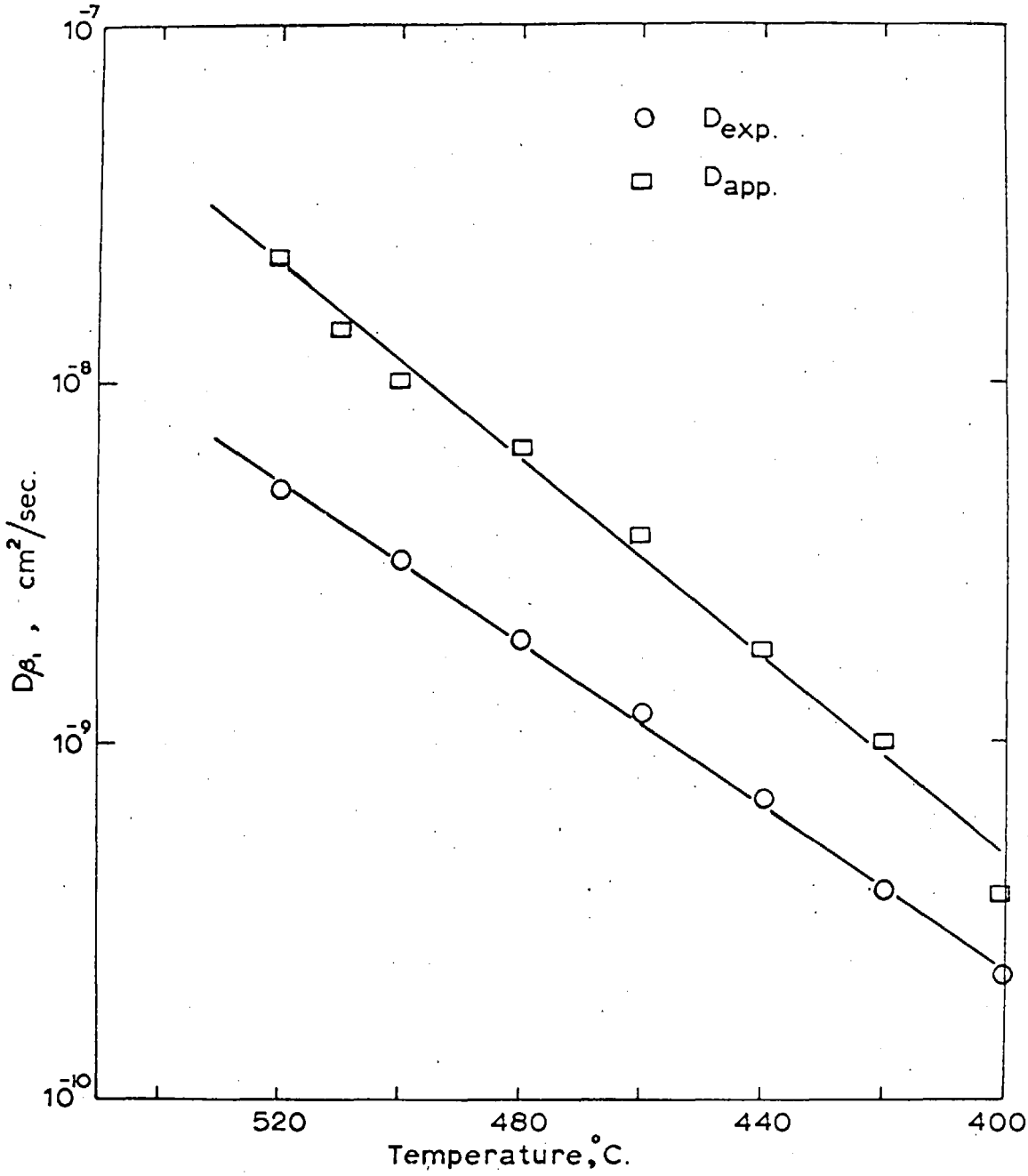

FIG. 45. Apparent And Experimental Diffusivity Values At Transformation Temperatures; 12·4% Al Alloy.

The results show that the Dapp values are larger by about a factor of 4 than the experimental values. This is not considered to be a large enough difference to suggest a shorter diffusion path for growth. The experimental diffusion data indicate that the diffusion coefficient of aluminium in the β phase is expected to increase with increasing aluminium concentration so that the value of Dexp in a 12.4% Al alloy is probably greater than in the 11.8% Al alloy. This would help in bringing the values of Dapp and Dexp closer together. Thus in this system also the growth of pearlite is controlled by volume diffusion of aluminium in the matrix β_1.

The thickness of the zone ahead of the pearlite interface, to which the diffusion fluxes are confined, is given by the ratio D_{Al}/G and varies with temperature as shown in Fig.46. In the case of steels this zone varies over orders of magnitude in the temperature range 600 to 720°C; in the present case it is about an order of magnitude.

(iv) The Pearlite Growth in Ternary Alloys

(a) Ferrous systems

Ternary alloying elements like chromium, manganese, nickel, molybdenum and cobalt affect the

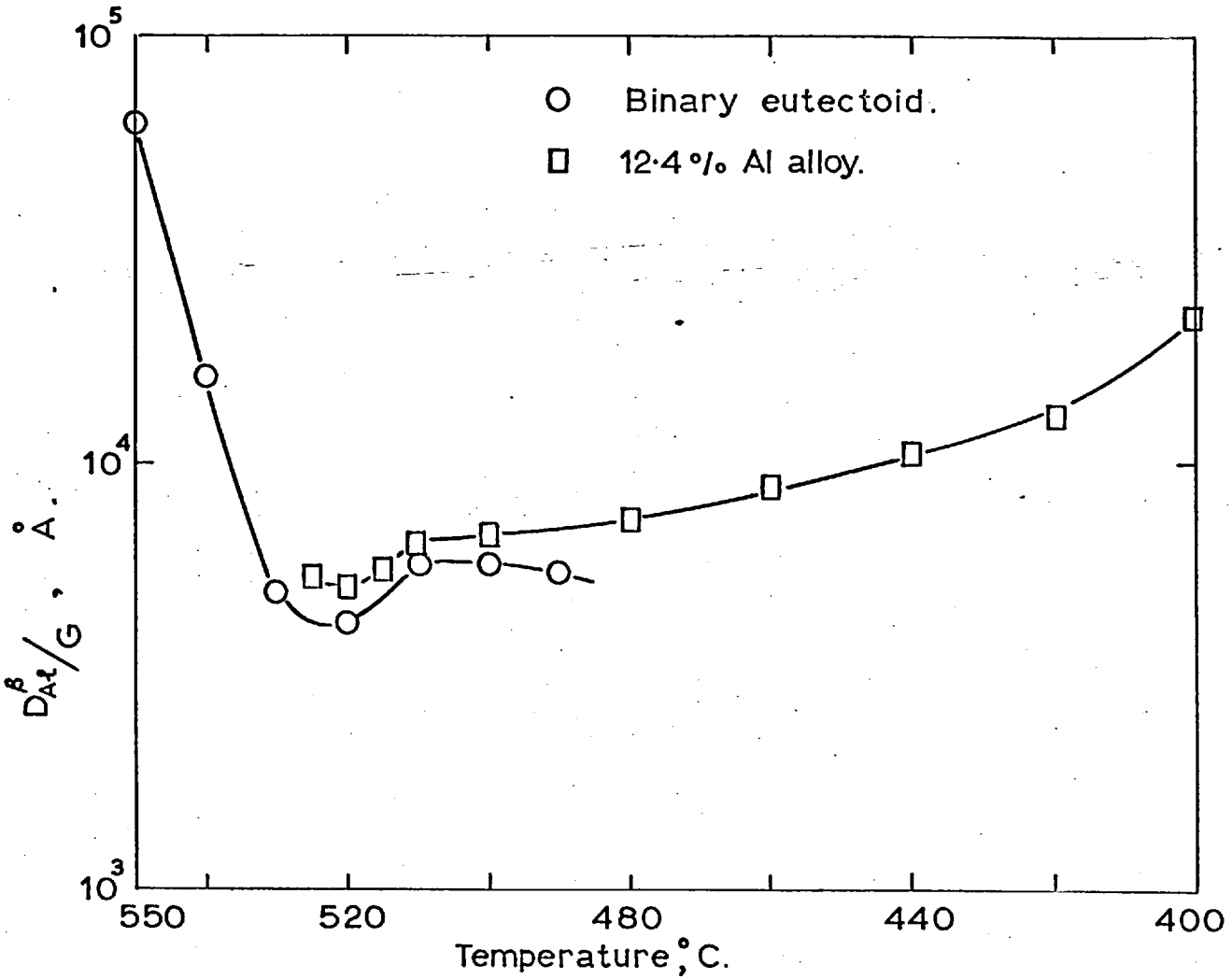

FIG. 46. Thickness Of The Diffusion Zone At Reaction Temperature

growth rate of pearlite markedly and are of considerable importance in the study of the hardenability characteristics of steels. However, the data on these steels seem incomplete[19,20] in respect of interlamellar spacing measurements and alloy partitioning behaviour so that a systematic analysis has not been reported.

There appears to be no general agreement regarding the effect of the ternary elements on the growth mechanism of pearlite. Brandt[21] suggested that alloying elements may change the eutectoid composition and alter the lower temperature limit at which pearlite can form. Zener[22] proposed that the growth rate of pearlite was affected indirectly by the effect of the alloying elements on the transformation free energy change. Although there is some experimental evidence[27] to substantiate this view Mehl and Hagel[18] criticize the suggestion as it does not explain the mechanism. Entin[31], Alksandrov and Lyubov[30] explain that the effect of alloying elements is two fold; these elements alter the activation energy for the polymorphic change $\gamma \rightarrow \alpha$ and may form special carbides giving rise to selective segregation to either of the phases in pearlite. Cahn and Hagel[19] consider the interaction

of the alloying elements as due to the thermodynamic effect of changing activity coefficients of one element brought about by the changing concentrations of the other element. Kirkaldy[35,36] has shown that in the case of manganese steels the effect of manganese is to reduce the carbon potential by virtue of the changed phase relations, thus effecting a change in the growth rate of pearlite in these steels. Darken and Fisher[34] propose that the alloying elements have an effect on the diffusion flux by changing the boundary conditions for the diffusion process. Another view[26,32] is that an alloying element increases the activation energy for the movement of the pearlite - austenite interface but this does not help in understanding the mechanism of pearlite growth.

Non - ferrous systems: Copper - Aluminium base ternary alloys

The only available quantitative data are due to Ranzetta and West[8] but no explanation is given for the observed decrease in growth rates in Cu - Al - Fe, Mn or Co bronzes. In the case of the Cu - Al - Mn system they expected the partitioning of manganese to the α phase to be the rate - controlling factor. Lacking diffusivity and complete

interlamellar spacings data they found it difficult to interpret the results. However the additions, of about 1% of Fe, Mn or Co, to the aluminium bronze, were found to have no measureable effect on the free energy change of the transformation[13]. Therefore it was inferred that the change in the kinetics of the $\beta \rightarrow \alpha + \gamma_2$ transformation was not due to any change in the free energy of transformation.

It has been demonstrated that the rate of growth of pearlite in a binary alloy is limited by the rate at which aluminium segregates to the γ_2 phase. Any change in this rate might therefore be reflected in the growth rate. When a ternary alloying element is present then there are at least two probable ways in which it can affect the segregation rate. It may change the diffusion rate or may change the driving potential gradient or both. The magnitude of the change in the diffusivity may be taken to be negligible since the concentration of the ternary element is very small. The diffusivities of tin and zinc are of the same order of magnitude and these elements seem to partition (if there is a selective segregation) during the growth of the pearlite itself. It is therefore possible that the effect on the growth rate is due to the change in the

potential gradient which causes the diffusion to occur. A measure of the potential gradient is obtained by the difference in the extrapolated values $(C_{\beta\alpha} - C_{\beta\gamma_2})$. In ternary systems it is not always simple to determine the above quantity because the phase α can have a range of compositions in equilibrium with a range of compositions of the phase γ_2 at a constant temperature.

Cahn and Hagel[19] suggested a method of obtaining the compositional differences - designated $(C'_{\beta\alpha} - C'_{\beta\gamma_2})$ - for the ternary systems. It is required to have isothermal sections of the ternary diagram with well defined boundaries of the phases involved in the reaction. However in the present case due to the lack of such data on isothermal sections of the Cu - Al - Zn and Cu - Al - Sn systems, approximate methods were used to obtain $C'_{\beta\alpha}$ and $C'_{\beta\gamma_2}$ values. The approximations made may be followed from a brief consideration of the appropriate method.

An isothermal section of a hypothetical diagram of a ternary system, at a temperature below that of the eutectoid reaction (in the binary system), is shown in Fig.47. If an alloy of eutectoid composition P is quenched from the β phase to the temperature

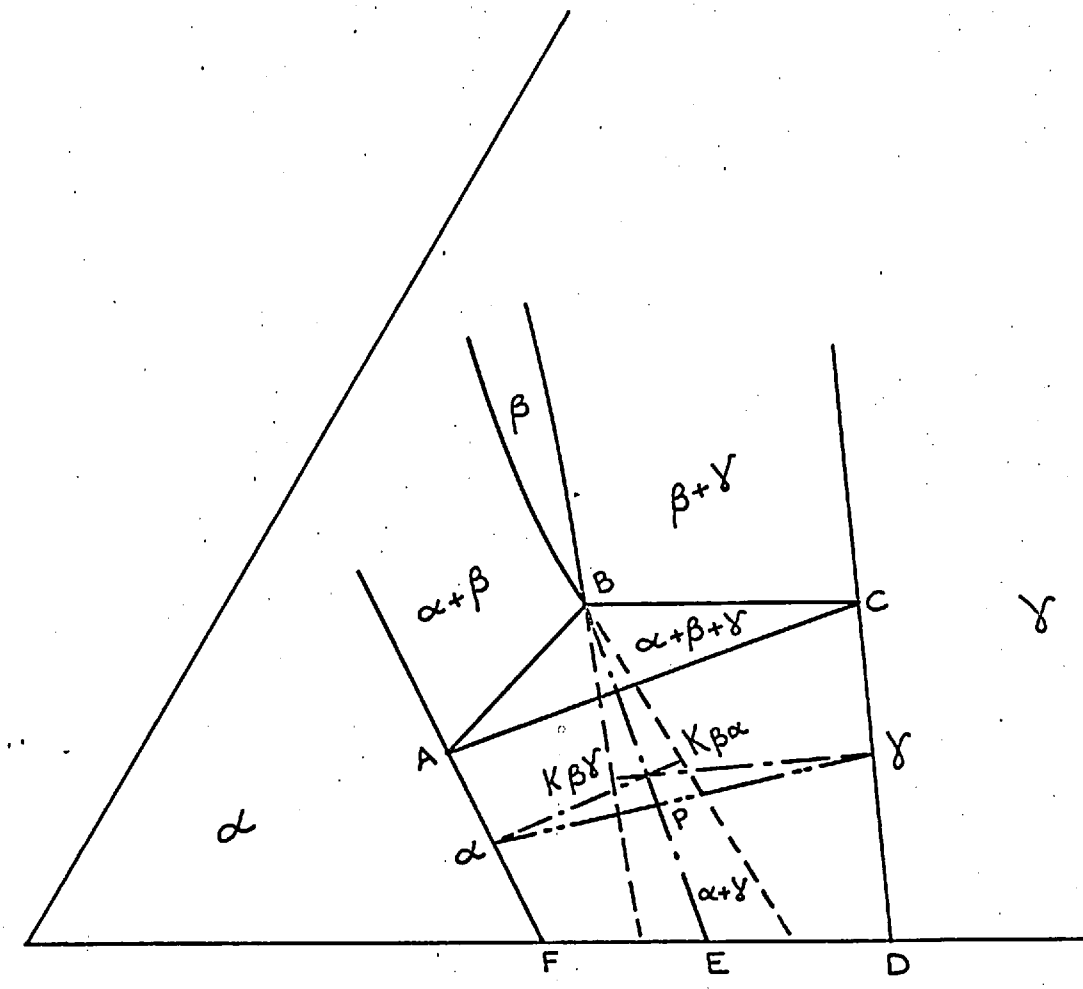

FIG. 47. Isothermal Section Of a Hypothetical Ternary Diagram For Estimating $(C'_{\beta,\alpha} - C'_{\beta,\gamma_2})$.

represented by the isothermal diagram, then at equilibrium, the phases α and γ are formed of compositions given by the points, say, α and γ. The points α, P and γ are connected by a tie line in the two phase region ACDF. The composition of β in metastable equilibrium with γ during the transformation is given by the point $K_{\beta\gamma}$, i.e. the point of intersection of the extrapolated β / β + γ phase boundary with the tie line $\gamma K_{\beta\gamma}$ in the extrapolated β + γ field. Similarly the composition of β in metastable equilibrium with α is given by the point $K_{\beta\alpha}$. The concentration potential is therefore given by $(K_{\beta\alpha} - K_{\beta\gamma})$.

The points $K_{\beta\alpha}$ and $K_{\beta\gamma}$ move towards the tie line αPγ as P moves towards/the binary line FD. Therefore if the three phase triangle ABC is farther away from P and P is nearer line FD, the points $K_{\beta\alpha}$ and $K_{\beta\gamma}$ may be (approximately) taken to be on the line αPγ. However, the effect of moving away the three phase triangle is to increase the uncertainties in the extrapolation of the β / α + β and β / β + γ phase boundaries. In such a case the projection of the composition difference in a binary alloy (at the same temperature) on the tie line αPγ may be a reasonable approximation of the quantity $(K_{\beta\alpha} - K_{\beta\gamma})$. The Cu - Al - Zn system may be considered to correspond to this situation.

There is also a possibility that the triangle ABC may be narrow enough to regard the point B to be on the line AC and this would also lead to the points $K_{\beta\alpha}$ and $K_{\beta\gamma}$ being considered as lying on the line $\alpha P\gamma$. This situation may correspond to the Cu - Al - Sn system. In this case also the concentration difference may be estimated from the corresponding binary value.

Thus in both the Cu - Al - Zn and Cu - Al - Sn systems the method of obtaining the concentration differences $(C'_{\beta\alpha} - C'_{\beta\gamma_2})$ was to correct the appropriate binary concentration difference $(C_{\beta\alpha} - C_{\beta\gamma_2})$; the magnitude of the estimated correction depended upon the inclination of the $\alpha - \gamma_2$ tie line with the aluminium concentration axis.

(b) Ternary Cu - Al - Zn System

The isothermal sections reproduced in Fig.48 have been used for the estimation of the quantity $(C'_{\beta\alpha} - C'_{\beta\gamma_2})$. Assuming equilibrium partitioning of zinc in the α and γ_2 phases the new concentrations of aluminium in the α and γ_2 phases are read from the diagram. Apparent diffusivity values, presented in table XII, for aluminium in the β phase are calculated in the same way as for the binary case. Comparison

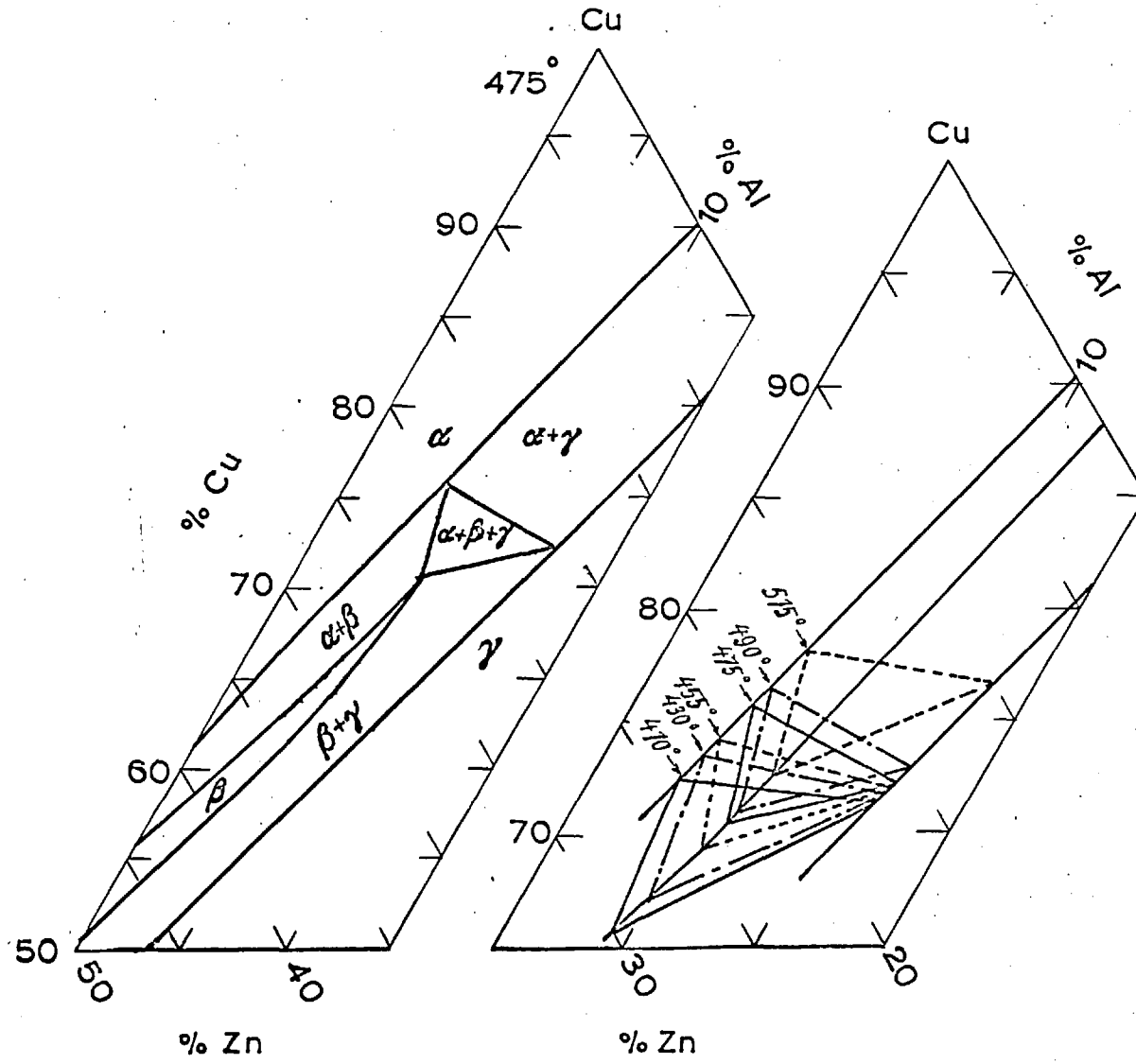

FIG. 48. Isothermal Sections Of Copper-Aluminium-Zinc System Showing The Phase Boundaries And The Three Phase Fields At Temperatures.

Temp °C	Dapp cm^2/sec	Dexp cm^2/sec	System
515	4.6×10^{-9}	4.4×10^{-9}	Cu - Al - Zn (2.4%)
530	6.7×10^{-9}	6.2×10^{-9}	Cu - Al - Sn (1%)
525	4.2×10^{-9}	5.5×10^{-9}	Cu - Al - Mn (0.5%)
525	3.6×10^{-9}	5.5×10^{-9}	Cu - Al - Mn (1%)

Table XII

Apparent and experimental diffusivity values for aluminium in the β phase in ternary alloys

with the experimental diffusivity data indicates that in the ternary Cu - Al - Zn system also the pearlite growth is controlled by the diffusion of aluminium in the β phase. The growth rate of pearlite in the ternary alloy is approximately the same (or most probably less) compared with the binary eutectoid alloy at higher reaction temperatures but becoming smaller and smaller until the β_1 reaction sets in. (See Fig.49). Further decrease in reaction temperature shows a reverse trend and an "apparent" increase in the ternary alloy. This conclusion is true for all the zinc alloys investigated.

An important effect of zinc in eutectoid aluminium bronzes is to decrease the $\beta \rightarrow \beta_1$ reaction temperatures by decreasing the concentration of aluminium; but the magnitude of the effect is not as much as it would be if there were no zinc at all. The net effect is that the ternary alloys of eutectoid compositions show the $\beta \rightarrow \beta_1$ reaction at lower temperatures than does the binary eutectoid alloy. This allows the Hultgren extrapolation in the binary alloy (from which the quantity $C'_{\beta\alpha} - C'_{\beta\gamma_2}$ for the ternary alloy is estimated) to be extended till the temperature at which β_1 begins to form. This has been done while calculating the apparent

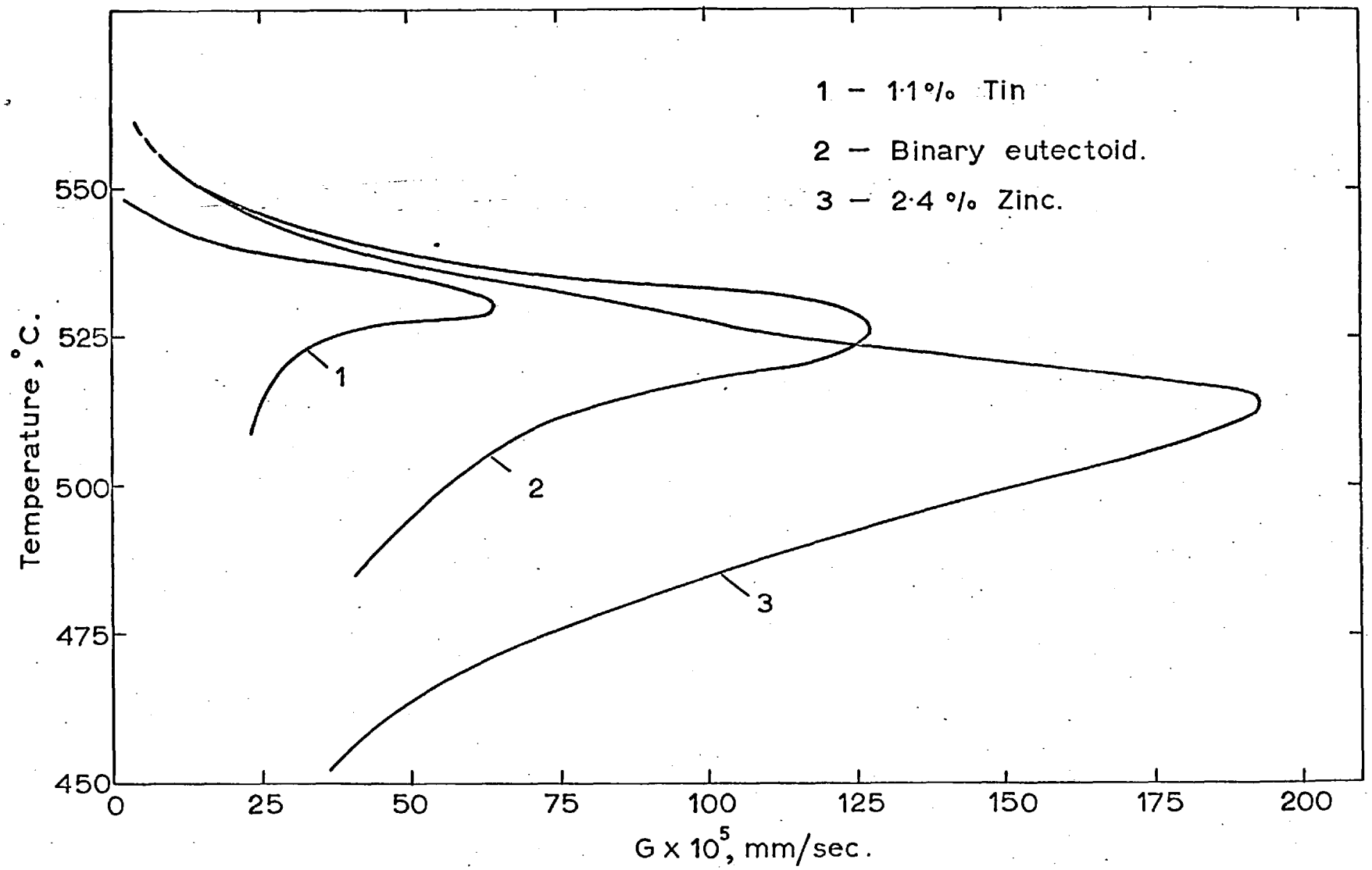

FIG. 49. The Growth Rate-Temperature Relation In Aluminium Bronzes.

diffusivity value given in table XII. The overall picture of the growth rates of pearlite in the zinc alloys therefore appears to give an impression of increased growth rates which in fact is the result of the lowering of the $\beta \rightarrow \beta_1$ reaction temperature.

(c) Ternary Cu - Al - Sn System

The addition of tin decreases the concentration of aluminium to a greater extent in the eutectoid alloys than in the case of the zinc alloys. The eutectoid temperature first decreases and then increases[14]. For a 1.1% tin alloy the decrease in eutectoid temperature is about 1°C and may be ignored. The three phase triangle ($\alpha + \beta + \gamma_2$) has not been established but is considered to be very narrow[14]. The probable two phase field, $\alpha + \gamma_2$, is shown in Fig.50. The tie line connecting α and γ_2 through the 1.1% tin composition is most probably lying at an angle to the aluminium axis. Estimation of the quantity, $C'_{\beta\alpha} - C'_{\beta\gamma_2}$ at 530°C, has been made as before and the result of the calculation for the Dapp value is given in table XII, along with the Dexp value. It may be noticed that the results are in good agreement considering the approximations made. Although it is not intended to claim absolute accuracy of the results obtained, the important

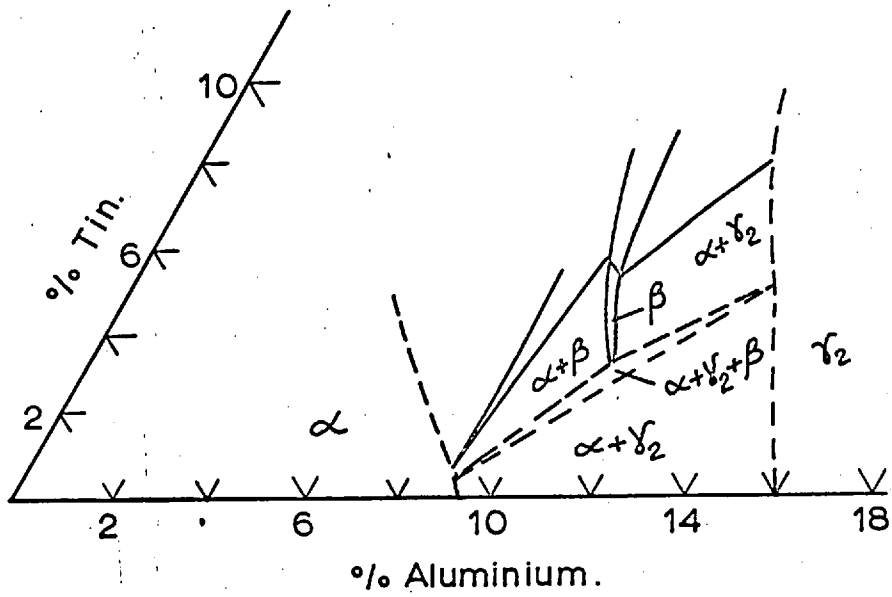

FIG. 50. The Copper-Aluminium-Tin System, 562 °C Isothermal Diagram.

factor in the growth rate of pearlite in the ternary Cu - Al - Sn system is the reduction in the driving potential. Thus it seems almost certain that the growth of pearlite in the Cu - Al - Sn ternary alloy is controlled by the diffusion of aluminium in the β phase.

It is mentioned earlier (Ref. Fig.14) that tin raises the $\beta \rightarrow \beta_1$ transformation temperature. The formation of β_1 is accompanied by a reduction in the potential gradient because the compositions of β_1 in metastable equilibrium with α and γ_2 do not appear to change with temperature. Therefore as soon as β_1 starts precipitating the growth rate shows a tendency to diminish and this tendency becomes more marked with increasing amounts of β_1. The peak in growth rate - temperature curves of the aluminium bronzes studied in the Cu - Al and Zn and Sn ternary alloys of eutectoid compositions is the result of the $\beta \rightarrow \beta_1$ reaction. As discussed in the interlamellar spacing section, the increase in spacing in the above alloys is due to the formation of $\beta_1 \rightarrow \alpha + \gamma_2$ pearlite.

The thickness of the diffusion zones ahead of pearlite in the β phase for the two ternary alloys along with that of the binary eutectoid alloy, at several reaction temperatures are shown in Fig.51.

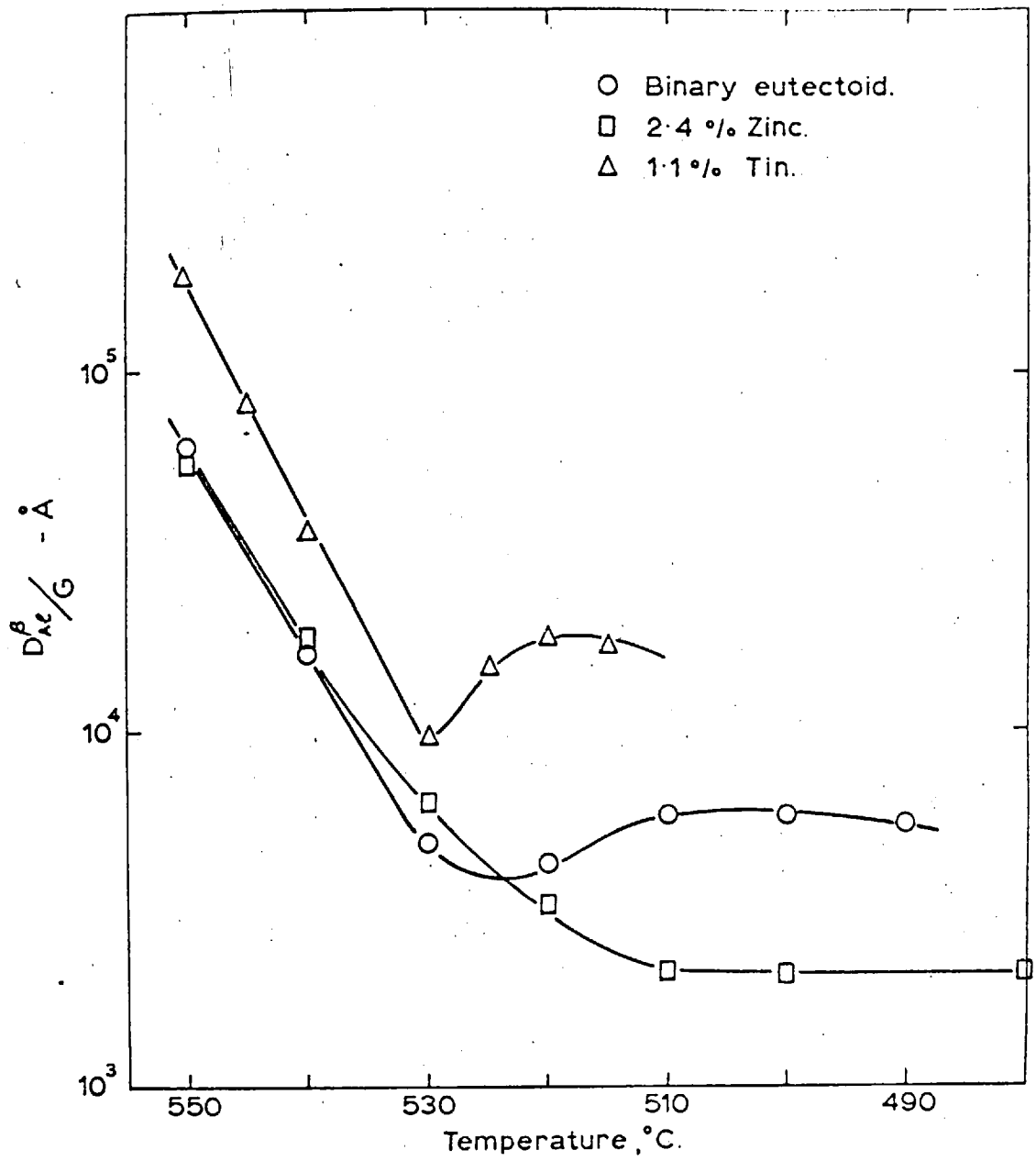

FIG. 51. Thickness Of The Diffusion Zone At Reaction Temperature.

In the case of the tin alloys, due to the slower growth rates, the thickness is larger than either in the binary or the ternary zinc alloy.

(d) The Cu - Al - Mn System

Although the present investigation excluded this system, the data available[5,7,8,11] on the equilibrium diagrams, the growth rates and the interlamellar spacings are adequate to examine the effect of manganese on the growth rate of pearlite. No approximations need be made in this case as was done for the zinc and tin alloys since the isothermal sections of this system are reasonably well established[11,59]. The calculations are carried out near the maximum in the growth rate vs temperature curves. From the isothermal section of the Cu - Al - Mn equilibrium diagram the value of $(C'_{\beta\alpha} - C'_{\beta\gamma_2})$ is determined by the method indicated in the hypothetical case. The growth rate and pearlite spacing values are taken from the results of Ranzetta[7]. The calculated Dapp values for aluminium in the β phase and the corresponding experimental values are given in table XII. Here also it seems that the growth rate of pearlite is controlled by the diffusion of aluminium in the β phase and the effect of manganese is to reduce the aluminium driving potential.

There are no data on the diffusion of manganese in the β phase and it is difficult to say whether partitioning of manganese has any effect on the growth rate. Results of partitioning experiments by Ranzetta[7] are not particularly useful since they refer to three phase fields; however they show a probable α - γ_2 tie line.

(iv) General Remarks

It may seem fortuitous to obtain such close agreement between apparent and experimental values of the diffusion coefficient of aluminium in the β phase in the ternary systems, in view of the approximations involved. But it is also possible that the ternary Cu - Al - Zn and Cu - Al - Sn systems satisfy the assumptions made in the development of the theory. For example it has been implicitly assumed in the solution of the diffusion equation (36) that the interaction terms between diffusing species are insignificant. As mentioned in the discussion on the diffusion of zinc and tin in the β (Cu - Al), the diffusion of aluminium in the β is practically independent of the gradients of either zinc or tin. The decomposition products α and γ_2 are expected to be of equilibrium compositions with respect to zinc or tin since the diffusion rates of these elements are comparable to that of aluminium.

The results of the present investigation strongly suggest that the effect of zinc and tin (and possibly manganese also) on the kinetics of growth of pearlite in Cu - Al based systems, is to reduce the aluminium potential and there - by to affect the growth rate. Still it would be quite difficult to calculate precisely the extent to which the growth rate is diminished by a known amount of reduction in the driving potential brought about by some other alloying element without data on interlamellar spacing. This is so because the growth rate would then depend upon the interlamellar spacing. The principle governing the selection of a particular spacing for a given growth rate appears to be obscure at the moment. It is quite possible that an alloying element affects the spacing as well. This may be judged from Fig.52 where the growth rates from the $\beta \rightarrow \alpha + \gamma_2$ reactions are plotted against interlamellar spacing in the alloys studied in this investigation. The tin alloy shows a smaller spacing than either the zinc or eutectoid alloy for a given growth rate, while the zinc and eutectoid alloys show similar trends in the relations of G vs S_o.

Apart from the determinations of the kinetic data necessary for the analysis of the growth

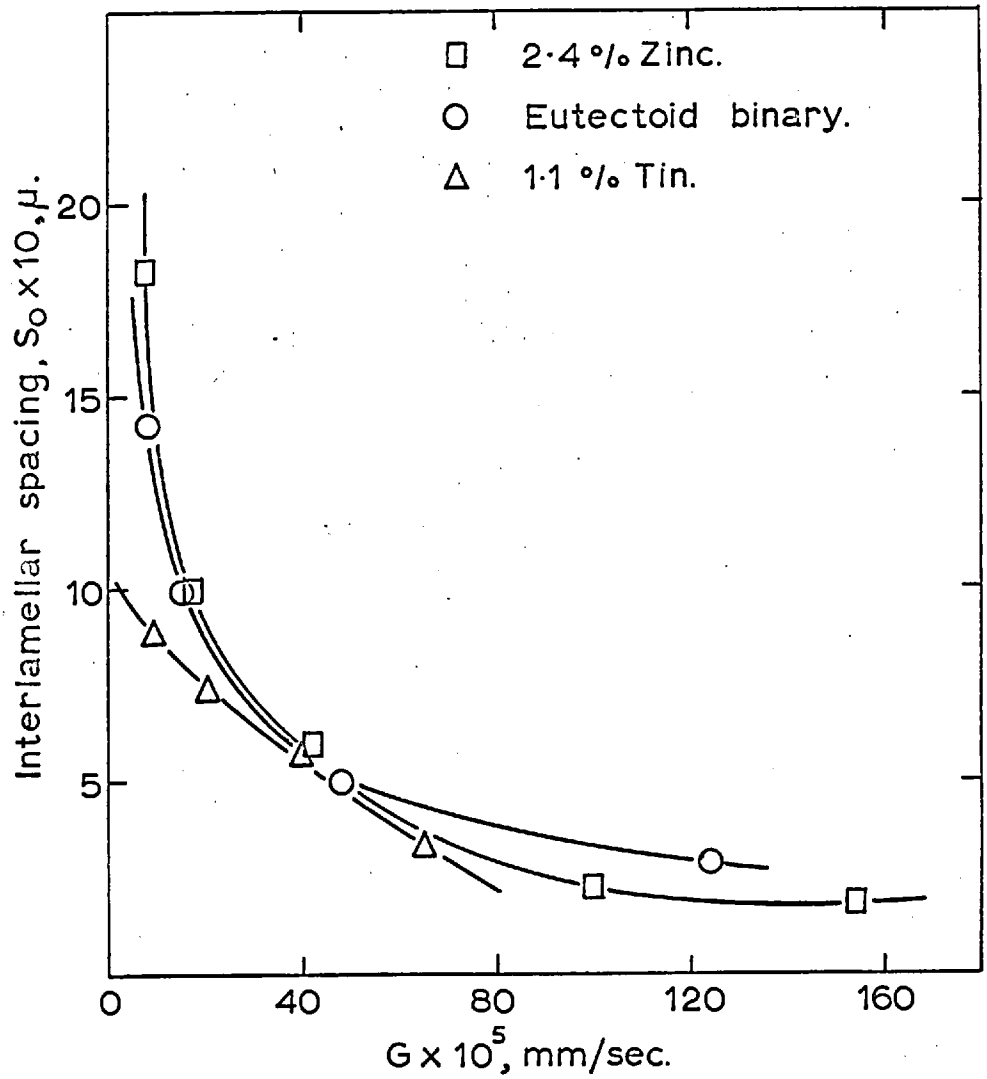

FIG. 52. Relation Between Interlamellar Spacing And Growth Rate.

mechanisms, some observations on the structures of pearlite in aluminium bronzes have been made. It is not intended to draw any definite conclusions from these structures but to suggest the possibility of further study in this direction.

Although lamellar pearlite is the most common type of the eutectoid reaction, sometimes simultaneous precipitation of α amd γ_2 occurred as shown in Fig.53. The decomposition of β, formed from the ~~peritectoid~~ reaction $\beta_1 \rightarrow \gamma_2 + \beta$ in the 12.4% Al alloy, appears to consist of $\alpha + \gamma_2$ mixture rather than $\alpha + \gamma_2$ pearlite; Fig.54.

It was observed by Hillert[33] that within a single colony the pearlite consists of two interwoven crystals i.e. the lamellae are inter - connected. In some instances it seems the lamellae extend into other colonies as well, as is seen in Fig.55, or the lamellae change direction abruptly as in Fig.56.

An interesting observation was made in alloys transformed partially to pearlite in the metastable $(\beta + \beta_1)$ region. A thin zone of β_1 appeared to envelop the growing pearlite as shown in Figs.57(a,b,c,d). It is doubtful whether this zone had formed during quenching. The likely explanation

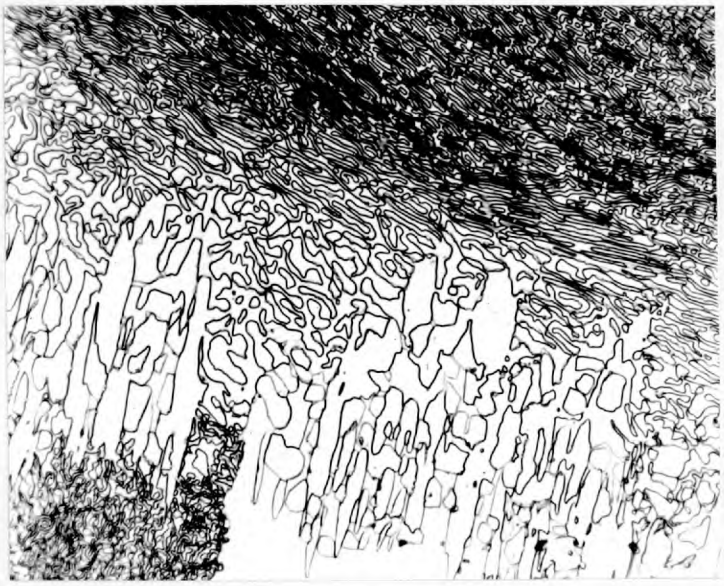

FIG.53 Precipitation of $\alpha + \gamma_2$ as a mixture.
11.8% Al alloy. x 525

FIG.54 α and γ_2 mixture from the decomposition of the β phase, resulting from the ~~eutectoid~~ reaction. $\beta_1 \rightarrow \beta + \gamma_2$ x 525
12.4% Al alloy.

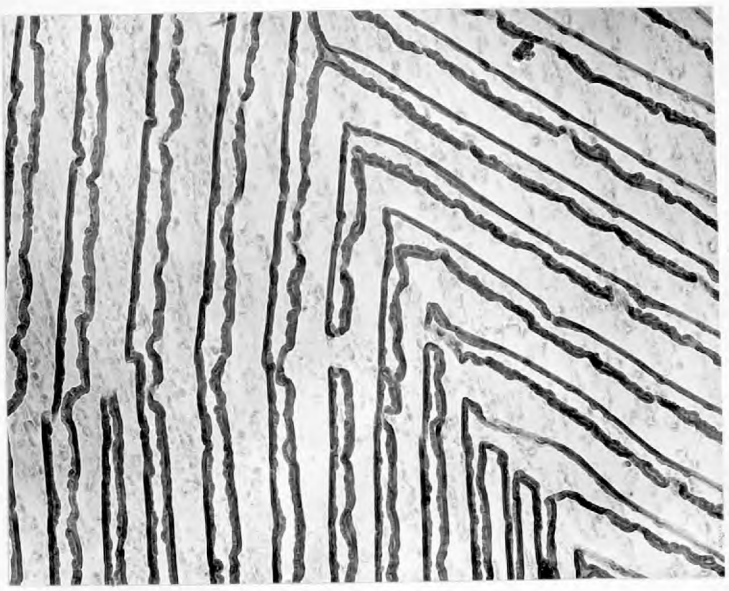

FIG.55 Lamellae extending into another colony of different orientation. x 10,000

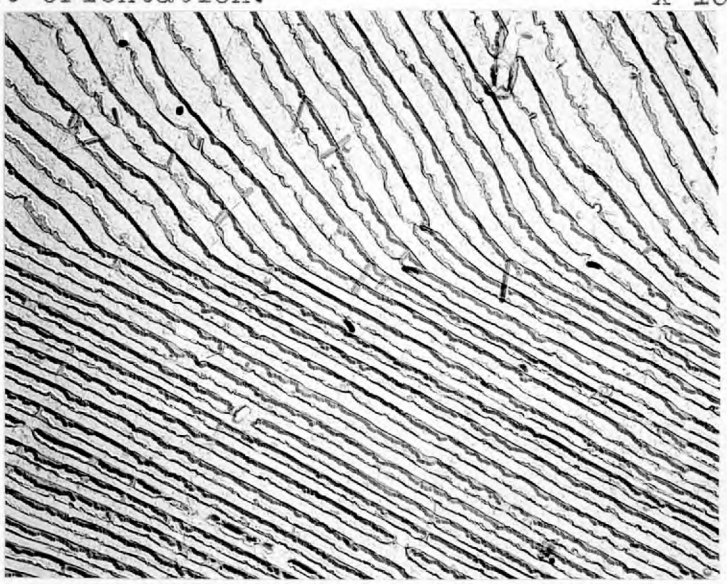

FIG.56 Lamellae changing direction. x 7,800

Enlarged 1.25 times for reproduction.

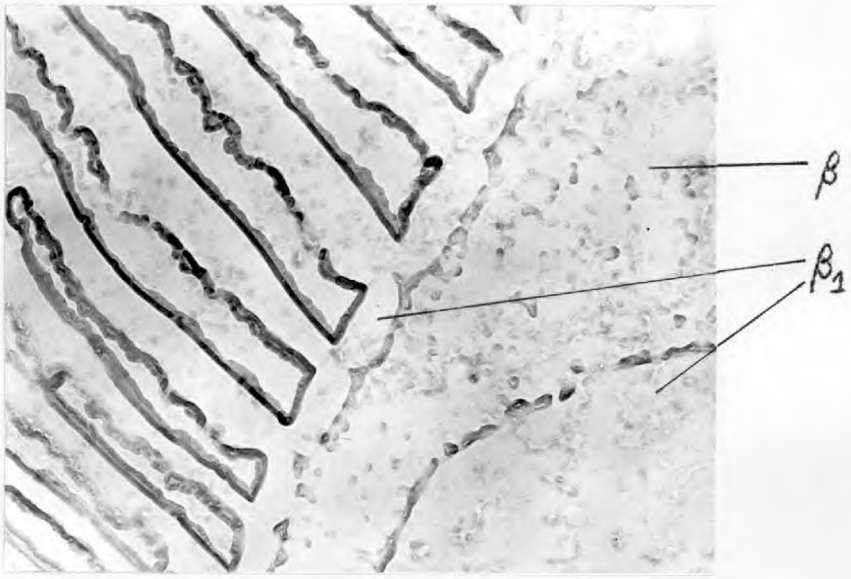

FIG.57(a) Zone of β_1 surrounding pearlite. x 10,000
Enlarged 1.25 times for reproduction.

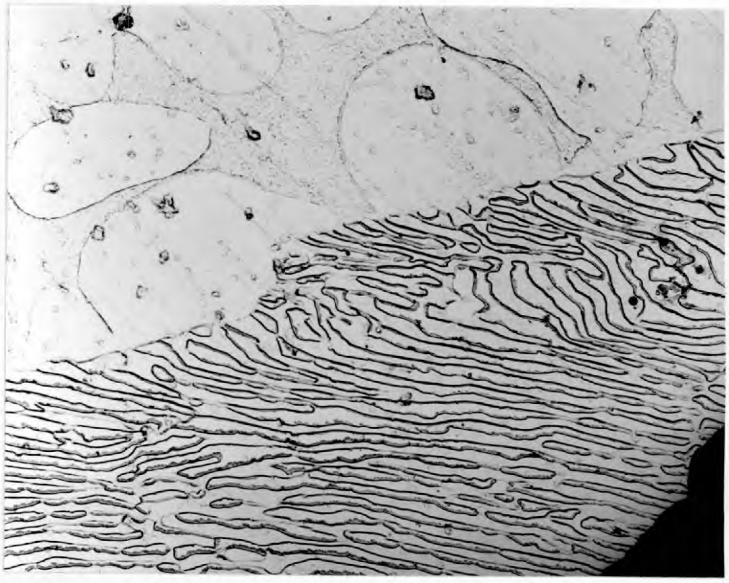

(b) β_1 separating pearlite and matrix $\beta + \beta_1$. x 7,800
Enlarged 1.25 times for reproduction.

FIG.57(c) β_1 in contact with pearlite. x 5000

Enlarged 1.25 times for reproduction.

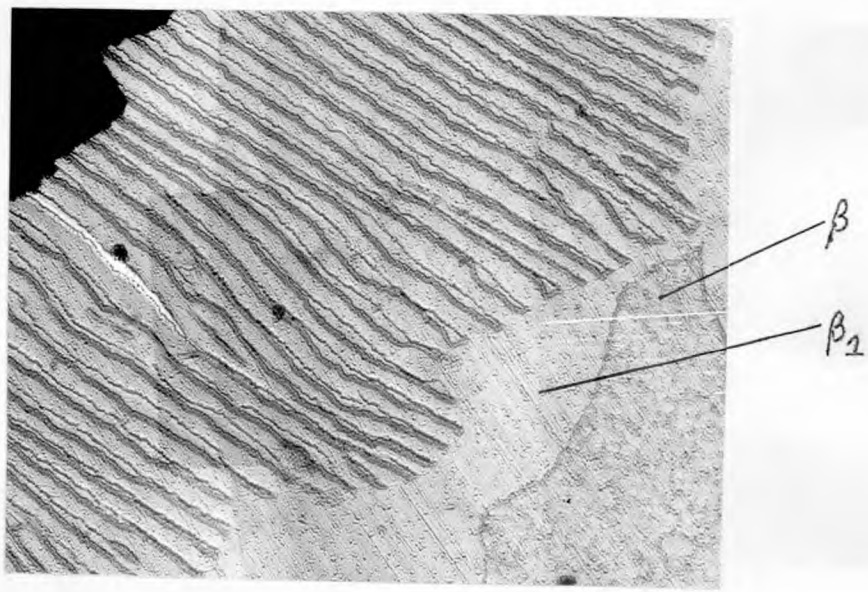

(d) β_1 in contact with pearlite. x 5000

Enlarged 1.25 times for reproduction.

for the β_1 film is that below the peritectoid horizontal the β phase in the $\beta + \beta_1$ mixture cannot precipitate γ_2 since the composition of the β lies outside the extrapolated $\beta + \gamma_2$ / β phase boundary. (See Fig.15). Therefore if any γ_2 is formed either as a proeutectoid α phase or as a constituent of the pearlite it could only be in metastable equilibrium with β_1 and not with β. Thus β_1 is found to separate pearlite from the $\beta + \beta_1$ mixture.

Conclusions:

The results of this investigation on certain aluminium bronzes have shown that the growth kinetics of the pearlite reaction are controlled by the volume diffusion of aluminium in the dissociating β phase. The theories developed for the pearlite reaction in steels explain the growth mechanism in Cu - Al system more satisfactorily than they do in the case of steels themselves.

The ternary alloying elements zinc and tin affect the growth rate by changing the driving potential for the diffusion process. The peak observed in growth rate - temperature curves in all the alloys is associated with the ordering reaction $\beta \rightarrow \beta_1$.

Interlamellar spacing of pearlite connot be related to undercooling by a simple reciprocity relationship in the pearlite reaction $\beta_1 \rightarrow \alpha + \gamma_2$. It depends upon the driving potential for diffusion, the diffusion coefficient and the growth rate.

The diffusion coefficient of aluminium in the β phase is very much larger than in the α phase and the activation energy for the diffusion process is almost half that in the α phase. Diffusivities of zinc and tin in the β (Cu - Al) phase are of the same order of magnitude and the activation energies nearly the same. Zinc and tin do not seem to affect the diffusivity of aluminium.

References

1. C. S. Smith and W. E. Lindlief
Trans A.I.M.E 104 (1933) 69

2. D. J. Mack
Trans A.I.M.E 175 (1948) 240

3. E. P. Klier and S. M. Grymko
Trans A.I.M.E 185 (1949) 611

4. R. Haynes
J. Inst. Metals 83 (1954 - 55) 105

5. D. L. Thomas
Ph.D. Thesis London Univ. 1957

6. A. H. Kasberg and D. J. Mack
J. Metals 191 (1951) 903

7. G. V. T. Ranzetta
Ph.D. Thesis London Univ. 1960

8. G. V. T. Ranzetta and D. R. F. West
J. Inst. Metals 92 (1963 - 64) 12

9. G. V. Raynor
Institute of Metals Annotated Equilibrium
diagram series 1944 No. 4

10. G. Wassermann
Metallwirtschaft 13 (1934) 133

11. D. R. F. West and D. L. Thomas
J. Inst. Metals 85 (1956 - 57) 97

12. T. V. Philip and D. J. Mack
Trans A.I.M.E 224 (1962) 34

13. G. V. T. Ranzetta and D. R. F. West
J. Inst. Metals (1961) 22 Supplement

14. J. S. L. Leach
Ph.D. Thesis Birmingham Univ. 1951

15. J. S. L. Leach and G. V. Raynor
Proc. Roy. Soc. A.224 (1954) 251

16. O. Bauer and M. Hansen
Zeit. für Metallkunde 24 (1932) 1 and 73

17. J. Fletcher
Unpublished work

18. R. F. Mehl and W. C. Hagel
Progress in Metal Physics Vol. 6 (1956) 74

19. J. W. Cahn and W. C. Hagel
"Decomposition of Austenite by Diffusional Processes" Interscience Pub. (1962) 131

20. F. C. Hull and R. F. Mehl
Trans A.S.M 30 (1942) 381

21. W. H. Brandt
J. Appl. Phys 16 (1945) 139
Trans A.I.M.E 167 (1946) 405

22. C. Zener
Trans A.I.M.E 167 (1946) 550

23. J. C. Fisher
'Thermodynamics in Physical Metallurgy'
A.S.M Seminar (1950) 201

24. M. F. Hawkes and R. F. Mehl
Trans A.I.M.E 172 (1947) 467

25. R. W. Parcel and R. F. Mehl
Trans A.I.M.E 194 (1952) 771

26. J. H. Frye, E. E. Stansbury and D. L. McElroy
Trans A.I.M.E 197 (1953) 219

27. W. C. Hagel, G. M. Pound and R. F. Mehl
Acta Met. 4 (1956) 37

28. J. J. Kramer, G. M. Pound and R. F. Mehl
Acta Met. 6 (1958) 763

29. M. Hillert
Jernkont. Ann 141 (1957) 757

30. L. N. Aleksandrov and B. Ya. Lyubov
Problems of Metallography and Physics of Metals
2 (1951) 256

31. R. I. Entin
'Decomposition of Austenite by Diffusional
Processes'
Intersc. Pub. (1962) 295

32. M. L. Picklesimer, D. L. McElroy, T. M. Kegley (Jr),
E. E. Stansbury and J. H. Frye (Jr)
Trans A.I.M.E 218 (1960) 473

33. M. Hillert
'Decomposition of Austenite by Diffusional Processes'
Intersc. Pub. (1962) 197

34. L. S. Darken and R. M. Fisher
Ibid (1962) 249

35. J. S. Kirkaldy
Ibid (1962) 39

36. J. S. Kirkaldy
Can. J. Phys. 36 (1958) 907

37. J. H. Woodhead
Private Communication

38. E. Scheil
Zeit. für Metallkunde 27 (1935) 199
28 (1936) 340

39. A. G. Spektor
Zavodskaya Laboratoria 15 (1949) 797

40. S. A. Saltykov
Zavodskaya Laboratoria 12 (1946) 816

41. G. E. Pellisier, M. F. Hawkes, W. A. Johnson and R. F. Mehl
Trans A.S.M 30 (1942) 1049

42. M. Gensamer, E. B. Pearsall, W. S. Pellini and J. R. Low
Trans A.S.M 30 (1942) 985

43. C. S. Smith and L. Guttman
Trans A.I.M.E 197 (1953) 81

44. H. A. Froot and L. S. Castleman
Trans A.I.M.E 227 (1963) 838

45. W. Jost
Diffusion in Solids, Liquids, Gases
Academic Press Inc. Publishers (New York)
(1952) 74

46. F. N. Rhines and R. F. Mehl
Trans A.I.M.E 128 (1938) 185

47. W. C. Hagel
General Electric Research Lab.
Report No. 63 - RL - 3320 M 1963

48. U. S. Landergren, C. E. Birchenall and R. F. Mehl
Trans A.I.M.E 206 (1956) 73

49. L. S. Darken
Trans A.I.M.E 180 (1949) 430

50. J. S. Kirkaldy
Can. J. Phys. 36 (1958) 899

51. J. S. Kirkaldy, Zia - Ul - Haq and L. C. Brown
Trans A.S.M 56 (1963) 834

52. F. E. Bowman and R. M. Park
Trans A.S.M 33 (1944) 481

53. F. E. Bowman
Trans A.S.M 35 (1945) 112

54. F. E. Bowman

Trans A.S.M 36 (1946) 61

55. A. Hultgren et al

Jernkontorets Ann (1951) 403

56. R. F. Mehl

A.S.M Symposium on hardenability of alloy steels (1938) 1

57. A. Hultgren

Discussion to the above paper

58. J. E. Hilliard and J. W. Cahn

"Progress in very high Pressure Research"

Published by J. Wiley 1961

59. D. F. Martin

D.I.C. Thesis Imperial College 1959

APPENDIX

Since no data on the β phase diffusion were available, a check on the validity of the diffusion coefficients obtained in the main investigation, was made. It consisted of deriving suitable equations in which diffusion coefficients of aluminium in the α and the β phase were involved so that from the known values in the α phase the data on the β phase could be checked with the data obtained by the method reported in Section VI A.

A schematic diagram, showing the conditions is depicted in Appendix Fig.1.

The initial conditions at $t = o$

$C = C''_o$ at $x < o$

$C = C_o$ at $x > o$

Conditions after a time i.e. $t > o$

$C = C_{\beta,\gamma_2}$ at $x = x_2 + o$. . . . . (1)

$C = C_{\beta,\alpha}$ at $x = x_1 - o$. . . . . (2)

$C = C_{\alpha,\beta}$ at $x = x_1 + o$. . . . . (3)

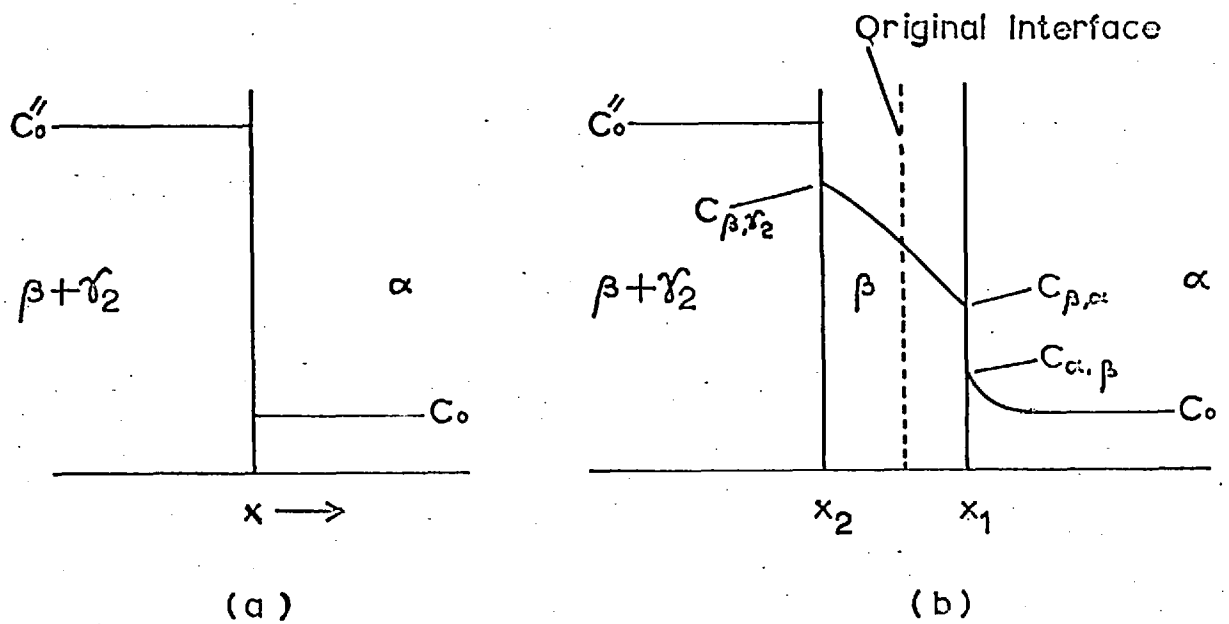

(Appendix) FIG.1 Diffusion In Three Phase System

(a) At $t = 0$

(b) At $t > 0$

The diffusion equations valid for β and α phases are

$$\frac{\delta C}{\delta t} = D_\beta \frac{\delta^2 c}{\delta x^2} \quad \text{for } x_2 < x < x_1 \quad \ldots\ldots\ldots \quad (4)$$

and

$$\frac{\delta C}{\delta t} = D_\alpha \frac{\delta^2 c}{\delta x^2} \quad \text{for } x > x_1 \quad \ldots\ldots\ldots \quad (5)$$

The mass balance equations at the interfaces are

$$C_o'' - C_{\beta,\gamma_2} \frac{dx_2}{dt} = D_\beta \left.\frac{\delta c}{\delta x}\right|_{x_2 + o} \quad \ldots\ldots \quad (6)$$

and

$$C_{\beta,\alpha} - C_{\alpha,\beta} \frac{dx_1}{dt} = -D_\beta \left.\frac{\delta c}{\delta x}\right|_{x_1 - o} + D_\alpha \left.\frac{\delta c}{\delta x}\right|_{x_1 + o} \quad \ldots \quad (7)$$

Solutions to the equations (4) and (5) are

$$C = A - B_\beta \operatorname{erf} \frac{x}{2\sqrt{D_\beta t}} \quad \text{for } x_2 < x < x_1 \quad \ldots \quad (8)$$

and

$$C = C_o + B_\alpha \left[1 - \operatorname{erf} \frac{x}{2\sqrt{D_\alpha t}}\right] \quad \text{for } x > x_1 \quad \ldots \quad (9)$$

where

A, B_β and B_α are constants determined by the boundary conditions.

From the conditions 1, 2 and 3 one obtains

$$C_{\beta,\gamma_2} = A + B_\beta \operatorname{erf} k_2 \quad \ldots\ldots\ldots\ldots \quad (10)$$

$$C_{\beta,\alpha} = A - B_\beta \operatorname{erf} k_1 \quad \ldots\ldots\ldots\ldots \quad (11)$$

and $$C_{\alpha,\beta} = C_o + B_\alpha\left[1 - \operatorname{erf}\left(k_1\sqrt{\Phi}\right)\right] \quad \ldots\ldots \quad (12)$$

where k_1 and k_2 are given by the assumptions

$$\frac{x_2}{\sqrt{t}} = k_2 \cdot 2\sqrt{D_\beta} \quad \ldots\ldots\ldots\ldots\ldots\ldots \quad (13)$$

$$\frac{x_1}{\sqrt{t}} = k_1 \cdot 2\sqrt{D_\alpha} \quad \ldots\ldots\ldots\ldots\ldots\ldots \quad (14)$$

and

$$\Phi = \frac{D_\beta}{D_\alpha} \quad \ldots\ldots\ldots\ldots\ldots\ldots \quad (15)$$

Differentiating equations (8) and (9) one obtains

$$\left(\frac{\delta c}{\delta x}\right)_{x_2 + o} = -\frac{B_\beta \cdot \exp\left(-k_2^2\right)}{\sqrt{\pi} \cdot \sqrt{D_\beta t}} \quad \ldots\ldots \quad (16)$$

$$\left(\frac{\delta c}{\delta x}\right)_{x_1 - o} = -\frac{B_\beta \cdot \exp\left(-k_1^2\right)}{\sqrt{\pi} \cdot \sqrt{D_\beta t}} \quad \ldots\ldots \quad (17)$$

$$\left(\frac{\delta c}{\delta x}\right)_{x_1 + o} = -\frac{B_\alpha \exp\left(-k_1^2\Phi\right)\sqrt{\Phi}}{\sqrt{\pi} \cdot \sqrt{D_\beta t}} \quad \ldots\ldots \quad (18)$$

Substituting the appropriate values in equations (6) and (7) one gets

$$C''o - C_{\beta,\gamma_2} = \left[\frac{D_\beta\sqrt{t}}{k_2\sqrt{D_\beta}}\right]\left[-\frac{B_\beta}{\sqrt{\pi}\cdot\sqrt{D_\beta t}\cdot\exp(k_2^2)}\right] + \frac{B_\beta}{\sqrt{\pi}\cdot k_2\cdot\exp(k_2^2)} \quad \ldots \quad (19)$$

Eliminating B_β through equations (10) and (11) one obtains

$$\frac{C_{\beta,\gamma_2} - C_{\beta,\alpha}}{Co'' - C_{\beta,\gamma_2}} = \sqrt{\pi}\cdot k_2\cdot\exp(k_2^2)\left[\operatorname{erf} k_1 + \operatorname{erf} k_2\right] \quad \ldots \quad (20)$$

Similarly eliminating B_β and B_α from the equation

$$C_{\beta,\alpha} - C_{\alpha,\beta} = \frac{B_\beta}{\sqrt{\pi}\cdot k_1\exp(k_1^2)} - \frac{B_\alpha}{\sqrt{\pi}\cdot\sqrt{\phi}\cdot k_1\exp(k_1^2)}$$

one obtains

$$C_{\beta,\alpha} - C_{\alpha,\beta} = \frac{C_{\beta,\gamma_2} - C_{\beta,\alpha}}{\sqrt{\pi}\cdot k_1\cdot\exp(k_1^2)\left[\operatorname{erf} k_1 + \operatorname{erf} k_2\right]} - \frac{C_{\alpha,\beta} - C_o}{\sqrt{\pi}\cdot\sqrt{\phi}\cdot k_1\cdot\exp(k_1^2\phi)\left[1 - \operatorname{erf}(k_1\sqrt{\phi})\right]} \quad \ldots \quad (21)$$

Equations (20) and (21) can be solved if C_{β,γ_2}, $C_{\beta,\alpha}$, $C_{\alpha,\beta}$, C_o, Co" and ϕ are known. The value of ϕ was determined from the data of Rhines and Mehl[46] and from the D_β values determined previously. An average activation energy of Q = 58.6 K.Cals / mol for α and an average value of D = 3.75×10^{-9} cm^2 / sec (at 880°C) have been used in the calculations.

A graphical method was used for evaluating k_1 and k_2. The rates of displacements of the α / β and $\beta + \gamma_2$ / β interfaces are given in Appendix table I. D_β values were determined from the equations (13) and (14). The average values have been used in the Arrhenius relation shown in Appendix Fig.2. The activation energy for diffusion is found to be 28.5 K.Cals / mol which is close to the one obtained by the other method.

Temp °C	$x_1^*/\sqrt{t}$ mm/h$^{1/2}$	k_1	$x_2^*/\sqrt{t}$ mm/h$^{1/2}$	k_2	D_β cm^2/sec
646	0.064	0.27	0.131	0.43	5.2×10^{-8}
672	0.091	0.30	0.182	0.52	7.3×10^{-8}
700	0.135	0.35	0.275	0.62	1.2×10^{-7}
725	0.175	0.37	0.416	0.73	1.9×10^{-7}
756	0.238	0.39	0.600	1.38	1.9×10^{-7}

Table I (Appendix)

Diffusion coefficient of aluminium calculated from rates of displacement and the constant parameter

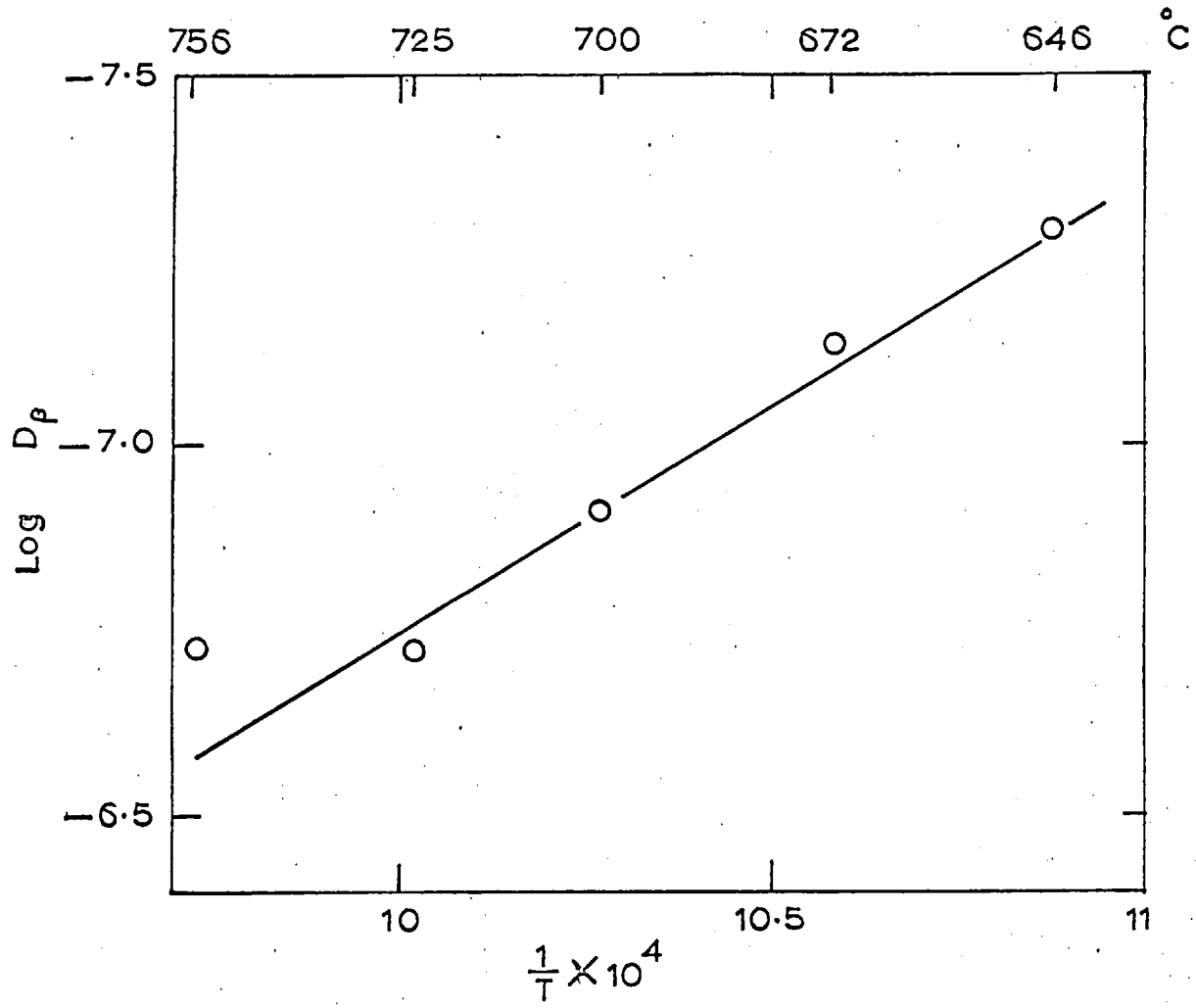

(Appendix) FIG. 2. Temperature Dependence Of Diffusion Coefficient.

Acknowledgements:

The author is indebted to Dr. D. R. F. West for the supervision, much kind criticism and encouragement throughout the course of this investigation. Grateful thanks are due to Professor J. G. Ball for the provision of research facilities. It is a pleasure to acknowledge the benefit of many a valuable discussion the author had with Dr. D. L. Thomas, Professor R. F. Mehl and Dr. J. Szekely and he wishes to express his sincere thanks.

This research programme was made possible through the award of a fellowship under the Colombo Plan by the British Council and the grant of leave of absence by the Indian Atomic Energy Establishment and the author most sincerely thanks them.

The author is especially grateful to the Department of Geology, Royal School of Mines, for carrying out microanalyses of the ternary diffusion couples and to Messrs. J. Stone and Co. Ltd. (Charlton) for chemical analyses of the alloys prepared for this investigation. He thanks his colleague Dr. K. I. Vasu for some of the chemical analyses reported in the binary diffusion work.

The willing cooperation and help received from the technical staff of the College is very warmly appreciated and thanks are due to them.